Modeling the Cost and Performance of Lithium-Ion Batteries for Electric-Drive Vehicles

Draft Report

EPA United States Environmental Protection Agency

Modeling the Cost and Performance of Lithium-Ion Batteries for Electric-Drive Vehicles

Draft Report

Assessment and Standards Division
Office of Transportation and Air Quality
U.S. Environmental Protection Agency

Prepared for EPA by
Argonne National Laboratory
Contract No. DE-AC02-06CH11357

NOTICE

This technical report does not necessarily represent final EPA decisions or positions. It is intended to present technical analysis of issues using data that are currently available. The purpose in the release of such reports is to facilitate the exchange of technical information and to inform the public of technical developments.

EPA United States Environmental Protection Agency

EPA-420-D-12-004
August 2012

TABLE OF CONTENTS

LIST OF FIGURES

LIST OF TABLES

ABBREVIATIONS

ASI	area specific impedance
BOL	beginning of life
DMC	dimethyl carbonate
EC	ethylene carbonate
EMC	ethyl methyl carbonate
EOL	end of life
EV	electric vehicle
Gr	graphite
GSA	General, Sales, and Administration
HEV	hybrid electric vehicle
HEV-HP	high-power assist hybrid electric vehicle
LCO	lithium cobalt oxide
LFP	lithium iron phosphate
Li	lithium
Li-ion	lithium-ion
LMO	lithium manganese spinel
LMR	lithium and manganese rich
LTO	lithium titanate spinel
microHEV	micro or mild power assist hybrid electric vehicle
NCA	lithium nickel cobalt aluminum oxide
NMC	lithium nickel manganese cobalt oxide
NMP	N-Methyl-2-pyrrolidone

OCV	open-circuit voltage
OEM	original equipment manufacturer
PE	polyethylene
PEP	polyethylene terephthalate
PHEV	plug-in hybrid electric vehicle
PP	polypropylene
R&D	research and development
SOC	state of charge
USGS	United States Geological Survey

LIST OF SYMBOLS

Section 3 and 5

a	ratio of interfacial area to electrode volume, cm^{-1}
A_{pos}	area of the positive electrode, cm^2
A_{term}	area of the terminal, cm^2
ASI_{energy}	area specific impedance for energy, ohm cm^2
ASI_{power}	area specific impedance for power, ohm cm^2
C	cell capacity, Ah.
C_p	specific heat capacity, J/g K
E	total energy, Wh
F	Faraday constant, 96485.3 C/mol
H_j	height of j, cm
H/W	aspect ratio of pouch cell
i_o	exchange current density related to the interfacial area, A/cm^2
I	average current density, A/cm^2
I_{lim}^{ionic}	ionic limiting current density, A/cm^2
I_n	local current density, A/cm^2
L_j	thickness of j, cm
m_j	mass of j, g
N_j	number of j
P	battery power, W
P_{batt}	maximum designed battery power, W
q	heating rate, W

Q	specific capacity of the electrode, mAh/g
r_C	C-rate, h^{-1}
$r_{C,lim}$	limiting C-rate, h^{-1}
r_j	radius of *j*, cm
$\overline{R}$	universal gas constant, 8.3144 J/mol K
R_j	resistance of *j*, ohm
T	temperature, K
t	time, s
$U_{ocv,P}$	open-circuit voltage at SOC for power, V
$U_{ocv,E}$	open-circuit voltage at SOC for energy, V
V_{cell}	cell voltage, V
v	square root of dimensionless exchange current
[V/U]	fraction of the open-circuit voltage
W_j	width of *j*
X_{comp}	compression factor
α	constant, ohm cm^3
β	constant, ohm cm^2
ε_{act}	volume fraction of active material
$\Phi_{1,k}$	metal potential of foil *k*, V
ρ_j	density of *j*, g/cm^3
σ_j	conductivity of *j*, S/cm

Section 4

C	capital cost of an installed equipment for the designed battery, $
C_o	capital cost of an installed equipment for the baseline plant battery, $
p	power factor
R	designed battery processing rate for specific process step
R_o	baseline plant processing rate for specific process step

ACKNOWLEDGEMENTS

Support from the Vehicle Technologies Program, Hybrid and Electric Systems, initially under Tien Duong and now David Howell, at the U.S. Department of Energy, Office of Energy Efficiency and Renewable Energy, is gratefully acknowledged. The submitted manuscript has been created by UChicago Argonne, LLC, Operator of Argonne National Laboratory ("Argonne"). Argonne, a U.S. Department of Energy Office of Science laboratory, is operated under contract no. DE-AC02-06CH11357. The U.S. Government retains for itself, and others acting on its behalf, a paid-up nonexclusive, irrevocable worldwide license in said article to reproduce, prepare derivative works, distribute copies to the public, and perform publicly and display publicly, by or on behalf of the Government. We especially thank Danilo Santini of Argonne's Transportation R&D Center for his support and suggestions in carrying out this study. Ralph Brodd reviewed our baseline plant and made several suggestions which we have incorporated in the present design. Fritz Kalhammer and Haresh Kamath of the Electric Power Research Institute have reviewed our work over several years and made suggestions that resulted in improvements. The work was done under the direction of Dennis Dees and Gary Henriksen of Electrochemical Energy Storage who provided guidance in carrying out the work and preparing this manuscript.

EXECUTIVE SUMMARY

This report details a design and cost model developed at Argonne National Laboratory for lithium-ion battery packs used in automotive transportation. The model designs the battery for a specified power, energy, and degree of powertrain electrification. The cost of the designed battery is then calculated by accounting for every step in the lithium-ion battery manufacturing process. The assumed annual production level directly affects each process step. The total cost to the original equipment manufacturer calculated by the model includes the materials, manufacturing, and warranty costs for a battery produced in the year 2020. At the time this report is written, this calculation is the only publically available model that performs a bottom-up lithium-ion battery design and cost calculation.

The purpose of the report is to document the equations and assumptions from which the model has been created. A user of the model will be able to recreate the calculations and perhaps more importantly, understand the driving forces for the results. Instructions for use and an illustration of model results are also presented. Almost every variable in the calculation may be changed by the user to represent a system different from the default values pre-entered into the program.

The model will be openly distributed to the public in the year 2011. Currently, the calculations are based in a Microsoft® Office Excel spreadsheet. Instructions are provided for use; however, the format is admittedly not user-friendly. Future work is proposed to create a more intuitive user-interface with tools to prevent inappropriate values from being entered. A version that is more user-friendly will allow for wider adoption of the model.

1. Introduction

The recent penetration of lithium-ion (Li-ion) batteries into the vehicle market has prompted interest in projecting and understanding the costs of this family of chemistries being used to electrify the automotive powertrain. The model described here-in is a calculation method that was developed at Argonne for estimating the manufacturing cost and performance of Li-ion batteries for electric-drive vehicles including hybrid-electrics (HEV), plug-in hybrids (PHEV), and pure electrics (EV). To date, a number of cost models of various levels of detail have been published in different forms.[1-10] Most available cost models for batteries are based on a single linear equation dependent on the power and energy required such as \$/kWh = $a + b$*kW. While a simplistic relation like this is attractive, it is only approximate and provides little guidance in reducing costs. The cost of a battery will change depending upon the materials chemistry, battery design, and manufacturing process.[11,12] Therefore, it is necessary to account for all three areas with a bottom-up cost model. Other bottom-up cost models exist but are not available to the general public and have not been explicitly detailed in an open document. The motivation for this work is based on a need for a battery cost model that meets the following requirements:

1. Open and available to the entire community
2. Transparent in the assumptions made and method of calculation
3. Capable of designing a battery specifically for the requirements of an application
4. Based on a bottom-up calculation approach to account for every cost factor

The model is the product of long-term research and development at Argonne National Laboratory. Over a period of years, Argonne has developed methods to design Li-ion batteries for electric-drive vehicles based on modeling with Microsoft® Office Excel spreadsheets.[11-18] These design models provided all the data needed to estimate the annual materials requirements for manufacturing the batteries being designed. This facilitated the next step, which was to extend the effort to include modeling of the manufacturing costs of the batteries. In the following sections of this document, a model is presented that meets the above criteria and may be used to analyze the effect of battery design and materials properties on the cost of the final battery pack. Use of the model requires some basic knowledge of battery packs; however, a user does not need to be an expert. For instance, the number of cells and thus battery pack voltage must be specified by the user. However, default values are available for more specific requirements such as experimentally measured values. In this way, a person with reasonable knowledge of batteries may be able to conduct cost comparisons and "what if" studies.

The battery pack design and cost calculated by the model represent projections of a 2020 production year and a specified level of annual battery production, 10,000-1,000,000. As the goal is to predict the future cost of manufacturing batteries, a mature manufacturing process is assumed. The model designs a manufacturing plant with the sole purpose of producing the battery being modeled. The assumed battery design and manufacturing facility are based on common practice today but also assume some problems have been solved to result in a more efficient production process and a more energy dense battery. Our proposed solutions do not have to be the same methods used in the future by industry. We simply assume the leading battery manufacturers, those having successful operations in the year 2020, will reach these ends by some means.

2. Battery and Cell Design Format

Various cell and battery design concepts are under development at battery manufacturers. The exact design of the battery does not have an important effect on the cost for a set cell chemistry system; the amounts of electrode materials and the number, capacity and electrode area of the cells, are the determining cost factors. The most common cell designs for batteries nearing large-scale production are cylindrical wound cells, flat wound cells, and prismatic cells with flat plates. Cylindrical cells probably have a slight advantage for the assembly of the electrode-separator unit because of the ease of making a cylindrical winding. For the different cell designs, there are small differences in the weights of the terminal extensions and the procedures for connecting these extensions to the current collector sheets, with a small advantage for flat plate cells. The flat-wound and flat-plate cells form a more compact module and have better heat rejection capabilities than the cylindrical cells; although, each cell design can be adequately cooled for most applications. These small differences would have minor effects on the cost of batteries produced in high volume in a mature, automated production plant. We conclude that the cost calculations would be relevant for batteries differing considerably from the selected design approach.

To provide a specific design for the calculations, a prismatic cell in a stiff-pouch container and a double-seamed module container was selected (Fig. 2.1). For this design, calculation of the current collector and terminal resistances are easily done. The electrical performance is near optimum in a compact, light-weight configuration. It is unlikely that we have selected the most viable design in this short study; there may be serious flaws in some details. However, the overall performance and low cost for the selected design will be challenging to match and will only be met by the most successful manufacturers, those that will dominate the market.

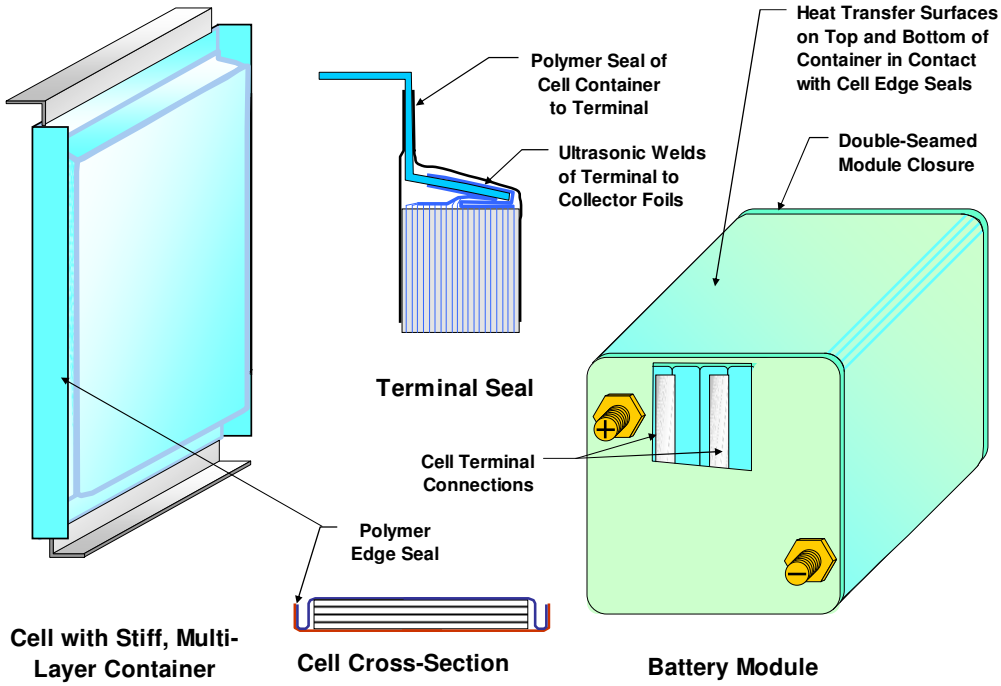

Figure 2.1 Prismatic cell and module design for battery packs

2.1 Cell Design

The prismatic cell of this design embodies individual positive and negative electrodes consisting of current collector foils coated with electrode materials on both sides. The current collectors are usually solid copper and aluminum foils for the positive and negative electrodes respectively. An illustration of a segment of the cell is detailed in Figure 2.2. Each electrode is made up of active material particles held together by a polymeric binder. A conductive additive, carbon black and/or graphite, is added to the positive electrode and sometimes to the negative electrode. The electrodes and separator each have porosity that is filled with the electrolyte solution. During discharge, the Li-ions move from the negative electrode particles into the electrolyte, across the separator, and then insert into the particles composing the opposite positive electrode. The electrons simultaneously leave the cell through the current collection system and then enter through the opposite side after doing external work. The materials currently used in Li-ion cells are based on an intercalation mechanism. In this process, the Li-ion is inserted into or removed from the crystal structure of the active material. The oxidation state of the active material, or host, is concurrently changed by gaining or losing an electron. Other electrode materials based on conversion reactions or electrodeposition could be implemented into the model if desired.

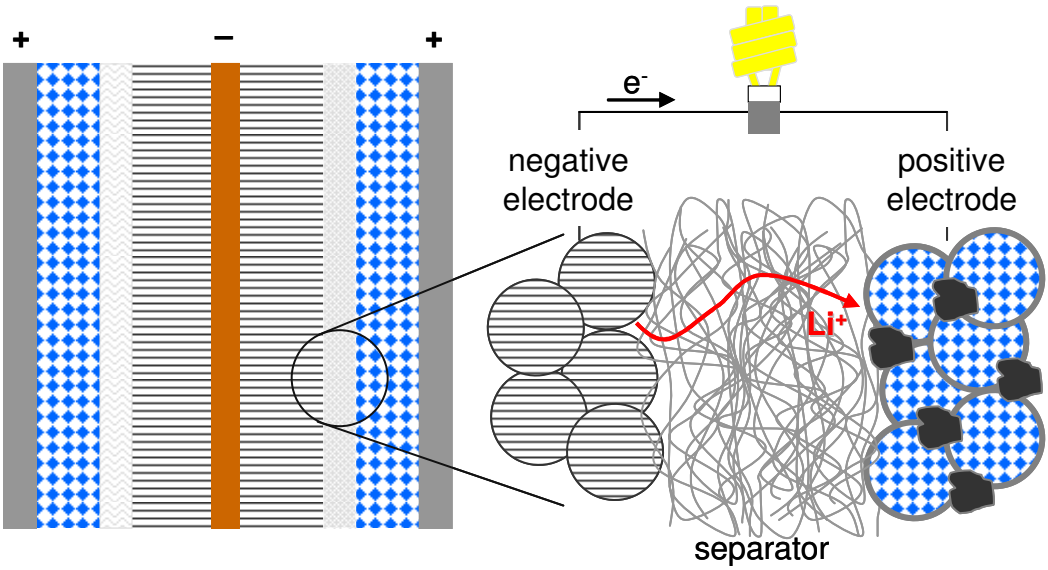

Figure 2.2 Cell sandwich inside of prismatic pouch cells.

The electrodes are efficiently prepared by coating wide sheets of foil (up to 2-meters in width) with uncoated strips running the lengths of the foil being coated. The individual electrodes can be cut from these sheets with little waste of electrode coating material or foil (Fig. 2.3). The separator for these cells can be handled as a single sheet that is folded back and forth as the electrodes are inserted. The electrodes are inserted so that all of the positive tabs extend beyond the separator sheet in one direction and the negative tabs extend in the opposite direction. The design model selects the number of electrodes for a set cell thickness determined by the type of cell: HEV, 6 mm; PHEV, 12 mm; EV, 14 mm. The cell terminals are formed from flat stock to be almost as wide as the entire cell. They are bent to the shape shown in Fig. 2.1 and ultrasonically welded to the current collector tabs. The cell stack is then sealed between the two halves of the cell container. The cell housing material is a tri-layer consisting of an outer layer of

polyethylene terephthalate (PEP) for strength, a middle layer of 0.1-mm aluminum for stiffness and impermeability to moisture and electrolyte solvent vapors and an inner layer of polypropylene (PP) for sealing by heating.[19,20] The two halves of the cell container are pre-shaped to facilitate assembly. The aluminum foil in the cell container material provides stiffness and it may be increased in thickness to assist in conducting heat to the module container.

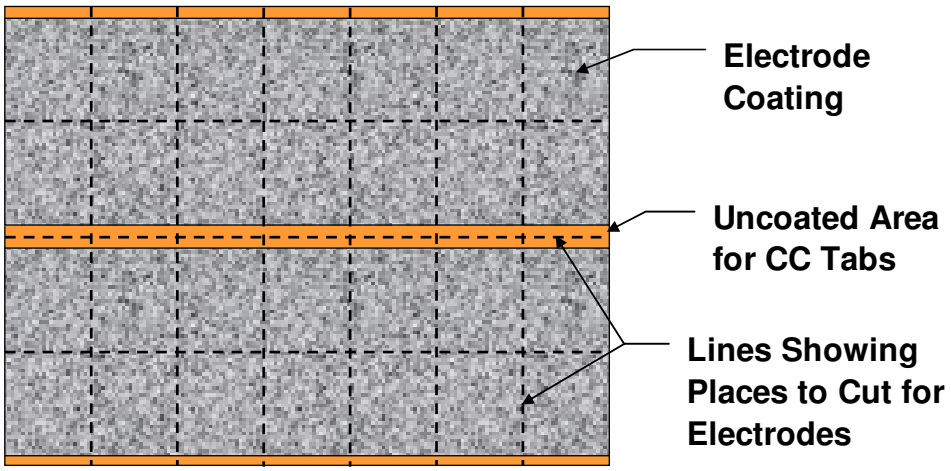

Figure 2.3 Coated current collector foil for prismatic electrodes

2.2 Module Design

The model designs a module casing of 0.5 mm aluminum that is sealed by double seaming, a process that is well established and inexpensive because it is automated, rapid, and uses low-cost capital equipment. The sealing of the module provides an additional barrier to the loss of electrolyte solvent from the cells and the entrance of water vapor. These deleterious transfers through the seals of pouch cells may shorten their lives to less than the desired fifteen years.[19] The cells are placed on their sides in the module and the terminals of adjacent cells are connected either mechanically with small bolts and flat springs to maintain contact or by laser welding.

Space is provided within the module casing on the left side, as sketched in Fig. 2.1, for an electronics package that includes cell monitoring for malfunctions (temperature and voltage) and for state-of-charge (SOC) control. The SOC control is activated whenever the battery is at rest and it diverts charge from the cells at highest voltage to those at lowest voltage.

In the model, we assume the module is cooled only by air flowing over the upper and lower surfaces of the module. This method of cooling is most practical if the amount of heat generated is kept to moderate levels by defining full power as that provided at 80 % or higher fraction of the open-circuit voltage. To enhance heat flow from the cells to the cooled walls of the module casing, the edge seals, which include two layers of 0.1 mm thick aluminum foil (one from each half of the cell container), can be pressed against the walls of the casing by springs shaped as hoops. The heat transfer can be further enhanced by increasing the thickness of the aluminum

layer in the cell pouches or by adding an aluminum plate between the cells. The modules can also be cooled internally by a dielectric fluid such as a transformer coolant. For that approach, the fluid would be brought to the module through metal tubing or be supplied to the battery jacket and enter the modules through slots. Corrugated plates inserted between the cells would provide flow channels for the cooling fluid. In the current model, only air cooling on the outside of the module is provided. Further discussion of thermal issues may be found in Section 7.

2.3 Battery Pack Design

The model designs the battery pack in sufficient detail to provide a good estimate of the total weight and volume of the pack and the dimensions of the battery jacket so that its cost can be estimated. The modules are arranged within the battery jacket either in a single row, with the terminals facing the same side of the pack, or in an even number of rows with the terminals in one row facing the terminal of an adjacent row. The terminals are laid out on the module so as not to interfere with those on the opposite row of modules, thus conserving space in the battery pack. The modules in a row are interconnected, negative to positive terminals, by copper connectors. The modules casings are compressed together by two steel sheets bound with steel straps at the front and back of the battery pack. The compression is necessary to ensure intimate contact between the active layers that make up the pouch cells that are tightly fit into the modules. The compressive force also serves to add structural support to the module casing.

The battery jacket consists of a sheet of aluminum on each side of a 10-mm thick layer of ridged, light-weight high-efficiency insulation. The thickness of each of the aluminum layers is selected by the modeling program to be 1- to 2-mm thick, depending on the total volume of the modules. The insulation slows the interaction of the battery with the external environment that cools the battery in the winter and heats it in the hot summer weather.[14]

3 Modeling of Battery Design and Performance

The design portion of the model calculates the physical properties of a battery based on user-defined performance requirements and minimal experimental data. An illustration of the model is shown in Figure 3.1. The user is asked to enter a number of design parameters such as the battery power, number of cells and modules, and target voltage at maximum power, etc. In addition, the user must enter one of the following three measures of energy: battery pack energy, cell capacity, or vehicle electric range. Defining one of these values will determine the value of the other two. An iterative procedure then solves for the user defined energy parameter (energy, capacity, or range) and remaining battery properties by varying the cell capacity and electrode thickness. The result is the dimensions, mass, volume, and materials requirements for the cells, modules, and battery pack.

The model has been designed to allow the user to enter as many customized values as desired. In this way, the model allows flexibility in the battery chemistries studies and some of the cell, module, and battery design aspects. Hence, the focus of this report is on the method of calculation and not the exact values chosen for a specific capacity or cell thickness. However, the default cell design parameters as well as experimental data measured at Argonne National Laboratory, for a number of different battery chemistries, are available for use within the model. There are five governing equations for battery performance that calculate the current density, battery energy, electrode area, electrode thickness, and resistance. The voltage at maximum power and the area specific impedance (ASI) are two important parameters in the design model for calculating the battery performance. Most of the discussion will be spent on these two properties.

3.1 Criteria for Power, Energy, and Life

In order to fully specify a battery design, the user of the design model must supply criteria for power, energy, and life. These criteria will depend on the application for which the battery will be used. While the user may change some of the settings as they prefer, we list our suggestions in Table 3.1. The battery type is defined by the end-use application. Hybrid electric vehicles (HEVs), plug-in hybrid electric vehicles (PHEVs), and electric vehicles (EVs) have increasing levels of electrification of the vehicle drivetrain. The model will use Table 3.1 or the user's explicit inputs to size the battery correctly for the chosen application.

Table 3.1 Criteria for designing batteries for a specific end-use application

Battery Type	microHEV	HEV-HP	PHEV	EV
SOC for Rated Power, %	50	50	25	25
Power Duration, sec	2	10	10	10
SOC Range for Useable Energy, %	40-65	40-65	25-95	15-95
Cell Thickness, mm	6	6	10	14

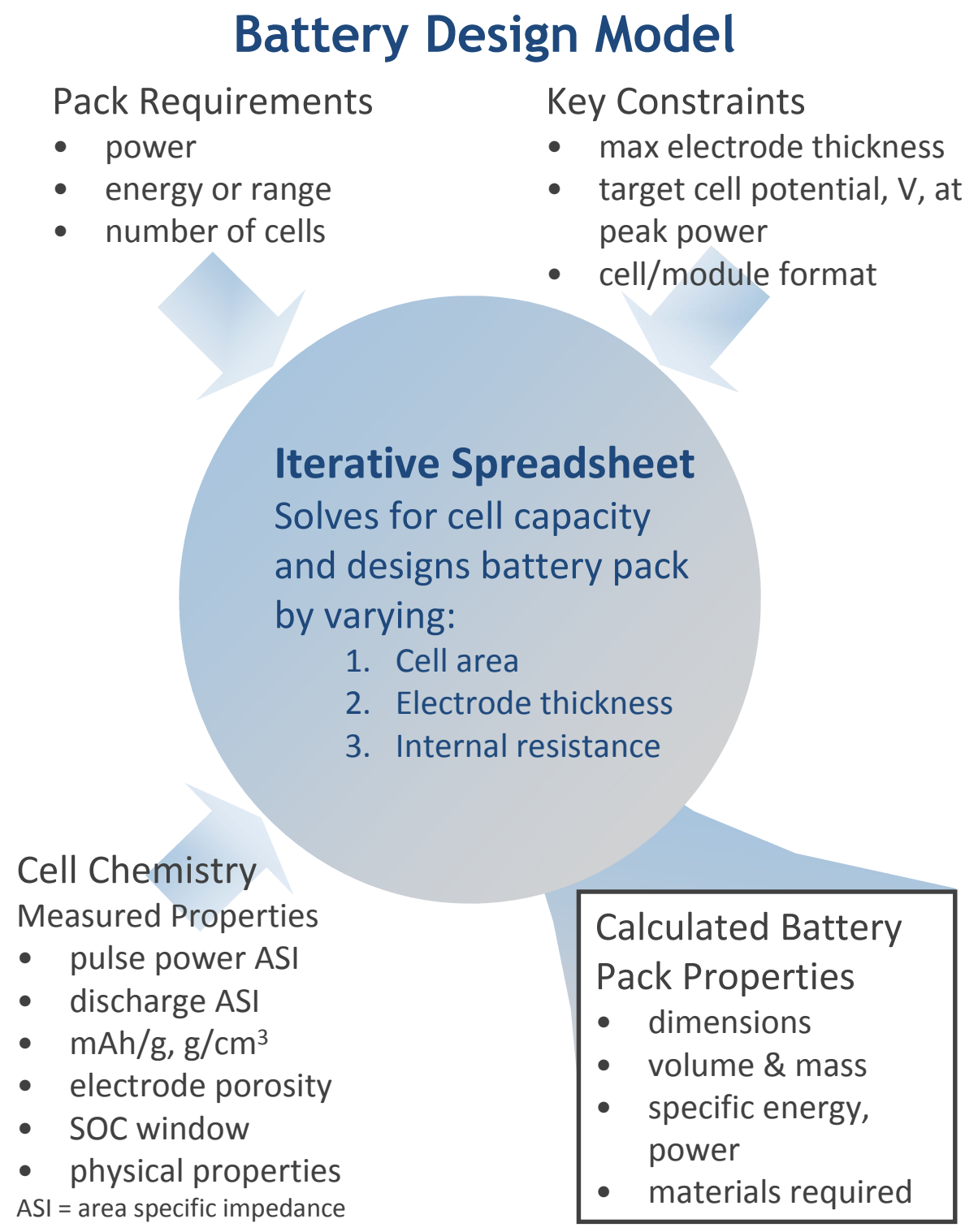

Figure 3.1 Summary flow of the design model

The microHEV is a micro or mild-hybrid that provides a moderate power level, ~25 kW, for two seconds. This design is best suited for cell chemistries capable of very high power-to-energy (P/E) ratios. The HEV-HP is a power-assist hybrid that provides the rated power for a full 10 second pulse. The power for both HEV applications is rated at 50 % state-of-charge (SOC). The energy available for discharge and charging is 25 % of the total energy to ensure long cycle life. As the capacity of the HEV cells is typically small, a cell thickness of 6 mm is used. The PHEV utilizes a much larger portion of the total energy, 70 %. At the end of discharge, the PHEV battery is operated in a charge sustaining mode. Therefore, the power rating for the battery is determined at 25 % SOC. PHEV cells should be much larger than HEV cells and thus a cell thickness of 10 mm is assumed. Finally, EV batteries use 80 % of their total energy with their power rated near the end of discharge. Cell thicknesses are set to 14 mm to accommodate a high capacity design. As noted later in the report, selecting a parallel arrangement of cells automatically assumes a cell thickness of 6 mm regardless of the end-use application. Additionally, the use of negative electrodes operating at potentials high above the lithium metal potential may extend the upper end of the available SOC range from 95 to 100 %. The lithium titanate spinel, $Li_4Ti_5O_{12}$ (LTO), negative electrode is an example of intercalation electrode with almost no risk of plating lithium metal during a charge pulse. On this basis, the available energy for LTO-based Li-ion chemistries is suggested to be 75 % for PHEVs and 85 % for EVs.

Accounting for capacity and power fade in the battery requires the user to design the battery with the appropriate excess energy and power at the beginning-of-life (BOL). Defining the voltage at which maximum power is achieved at BOL is one way to set the allowable power fade over the life of the battery. This is discussed in detail in the following section. Capacity or energy fade must be accounted for by over-sizing the battery at BOL. If the user has a certain fade requirement, then the BOL energy may be increased to meet the end-of-life (EOL) target. The design model does not attempt to predict fade rates or even suggest an allowable fade for a specific application. It is our view that many aspects of materials chemistry, cell design, and battery use directly affect the decay of the battery pack. Hence, we allow the user to make accommodations for decay as he or she believes is necessary.

3.2 Voltage at Maximum Power

The voltage at which a cell reaches the designed maximum power is one of the most important factors in the design of a battery. However, this specification is one of the least discussed aspects of battery design. The voltage at maximum power, V_{cell}, is a measure of the largest polarization the cell will undergo during operation at the BOL. This initial value has a direct effect on round-trip battery efficiency, heat removal requirements, cold-cranking power, and allowable power fade. A basic calculation shows the maximum achievable power for a battery at BOL is at 50 % of the open-circuit voltage (OCV). Operating at these conditions would result in an inefficient battery and require a significant cooling system to reject heat. More importantly, the battery will never be able to reach this power level after any increase in impedance occurs. With all certainty, the impedance of a battery will rise with time and the power rating of battery will no longer be accurate. The remainder of this section presents a discussion for setting the BOL voltage at maximum power at no less than 80 % of the open-circuit voltage. Defining the voltage as a fraction of the OCV, [V/U], allows for direct calculation of all the necessary battery properties (see for example Eq. 3.6 or 3.8 in the section 3.3).

The allowable increase in battery resistance over the life of the battery is a function of the designed voltage for maximum power. In general, designing the battery to achieve maximum power at a higher [V/U] allows for larger resistance or impedance increases over the lifetime of the battery. Figure 3.2 created from Eq 3.1 displays how the voltage at maximum power will change to meet the designed power as the internal resistance of the battery increases. Clearly, achieving BOL power at a high fraction of the OCV allows for greater degradation within the usable lifetime of a battery. If the minimum voltage is 55 % of the OCV, the allowable increase in resistance for batteries designed for BOL max power at 70, 80, and 90 % OCV is 18, 55, and 175 %. The consequence of achieving the power at lower and lower fractions of the open-circuit voltage is that both electric current and heat generation will increase over the lifetime of the battery, Figure 3.2b and Figure 3.3. The proper design of a battery will account for the changes over the entire lifetime and not just desired behavior at BOL.

$$\left[\frac{V}{U}\right]_2 = \frac{1}{2}\left\{1+\sqrt{1-4\frac{R_2}{R_1}\left[\frac{V}{U}\right]_1\left(1-\left[\frac{V}{U}\right]_1\right)}\right\} \tag{3.1}$$

The level of heat production is significantly different at BOL for batteries designed to meet maximum power at differing fractions of the open-circuit voltage. We may compare the differences in designed [V/U] by assuming the resistive heating (joule heating) is the most significant factor in determining the heat generation, Eq. 3.2. We also reasonably assume the ASI will not change significantly in the range of current densities and electrode thickness we vary in the comparisons. From this point, we can analyze the difference in heat generation from different designed [V/U] values, Eq 3.3.

$$q_j = \left(A_{pos} I\right)^2 R_j = \frac{U^2\left(1-\left[\frac{V}{U}\right]_j\right)^2}{R_j} \tag{3.2}$$

$$\frac{q_2}{q_1} = \frac{R_1\left(1-\left[\frac{V}{U}\right]_2\right)^2}{R_2\left(1-\left[\frac{V}{U}\right]_1\right)^2} \tag{3.3}$$

The ratio of resistances may be found by equating the power for the two cases. Then the resistances, and areas if the ASIs are equivalent, are determined solely by the fraction of the open-circuit voltage at which they achieve maximum power, Eq 3.4. Then substitution will give the ratio of heat production at maximum power for the two cases, Eq. 3.5. A battery that achieves maximum power at 80 % of OCV will have a heat production at maximum power that is 2.3 times higher than one designed at [V/U] = 90 %. A battery producing power at 70 % of the OCV will have 3.9 time higher heat generation than at [V/U] = 90 %.

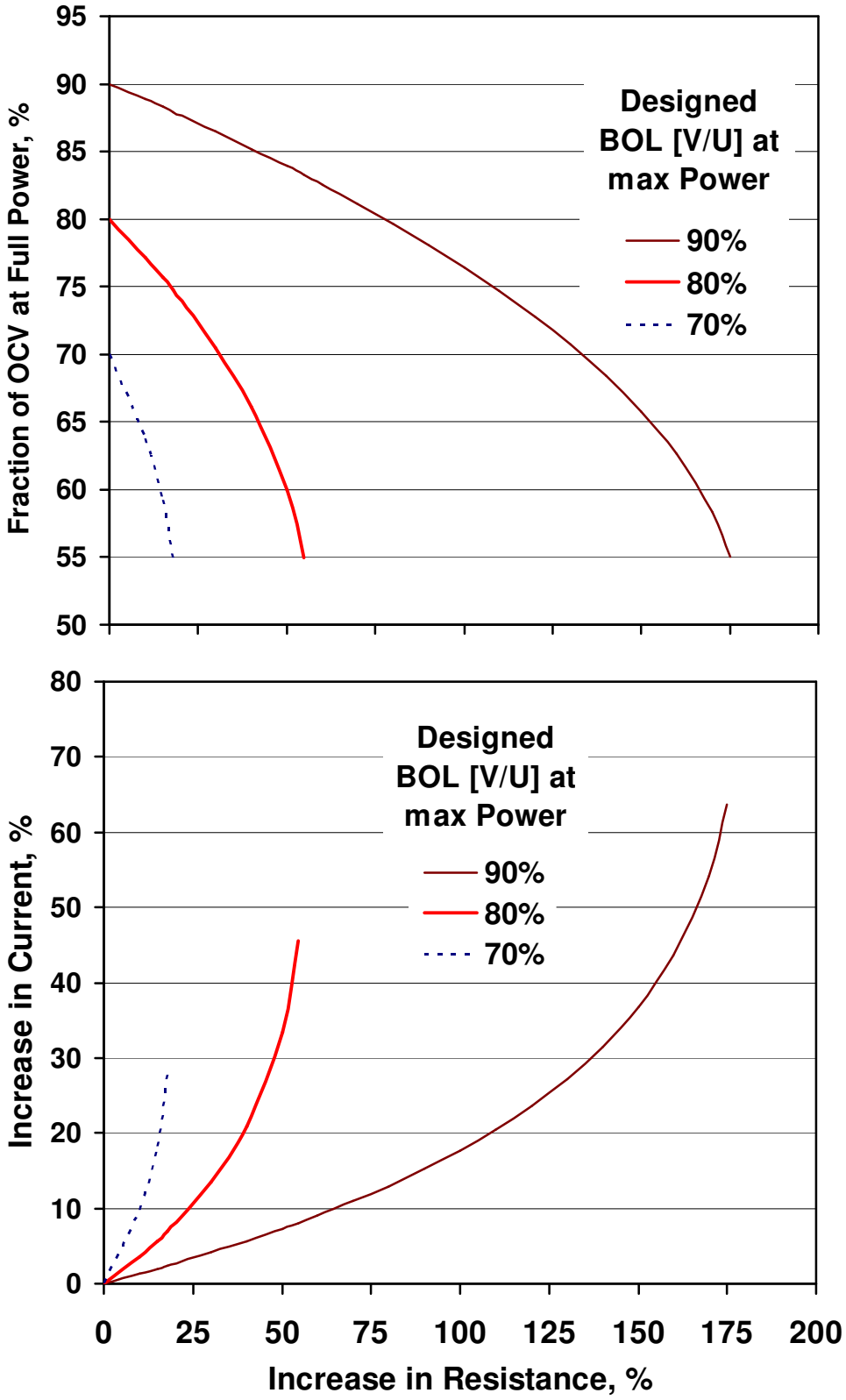

Figure 3.2 a) Required change in [V/U] to maintain rated power with increases in internal resistance over the life of the battery. b) Increase in current due to lowered [V/U].

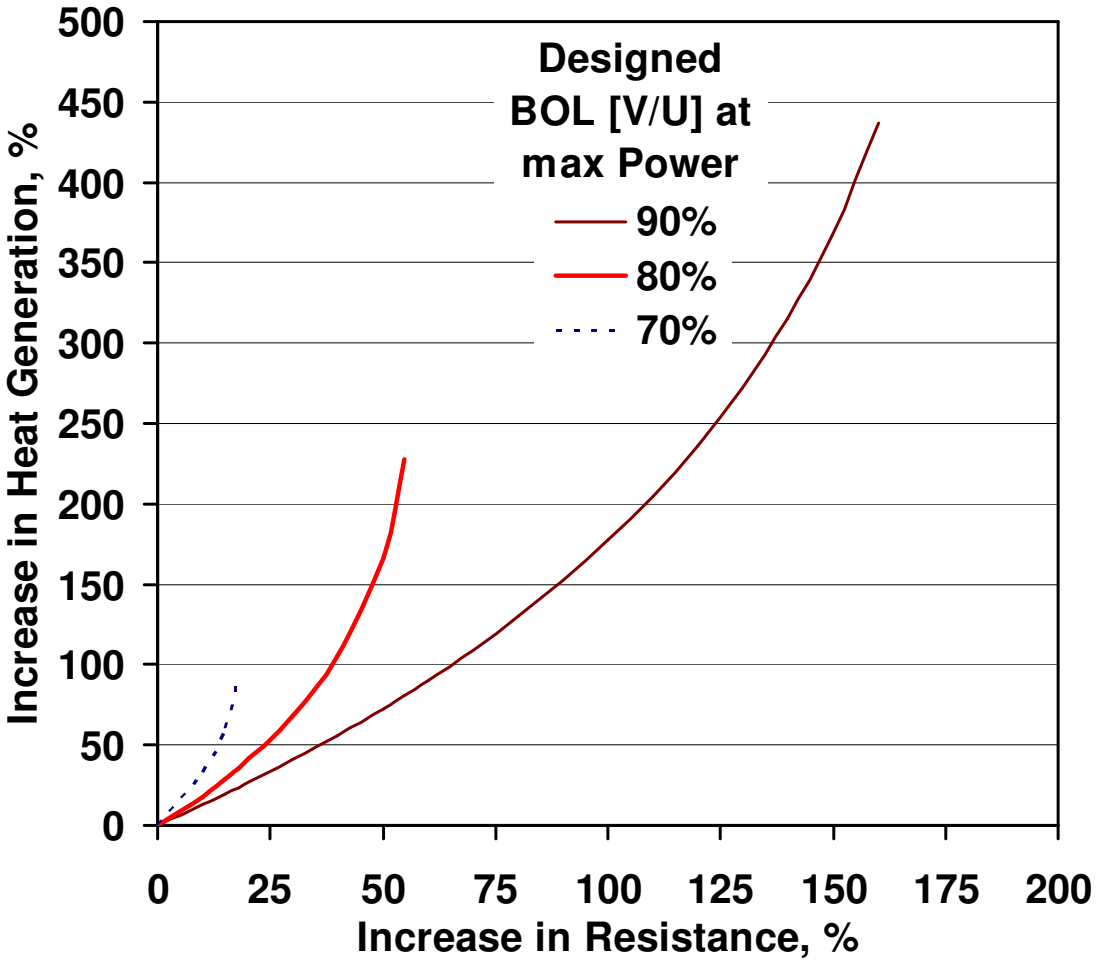

Figure 3.3 Change in heat rejection requirement from increases in resistance for batteries with different designed voltages at maximum power.

$$\frac{R_1}{R_2} = \frac{ASI_{power1} A_{pos2}}{ASI_{power2} A_{pos1}} = \frac{\left[\frac{V}{U}\right]_1 \left(1 - \left[\frac{V}{U}\right]_1\right)}{\left[\frac{V}{U}\right]_2 \left(1 - \left[\frac{V}{U}\right]_2\right)} \tag{3.4}$$

$$\frac{q_2}{q_1} = \frac{\left[\frac{V}{U}\right]_1 \left(1 - \left[\frac{V}{U}\right]_2\right)}{\left[\frac{V}{U}\right]_2 \left(1 - \left[\frac{V}{U}\right]_1\right)} \tag{3.5}$$

Two straightforward design changes will enable operating a battery at 90 % of OCV compared to 80 % while maintaining the same power output. First, a second identical battery may be connected in parallel to the original battery. This will lower the resistance of the battery pack by one half but will also double the energy and cost of the battery. A more realistic approach is to reduce the electrode thickness by coating a larger separator area. The capacity of the cell is maintained while minimizing increases in cost from a larger separator, current collector and packaging area. This approach is feasible as long as the reduced electrode thickness is above the increase in ASI, > 20 microns as discussed in detail below.

The efficiency of a battery defines the heat rejection requirements and may be measured or calculated. Measurement of round-trip efficiency of a battery is best performed by using a calorimeter to measure the heat given off during the cycling of the battery. The calorimeter removes the requirement of knowing the exact SOC of a battery during the entire drive cycle. Calculation of the round-trip efficiency of a battery requires a detailed transient battery model within a vehicle simulation program to exercise the battery over the many acceleration and deceleration periods that occur during a drive cycle. The interesting result is that the same battery will have different power ratings depending on what level of round-trip efficiency the user is willing to accept.

Figure 3.4 shows the efficiency of a battery as a function of the designed potential at which the battery reaches maximum power. The figure is created using Equations 3.1 and 3.4 above. Each line may be considered a different drive cycle, or duty load, for a battery with the same energy but different impedance (changing separator area). The straight, solid black line represents the efficiency of the battery operated only at maximum power, $P/P_{max} = 1$. In example, a battery designed at [V/U] = 0.8 will have 80 % efficiency for a single discharge pulse at maximum power. Likewise, a battery designed at 0.9 will be 90 % efficient at maximum power. Batteries are normally operated in the area above the line of the maximum power. Therefore, the other curves represent the efficiency of discharging a battery at power levels below maximum power (typical driving conditions). Consider two batteries each designed for a maximum power of 100 kW although one achieves this power at a [V/U] = 0.9 and the other at 0.7. If the two batteries are discharged at 45 kW, $P/P_{max} = 0.45$, the battery designed at [V/U] = 0.9 will be 6.4 % more efficient. This is significantly less than the 20 % efficiency improvement realized when operated at maximum power. The efficiency penalty is reduced as the battery operates less and less near the designed maximum power.

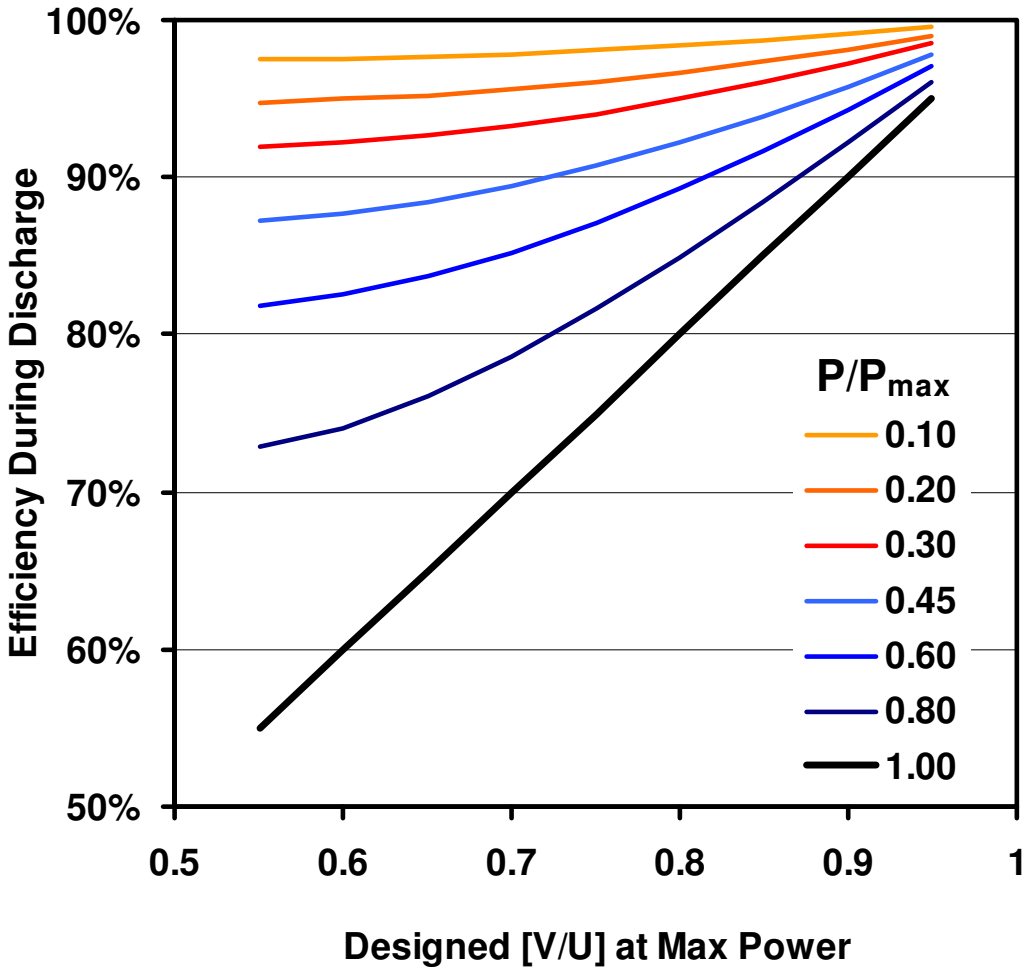

Figure 3.4 Efficiencies for batteries designed to achieve maximum power at different fractions of their open-circuit voltage. Comparative efficiency lines are shown for equivalent power demands over a period of battery operation.

3.3 Governing Equations

The five coupled, algebraic equations that govern the battery design are presented in this section. While these equations are perhaps the most important, many other equations are used to fully define the battery mass and volume. These other equations will be specified where necessary in the following subsections.

The user of the model specifies the required maximum power, P_{batt}, of the battery. This power is translated to a current density, I, in Eq 3.6 using the area of the positive electrode, A_{pos}, the number of cells, N_{cell}, the open-circuit voltage at the SOC for power, $U_{ocv,P}$, and the fraction of the open-circuit voltage at which maximum power is achieved, [V/U].

$$I = \frac{P_{batt}}{A_{pos} N_{cell} U_{ocv,P} \left[\frac{V}{U}\right]} \tag{3.6}$$

The relationship between capacity and battery energy is described by Equation 3.7. Formally, the energy of a battery is the product of the capacity and the average voltage at which the energy is obtained. The average cell voltage is approximated in Eq. 3.7 by subtracting the polarization from discharging the battery at a C/3 rate from the open-circuit voltage at the SOC for energy, $U_{ocv,E}$. The energy for all batteries designed by the design model is calculated at a C/3 rate and the average open-circuit voltage at 50 % SOC. The remaining necessary values are the capacity of the cell, C, ASI for energy, ASI_{energy}, number of cells, and area of positive electrode. Either the battery energy or capacity may be specified. The energy may alternatively be determined from a stated range, fraction of total energy available, and energy usage rate for the vehicle (Wh/mile).

$$E = N_{cell} C \left(U_{ocv,E} - \frac{C}{3} \frac{ASI_{energy}}{A_{pos}} \right) \tag{3.7}$$

The area of the positive electrode in Eq. 3.8 is determined largely by the area specific impedance for power, ASI_{power}, and resulting voltage drop. The voltage of cell at max power, $V_{cell,P}$, is found from the product [V/U]$U_{ocv,P}$. In general, the area of the cell will increase if the ASI for power increases. The areas of the negative electrode and separator are determined from the area of the positive electrode. The negative electrode is taken to be 1 mm larger than the positive electrode in both height and width to alleviate concerns of lithium plating during charge pulses. The separator area is slightly larger than the negative electrode to prevent the electrical shorting of the two electrodes.

$$A_{pos} = \frac{ASI_{power} P_{batt}}{N_{cell} \left(U_{ocv,P}\right)^2 \left[\frac{V}{U}\right] \left(1 - \left[\frac{V}{U}\right]\right)} \tag{3.8}$$

The positive electrode thickness, L_{pos}, in Eq. 3.9 is determined from the capacity of the cell, C, specific capacity of the electrode, Q, volume fraction of active material, ε_{act}, bulk density of the

active material, ρ, and the positive electrode area. The negative electrode thickness is determined by its specific reversible-capacity and the designed excess-capacity to prevent lithium plating during charging. We have chosen a ratio of 1.25 negative to positive reversible-capacity (N/P ratio) for the default value for the cells with graphite negative electrodes. LTO negative electrode based cells are designed at a 1.1 N/P ratio because of the previously mentioned minimal possibility of lithium deposition. The maximum allowable electrode thickness is a user defined value. The calculation for the electrode area changes when the designed thickness is greater than the maximum allowed (Section 3.6.1).

$$L_{pos} = \frac{C}{Q\rho\varepsilon_{act}A_{pos}} \tag{3.9}$$

Finally, the ASI for power (and for energy to a lesser extent) is calculated using an expression that is based on the electrode thicknesses, the current density, and the C-rate. The exact expression will be discussed in the next session. The ASI in Eq 3.10 shows the basic dependencies with α and β being constant valued parameters.

$$\text{ASI} = \frac{\alpha + f(I)}{L_{pos}} + \beta \tag{3.10}$$

3.4 Calculation of the ASI

In most battery design scenarios, the ASI directly determines the electrode thickness to meet a specified power-to-energy (P/E) ratio. From this electrode thickness, the area of the electrode is set to meet the capacity requirements. Clearly, the ASI plays a significant role in the design of a battery and particularly in the case of the P/E ratios required by automotive applications. However, the ASI is not an inherent constant of a specific battery chemistry or cell design. The measured value of the ASI is a complex combination of resistances within the battery resulting from the physical processes occurring at different length and time scales. Consequently, the measured value is a function of many factors (state of charge, pulse length, current density, C-rate, particle size, transport and kinetic parameters, etc). The calculation used for the ASI in this battery design model has been discussed in detail elsewhere.[18] The physical meaning of the equation will be discussed but those interested in the derivation are directed to the separate publication. We note that the ASI described here is slightly different than the one addressed in the paper. The thermodynamic component is removed that originated from the change in open-circuit potential with concentration for the intercalation materials. Equation 3.11 contains the definition of the ASI used in this document. I_{t1} is a positive valued current density for a discharge pulse. I_{t2} is equal to zero as it is during the relaxation period after the pulse. Time 0, *t0*, is the time just before a current pulse begins, time 1, *t1*, is the time just before the current pulse ends, and time 2, *t2*, is the time long after the current pulse when the cell is at open-circuit and the concentration gradients have relaxed. Therefore, this ASI measurement is not troubled by accounting for a change in open-circuit voltage with the passage of current. In general, the ASI measured with this definition is similar, although smaller, in value to those produced using the more standard definition used elsewhere.

$$ASI = \frac{V_{t2} - V_{t1}}{I_{t1} - I_{t2}} \tag{3.11}$$

The ASI for the electrochemical charge and discharge process is referred here-in as ASI_{echem}. Our calculation approach for both the ASI for power and for energy involves adding three components together to reach the ASI_{echem}, Eq. 3.12. The first two factors include impedance that arises from the interfacial charge transfer and transport. The third factor is a lumped parameter used to capture the remaining impedance.

$$ASI_{\text{echem}} = ASI_{\text{intf}}^{pos} + ASI_{\text{intf}}^{neg} + ASI_{\text{const}} \tag{3.12}$$

The interfacial impedance for positive and negative electrodes both contain the charge transfer resistance component $RT/(i_o aLF)$ as shown in Eq. 3.13 and 3.14. Here, i_o is the exchange current density related to the interfacial area and a is the ratio of interfacial area to electrode volume. An approximation often used for a relates the parameter to the volume fraction of the active material and the particle radius, $a = 3\varepsilon_{\text{act}}/r_p$. The variables i_o and a should be specified to relate to the same area as they are often not independently determined. $\overline{R}$ and T correspond to the universal gas constant and absolute temperature respectively. F is Faraday's constant. The influence of the interfacial impedance is that the ASI_{echem} increases as the electrode thickness is reduced. This behavior is typically observed at electrode thicknesses less than 30 microns for common Li-ion battery materials.

$$ASI_{\text{intf}}^{\text{neg}} = \frac{\overline{R}T}{i_o aL_{neg}F} \tag{3.13}$$

$$ASI_{\text{intf}}^{\text{pos}} = \frac{\overline{R}T}{i_o aL_{pos}F}\left\{\left(1 - \frac{I}{I_{\text{lim}}^{ionic}}\right)\left[1 - \left(\frac{r_C}{r_{C,\text{lim}}}\right)^2\right]\right\}^{-0.5} \tag{3.14}$$

The positive electrode interfacial impedance also includes two factors that account for the physical limitations that occur from depleting the concentration of the reactants within the porous electrode. The I_{lim}^{ionic} term is the limiting ionic current for lithium cation transport through the porous separator. The $r_{C,\text{lim}}$ term is the limiting C-rate for solid state diffusion of lithium in the active materials. The C-rate may be related to the current density with Eq. 3.15. Here, the specific capacity, Q, the active material density, ρ, active material volume fraction, ε_{act}, and the electrode thickness, L, are used. If either the limiting C-rate or limiting ionic current are approached, the ASI will begin to approach an infinite value. The parameters required for the ASI expression are fit to experimental measurements. The ASI values are corrected for the interfacial contributions present during measurement so that the correct ASI may be determined at different electrode thicknesses.

$$I = r_C Q \rho \varepsilon_{act} L_{pos} \tag{3.15}$$

The cell ASI for energy, ASI_{energy}, and power, ASI_{power}, are determined by adding the ASI_{echem} to that of the current collectors, ASI_{cc}, as discussed in the next subsection. The difference between ASI_{energy} and ASI_{power} is that the limiting currents are not important during the C/3 discharge for energy and the ASI_{const} is a different value for two cases. ASI_{energy} will always be higher than ASI_{power} if a battery is operated far from the limiting current. The higher impedance is due to the formation of significant concentration polarizations during the longer time scale of the energy discharge. A reasonable rule-of-thumb is that the ASI_{const} for energy is 2.2x the value for power in layered oxide materials such as $LiNi_{0.80}Co_{0.15}Al_{0.05}O_2$.

3.4.1 Current Collection Resistance

The resistance from the conductors used to collect the current must be accounted for as they can contribute significant ohmic drop to the battery. The ASI used to calculate the required cell separator area, ASI_{power}, is larger than the ASI for the electrochemical charge and discharge processes, $ASI_{echem,P}$, as shown in Equation 3.16. The ASI_{echem} value is typically measured from experiments and must be added to the external resistances that arise from the materials used to conduct the electric current. These resistances come from current collection in the cell and also those on the module and battery pack level.

$$ASI_{power} = ASI_{echem,P} + ASI_{cc} + ASI_{term}^{cell} + \frac{R_{cnct} A_{pos}}{N_{cells}} \tag{3.16}$$

The current collector foil impedance, ASI_{cc}, is determined from an analytical expression, Eq. 3.17, which accounts for the coated and uncoated region of the foil, labeled *act* for active and *tab* respectively. The resistance factor, R_f, and the resistance of the current collector foils, R_{cc}, are also shown for clarity in Eq 3.18 and 3.19. The factor of 2 in the R_f term is due to assuming half of the foil thickness carries the current produced on one side of the foil. While all of the current passes through the tab region, the magnitude of the current varies along the height of the coated foil as the reaction area continually contributes current to the foil. An equivalent length for the resistance calculation may be determined so that multiplication by the total current for a cell will give the correct ohmic drop. This equivalent length is H/3 if the current density is relatively constant over the entire area. The derivation of this equivalent length as well as an in-depth discussion of the voltage and current distribution in the foils may be found in subsection 3.4.2. Also in the later subsection, the assumption of constant current density is verified with numerical modeling.

$$ASI_{cc} = H_{act} W_{act} R_{cc} = R_f \left(\frac{(H_{act})^2}{3} + H_{act} H_{tab} \right) \tag{3.17}$$

$$R_f = \left(\frac{2}{\sigma_{foil,neg} L_{foil,neg}} + \frac{2}{\sigma_{foil,pos} L_{foil,pos}} \right) \tag{3.18}$$

$$R_{cc} = R_f \left(\frac{H_{act}}{3W_{act}} + \frac{H_{tab}}{W} \right) \tag{3.19}$$

The cell terminals are ultrasonically welded to the ends of the current collector foil tabs. While the welding removes this contact resistance, the ASI of the terminal must be included in the total cell resistance. The ASI of the cell terminals, $ASI_{\text{term}}^{\text{cell}}$, is the summation of the positive and negative cell terminals as shown in Eq 3.20. The dimensions for these terminals are set by the calculated width of the cell and the user defined terminal thickness and height.

$$ASI_{\text{term}}^{\text{cell}} = \left(\frac{1}{\sigma_{term,neg}} + \frac{1}{\sigma_{term,pos}} \right) \frac{H_{term}}{W_{term} L_{term}} A_{pos} \tag{3.20}$$

The ASI for connection losses is the last term in the ASI summation stated in Eq. 3.16. This ASI value is calculated by multiplying the ratio of cell positive electrode area to number of cells by the summation of the resistances, R_{cnct}, for cell terminals, module terminals, module interconnects, and batteries terminals. In this way, each cell shares in the burden of overcoming the system losses from carrying the electric current. The calculation of R_{cnct} is detailed in Eq. 3.21 with the individual sources of connection losses shown. The voltage drop resulting from cell-to-cell contact resistance, R_{cntct}^{cell}, is taken to be $10^{-4} U_{\text{ocv,E}}$ in Eq. 3.22, a small fraction of the open-circuit voltage. A battery manufacturer would only tolerate a minimal voltage drop from cell-to-cell contact. One connection method is to physically press the two cell terminals together. This resistance could be lowered by increasing the physical pressure and contact area, or by laser welding the terminals together. Regardless, the value used in the model is left to the choice of the user to leave as is or to change to a different value.

$$R_{cnct} = N_{cell} R_{cntct}^{cell} + N_{\text{mod}} R_{term}^{\text{mod}} + \left(N_{\text{mod}} - 1 \right) R_{incnt}^{\text{mod}} + R_{term}^{batt} \tag{3.21}$$

$$R_{cnct}^{cell} = 10^{-4} \frac{N_{cell} U_{ocv,E}}{I A_{pos}} \tag{3.22}$$

The module terminal resistance, R_{term}^{mod}, calculation in Eq. 3.23 is shown as an example of how the terminal and interconnect resistances are calculated for the module and battery pack. The size of the terminals and thus their resistance are determined from a calculation based on a pre-determined allowable rate of temperature rise for the conductor. This approach is explained in more detail in subsection 3.4.3.

$$R_{\text{term}}^{\text{mod}} = \frac{H_{term}}{\sigma_{term} \pi \left(r_{term} \right)^2} N_{term}^{\text{mod}} \tag{3.23}$$

3.4.2 Potential and Current Distribution in the Current Collection Foils

The designed current collection system was evaluated using a numerical simulation package. Equations 3.24-3.26 were solved for a steady state, isothermal, and 1-D simulation. Here, the conductivity, σ_j, is the effective conductivity of ½ of the foil (the other half carries the current from the opposite side). The bulk conductivity value, σ_j^0, is multiplied by the thickness of the conductor, $L_j/2$, to lower the dimension of transport.

$$I_n = \frac{U_{ocv} - \left(\Phi_{1,pos}(x) - \Phi_{1,neg}(x)\right)}{ASI_{echem}} \tag{3.24}$$

$$\nabla \cdot \left(\sigma_{pos} \nabla \Phi_{1,pos}\right) = -I_n \tag{3.25}$$

$$\nabla \cdot \left(\sigma_{neg} \nabla \Phi_{1,neg}\right) = I_n \tag{3.26}$$

The boundary conditions were set for both ends of each foil. The tab ends of the foils were set to a specified voltage and the opposite ends of the foils were restricted to a no flux condition. The simulation was performed using the foils defined in our battery design: 12 micron thick copper foil and 20 micron thick aluminum. The cell length was 20 cm, the ASI_{echem} was 30 ohm cm^2, and the U_{ocv} and V_{cell} were set to 3.72 and 3.57 V respectively. Figure 3.5 shows the current and potential distribution in the foils and in the cell resulting from the simulation. The cell potential along the length of the foil varies only by 1.5 mV from maximum to minimum difference. The 0.4 % variation in voltage results in a 0.9 % variation in current density. This verifies the current density is uniform along the length of the foil. This is also obvious from the linear relationship of current with foil height in Fig. 3.5. The assumption of constant current density was tested in cell heights up to 100 cm and found to be satisfactory. The assumption should be reasonable as long as the ASI_{echem} is at least twice the value of ASI_{cc}. The simulated resistance of the foils is found to raise the ASI_{echem} by 0.7 for an ASI_{power} of 30.7 ohm cm^2. Additionally, the numerical result verified that H/3 is the correct equivalent length to represent the ASI_{cc} for the cell. This may also be found analytically, Eq. 3.27-3.29, if you assume an even current distribution as we have shown is a reasonable assumption.

$$\Phi_{1,pos} = V_{cell} + \frac{I_n}{2\sigma_{pos}}\left(H^2 - x^2\right) \tag{3.27}$$

$$\Phi_{1,neg} = \frac{I_n}{\sigma_{neg}}\left(\frac{x^2}{2} - xL\right) \tag{3.28}$$

$$ASI_{echem} + ASI_{cc} = \frac{1}{H}\int_0^H \frac{\Phi_{1,pos} - \Phi_{1,neg}}{I_n} dx = \frac{V_{cell}}{I} + \frac{H^2}{3}\left(\frac{1}{\sigma_{pos}} + \frac{1}{\sigma_{neg}}\right) \tag{3.29}$$

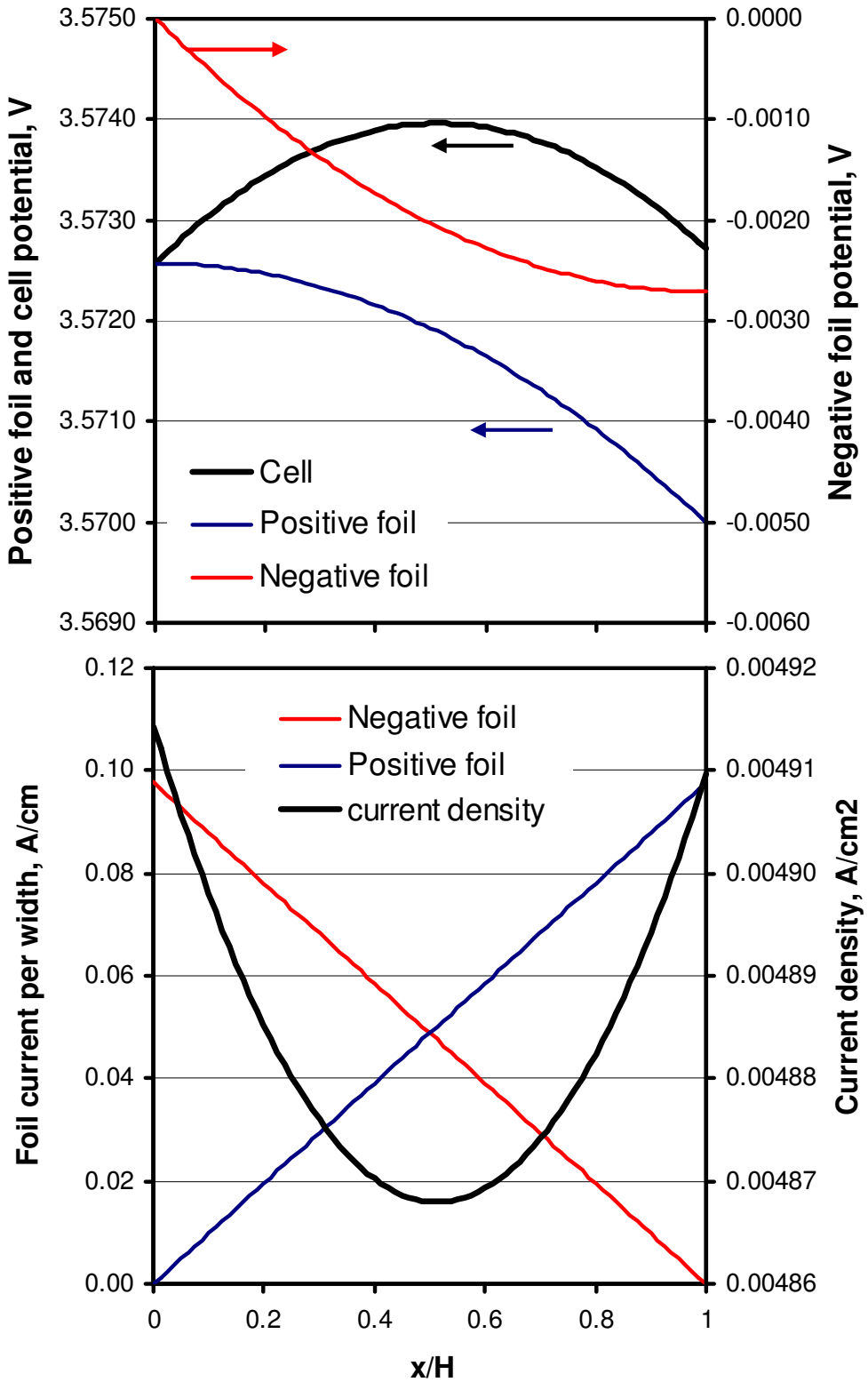

Figure 3.5 The change in current and potential within the positive and negative foils. The current collection design results in a uniform current distribution along the length of the foil.

An analogous problem has been solved by Euler and Nonnemacher and then communicated repeatedly by Newman *et al*.[21, 22] The analytical solution they presented may be used after a slight alteration to dimensionalize the current density to the geometry of our concern, Eq. 3.30 and 3.31. This solution was reached assuming linear polarization behavior and is valid for cases where the current density varies along the height of the current collector foil. Thus, this approach is a more general solution than the one we use in the design model.

$$\mathrm{ASI}_{echem} + \mathrm{ASI}_{cc} = \frac{U_{ocv} - \left(\Phi_{1,pos} - \Phi_{1,neg}\right)}{I} = \frac{H^2}{\sigma_{neg} + \sigma_{pos}} \left[1 + \frac{2 + \left(\frac{\sigma_{neg}}{\sigma_{pos}} + \frac{\sigma_{pos}}{\sigma_{neg}} \right) \cosh v}{v \sinh v} \right] \quad (3.30)$$

$$v^2 = \frac{H^2}{ASI_{echem}} \left(\frac{1}{\sigma_{pos}} + \frac{1}{\sigma_{neg}} \right) \quad (3.31)$$

3.4.3 Determination of Module Terminal, Battery Terminal, and Module Inter-connect Size

An important factor for setting the resistances of a module terminal, battery terminal, or module interconnect is the allowable rate of temperature rise in the conductor at full power. We set the acceptable rate of temperature rise, dT/dt, at 0.2 °C/sec or a 2 °C rise for a 10-sec power burst under adiabatic conditions. The heating rate, q, is then used to determine the mass, m, of the terminal required for the designed battery in Eq. 3.32. Since the heating rate may also be determined by Eq. 3.33, we may determine the cylindrical terminal radius and mass by assuming a length, H_{term}. In this way, the size of the module terminal is redesigned during each simulation to meet the specified power requirements and allowable temperature rise, Eq. 3.34. The mass of the conductor is found to be inversely proportional to the allowable temperature rise.

$$q = mC_p \frac{dT}{dt} \quad (3.32)$$

$$q = \frac{H_{term}}{A_{term}\sigma_{term}} \left(IA_{pos}\right)^2 \quad (3.33)$$

$$A_{term} = IA_{pos} \left[\rho_{term}\sigma_{term} C_p \frac{dT}{dt} \right]^{-1/2} \quad (3.34)$$

3.5 Calculation of Battery Dimensions

The goal of the model is to quantify how the various components of a specific battery design sum to make the mass and volume of the battery pack. In this way, a true energy and power density can be calculated as well as the exact materials requirement to meet this design.

Summing the mass of the components is relatively straight forward. Determining the total volume that contains the components and required free volume is not as obvious. The exact calculations used in the design model are detailed below for the cell, module, and battery pack.

3.5.1 Cell Dimensions

The number of layers in each cell is approximated in Eq. 3.35 by accounting for the compression factor, X_{comp}, and the individual thicknesses of the current collector foils, L_{foil}, electrodes, L_{pos} and L_{neg}, separator, L_{sep}, and container, L_{cont}. X_{comp} is usually taken to be 0.97. The Li-ion battery chemistries this model was designed for are assumed to undergo negligible volume change on the cell level. No effort was made to address possible changes in electrode volume upon cell discharge or charge.

$$N_{layers} = X_{comp} \frac{L_{cell} - 2L_{cont} + L_{foil}^{neg}}{L_{foil}^{neg} + L_{foil}^{pos} + 2(L_{sep} + L_{neg} + L_{pos})} \tag{3.35}$$

The N_{layers} approximation is necessary as the cell thickness is a user defined parameter. The aspect ratio of the cell is also user defined; therefore, solving for the width also determines the height of the cell as seen in Eq. 3.36. The width is calculated from the number of layers and the aspect ratio, H/W. The factor of 2 enters the denominator as both sides of the foil are assumed to be coated.

$$W_{pos} = \sqrt{\frac{A_{pos}}{2\frac{H}{W}N_{layers}}} \tag{3.36}$$

Having determined the width and height of the electrode, the rest of the cell dimensions are relatively straightforward, Eq. 3.37 and 3.38. The width of the cell, W_{cell}, is 8 mm wider than the positive electrode to allow for the larger separator area and pouch seals. The pouch seals are folded up, pressing along the inside wall of the module casing. The height of the cell, H_{cell}, is the height of the positive electrode in addition to the distance for the terminals and connections to the foil tab, $L_{term,cnt}$. Our assumed design requires 15 mm for this distance. The volume of the cell is the product of the three dimensions.

$$W_{cell} = W_{pos} + 8 \tag{3.37}$$

$$H_{cell} = H_{pos} + 2L_{term,cnt} \tag{3.38}$$

3.5.2 Module Dimensions

The module dimensions are defined by Eq. 3.39-3.41. The height and length of the module are both just 2 mm wider than the cell dimension. The width of the module is related to the total thickness from all of the cells with allowance for a SOC controller at one end.

$$H_{\text{mod}} = W_{cell} + 2 \tag{3.39}$$

$$L_{\text{mod}} = H_{cell} + 2 \tag{3.40}$$

$$W_{\text{mod}} = L_{cell}\left(N_{cell/\text{mod}} + 1\right) + 1 \tag{3.41}$$

3.5.3 Battery Pack Dimensions

The battery pack volume includes all of the modules, spacing for connections between modules, channel for the cooling air to flow, H_{air}, thickness of the module compression plates, L_{comp}, and the battery pack jacket, L_{jack} (Eq. 3.42-3.44). L_{jack} includes a 10 mm thick insulation layer sandwiched between two aluminum walls for the container. The thickness of the aluminum wall increases from 1 to 1.5 to 2 mm as the battery volume increases from < 20 L to < 40 L to larger dimensions. The layout of the modules, number per row, $N_{mod/row}$, and number of rows, N_{row}, is also included. The final volume of the battery is the product of the three dimensions. The space left for connections between modules, L_{gap}, is a function of the number of rows of modules. L_{gap} is equal to 8, 10, or 20 depending if there is one, two, or four rows of modules. Three rows of modules are not allowed as the positive and negative terminal for the battery would be on opposite ends and thus not very practical. A number greater than four rows of modules is deemed unnecessary.

$$H_{batt} = H_{\text{mod}} + 2H_{air} + 2L_{jack} \tag{3.42}$$

$$L_{batt} = N_{\text{mod}/row} W_{\text{mod}} + H_{air} + 2L_{comp} + 2L_{jack} \tag{3.43}$$

$$W_{batt} = N_{row} L_{\text{mod}} + L_{gap} + 2L_{jack} \tag{3.44}$$

3.6 Additional Considerations

A few situations may arise that require a change in the calculation method. These situations are addressed in the subsections below. The inclusions of these calculations into the model allow for a more realistic depiction of limitations often encountered by cell manufactures.

3.6.1 Maximum Electrode Thickness

A practical limitation exists for the maximum achievable electrode thickness. This limitation may be set by manufacturing capabilities, ionic and electronic current transport within the porous electrode, or aging characteristics related to adhesion to the current collector. When the maximum electrode thickness, L_{max}, has been reached on either the positive or negative electrode, the electrode area equation is modified as shown in Eq 3.45. The electrode thickness, L_{tgt}, is the largest electrode thickness, negative or positive, calculated at the targeted fraction of the OCV [V/U].

$$A_{pos}^{L\max} = \frac{L_{tgt}}{L_{\max}} A_{pos} \tag{3.45}$$

The area of the electrode is now determined by the cell capacity requirement to meet the battery energy demands and not the target voltage at maximum power. As a consequence, the battery pack will operate at a higher [V/U] than originally selected by the battery designer. The new [V/U] may then be calculated from Eq. 3.46 which is the solution to the quadratic found in Eq. 3.47.

$$\left[\frac{V}{U}\right] = \frac{1}{2U_{cell}}\left[U_{cell} + \sqrt{(U_{cell})^2 - 4\frac{P_{batt}ASI_{power}}{N_{cells}A_{pos}}}\right] \tag{3.46}$$

$$V_{cell} = U_{cell} - \frac{P_{batt}ASI_{power}}{V_{cell}N_{cells}A_{pos}} \tag{3.47}$$

The maximum electrode thickness has a large impact on the energy density and cost of cells designed for high energy and range. Nelson et al. demonstrated this concept in 2009 assuming a 100 micron maximum electrode thickness.[11,17] In 2010, Santini et al. relaxed this assumption to 300 micons; although, the thickest electrode discussed in the paper was a 225 micron graphite electrode in the LMO-Gr EV with 100 mile range.[12] In conversations with manufactures, 100 microns appears to be the general electrode thickness used for EV type cells at the present time. However, Santini et al. has shown substantial increases in energy density and decreases in cost if larger electrode thicknesses may be utilized. The challenges to achieving thick electrodes, in addition to those already mentioned, relate to fast charging while avoiding lithium metal deposition, removing gases formed during formation cycling, wetting the full porosity of the electrode, achieving defect free coatings, and drying the thick electrode at high rates. Our opinion is that the successful cell manufacturers will engineer ways to overcome these challenges to increase energy density and lower cost.

3.6.2 Accounting for Parallel Cell Arrangements

The user of the design model may wish to use a parallel arrangement of cells within the larger series arrangement of the battery pack. Several motivations exist for a parallel cell arrangement. For example, a battery supplier may wish to only produce cells of a specific capacity. The manufacturer may only have the equipment to produce a certain size cell or they may encounter engineering design problems for very large cells (> 60 Ah). Thus, a cell group composed of parallel connected cells may be necessary to meet the energy requirements while staying within battery pack voltage and current requirements.

When the user chooses to have cells connected in parallel, the design model calculation includes the appropriate factors necessary to account for changes in the resistance, volume, and mass of the battery. The end result is a lower energy density for the battery from including the cell group interconnects and additional inactive material for each cell. Furthermore, the thickness of the cells is reduced to 6 mm to better suit the smaller cell format.

4. Modeling of Battery Pack Manufacturing Cost

4.1 Approach

The manufactured cost of a battery pack is calculated with input from the design information generated in modeling the cell and battery pack performance. The design modeling determines the annual materials and purchased items requirements. The manufacturing cost is then added to these materials costs, along with a warranty cost, to reach the unit cost of a single battery pack. The manufacturing costs for the designed battery are scaled from a baseline plant. The baseline plant was designed for a battery of intermediate size and production scale so as to establish a center-point for other designs. The baseline plant accounts for the size, speed, number of units, direct labor, and depreciation of the capital cost for each processing step. These costs are adjusted to meet the requirements for a plant producing the battery under study. The process expenses are summed with the additional costs of operating the manufacturing facility. These costs include launch costs, working capital, variable overhead, general, sales, administration (GSA), research and development, depreciation, and profit.

In this analysis, all costs are evaluated for 2020 when large battery manufacturing plants are built. All dollar values are brought back to 2010 with allowance for inflation. Some materials and battery manufacturing costs are lower than recent values, where we judged that processing improvements for high volume production of materials would reduce costs.

The baseline manufacturing plant was calculated for an annual production rate of 100,000 batteries. The cost model accounts for different scales of manufacture by recalculating the costs of each individual step in the manufacturing process. The changes in capital and operating costs will change the calculated unit cost of the battery pack. However, the parameters were determined to provide reasonable estimates for manufacturing rates of 20-500 % of the baseline rate. Thus, for a plant that is far different in size from the baseline plant, for instance a pilot plant having an annual production of only 5,000 battery packs per year, the estimate from this study would be expected to be less accurate than if determined in a study dedicated to that purpose.

To simplify the cost calculations, it was assumed that all hardware items for the cells, modules and battery will be purchased from a vendor specializing in similar products. The costs for these items were estimated to be a fixed value plus an additional value proportional to the weight of the item, which is calculated during the battery design. In mature manufacturing plants in 2020, toward which this study is directed, some items which are assumed to be purchased in this study might actually be internally manufactured from raw materials. This would increase the number of processing steps needed in our manufacturing simulation and thus complicate the cost calculations. Assuming that some parts would be purchased if they would actually be produced from raw materials would tend to underestimate capital and labor costs and overestimate purchased items expenses. However, the net effect would be a very small change to the overall unit cost of the battery pack.

4.2 Materials Costs and Purchased Items

The end battery pack cost depends significantly on the cost of both the active and inactive materials that compose the design. In this subsection, the assumed material costs and the rational behind them are presented. While we state suggested materials costs, the user of the cost model may enter any value that they desire.

4.2.1 Battery Specific Materials Cost

The largest contributions to the materials cost of the battery are from the following components: positive and negative electrode active material, separator, electrolyte, and current collector foils. The choice of the materials often defines the size and performance of the battery as well as the cost. Many different variations of materials are possible in the Li-ion family of chemistries. However, we have chosen to focus on the different available positive electrode materials with less attention on the negative electrode. This reflects the current research and manufacturing activities. The separator and the electrolyte are also both active areas of development. However, the following battery designs are based on a single electrolyte and separator combination. Including the cost and effect of additives and enhanced separators is beyond the scope of this work. The user is always able to modify the dimensions, cost, and ASI that may be required to account for changes in these materials.

The price of specific battery materials is of some debate. The values presented in Table 4.1 compare our suggested costs to those reported recently in the open literature. Our values, as well as the others in the table, are derived from conversations with material, cell, and original equipment manufacturers. The sources are commonly anonymous and the accuracy of the values is generally unknown. We present the comparison of published values so that the user of the cost model may appreciate the accepted range of values for commonly used materials.

4.2.1.2 Positive Electrode Active Materials

The cost of positive electrode materials is driven to a large extent by the cost of the raw materials from which it is made. The archetype Li-ion positive electrode material, lithium cobalt oxide (LCO), was the original material commercialized in Li-ion batteries for consumer electronics. LCO has many excellent characteristics but is not considered a viable choice for use in Li-ion batteries for automotive applications. One of the largest drawbacks of LCO, other than safety concerns, is the cost of the cobalt. While tolerable in the consumer electronics market, the cost is too high for use in an automobile battery. Many other materials are in a commercially viable state of development and are currently utilized in Li-ion batteries produced today (Table 4.1).[3,6] The relative advantages and disadvantages of each material will not be discussed here.

The amount of cobalt and nickel, as well as ease of manufacture, controls the end price for a positive electrode material. For example, the NMC-441 is less expensive than the NMC-333 as the cobalt quantity is significantly reduced. The market price for cobalt and nickel metal varies dramatically from year to year. Reducing the quantities of these materials will reduce the

Table 4.1 Details of stated costs for cathodes, anodes, electrolyte, and separator.[3,6]

Material	Chemistry	Abbreviation	unit	ANL 2010	TIAX 2010	CARB 2007
Manganese spinel cathode	$Li_{1.06}Mn_{1.94}O_4$	LMO	$/kg	10	12 - 16 - 20	8 - 10
Phospholivine cathode	$LiFePO_4$	LFP	$/kg	20	15 - 20 -25	16 - 20
Layered oxide cathode	$LiNi_{0.80}Co_{0.15}Al_{0.05}O_2$	NCA	$/kg	36	34 - 40 - 54	28 - 30
Layered oxide cathode	$Li_{1.05}(Ni_{1/3}Mn_{1/3}Co_{1/3})_{0.95}O_2$	NMC-333	$/kg	40	40 - 45 -53	22 - 25
Layered oxide cathode	$Li_{1.05}(Ni_{4/9}Mn_{4/9}Co_{1/9})_{0.95}O_2$	NMC-441	$/kg	33	-	-
Li & Mn rich layered cathode	$xLi_2MnO_3 \cdot (1-x)LiNi_yMn_zCo_{1-y-z}O_2$	LMR-NMC	$/kg	25	24 - 31 - 39	-
Layered oxide cathode	$LiCoO_2$	LCO	$/kg	-	-	30 - 40
Graphite anode	C_6	Gr	$/kg	19	17 - 20 - 23	-
Titanate spinel anode	$Li_4Ti_5O_{12}$	LTO	$/kg	12	9 - 10 - 12	-
Electrolyte	1.2 M $LiPF_6$ in EC:EMC		$/kg	19	18.5 - 21.5 -24.5	-
Separator	PP/PE/PP		$/m^2	2	1 - 2.5 -2.9	-
Current collector foil	Copper		$/m^2	3.00	-	-
Current collector foil	Aluminum		$/m^2	0.80	-	-

positive electrode material price and price volatility. Researchers at TIAX LLC have treated this variation and shown the significant effect on end battery cost.[10] The average metal prices for the last 20 years is 48 $/kg and 15 $/kg for cobalt and nickel respectively. These numbers are based on historical prices for the metals as collected by the United States Geological Survey (USGS).[23] The metal prices are best used as indicators for how the intercalation material cost will relate when compared to one another. The fact these materials are not earth abundant means they will not benefit as much as other materials from increased scales of production.

In general, earth abundant elements should be the dominate transition metal used if a low positive electrode cost is desired. Both iron and manganese are abundant and inexpensive transition metals for intercalation materials. Comparison of the iron phosphate, LFP, to manganese spinel, LMO, reveals how processing costs contribute to the end price of a material. LMO is relatively easy to manufacture. In contrast, LFP requires a reducing atmosphere and a carbon coating step to reach the end product. The increased complexity in the manufacturing process is realized in the price. However, one could argue that the manufacturing cost will decrease with increased knowledge from larger scales of production.

4.2.1.2 Negative Electrode Active Materials

While multiple negative electrode materials exist for Li-ion batteries, carbon materials in the form of graphite and/or hard carbon are still used in the vast majority of commercial cells. Graphite offers the greatest energy density while hard carbon is said to enable high rate capability with decreased risk of lithium plating (an undesired side reaction) during high charge rates. We have chosen synthetic graphite as a generic carbon electrode in our model. The price of graphite is much better understood than that of most of the positive electrode materials. However, significant differences in cost and performance will exist between synthetic, natural, and coated-natural graphite. The method of production and necessary heat-treatment will control the end cost. Graphite, although in different purity grades or microstructure forms, is used in many industries. This is in stark contrast to the positive electrode materials.

The lithium titanate electrode, LTO, offers an interesting option compared to graphite. Unlike graphite, LTO operates within the stability window of the electrolyte. The higher electrode potential dramatically reduces or eliminates the formation of the solid electrolyte interphase (SEI). As a result, nanoparticle-based LTO may be implemented without concerns of increased side reactions with the electrolyte. The reduced dimensions increase the available surface area for reaction while simultaneously shortening the diffusion length. Both of these factors combined with the lack of SEI dramatically reduce the impedance of the electrode.

4.2.1.3 Electrolyte and Separator

The electrolyte used in this model is based on a lithium hexafluorophosphate salt, $LiPF_6$, dissolved in a carbonate based solvent system. The carbonate solvent system is a blend of ethylene carbonate, EC, and a linear carbonate such as ethyl methyl carbonate, EMC, or dimethyl carbonate, DMC. Other chemical additives may be used to lower the capacity and power fade of the battery over time. Polymers may be added to the electrolyte as either a minor or major

component. This is not discussed in any further detail in this work. The price of $16/L, about $19/kg, is only for the base electrolyte (i.e. no additional additives).

The separator is typically a porous membrane based on polypropylene (PP) and sometimes includes a polyethylene (PE) middle layer. PP and PE are very inexpensive raw materials and thus the suggested cost of $2/m^2 is in large part due to the manufacturing process required to form the porous network in the membrane. As competition and scale of manufacture increase, the prices of the separator may fall closer to $1/m^2. However, the cost of improved technology may offset some of this cost reduction, so we have retained our cost estimate of $2/m^2.

As safety is a major concern for Li-ion batteries, the separator plays a key role in isolating the oxidant from the fuel. If the two charged electrodes contact each other (short), then a run-away reaction is possible. Separators have been designed to "shut-down" or melt at key temperatures. The middle PE layer is the shut-down feature in our proposed separator. Ceramic coatings have also been used to ensure structural integrity. Many other approaches are being developed to increase the safety of Li-ion batteries. The user of the cost model should account for the increased technology in the price and dimensions of the separator as needed.

4.2.1.3 Current Collector Foils

The current collector foils are based on copper metal for the negative electrode and aluminum for the positive electrode. However, the LTO anode material, because of its high voltage relative to lithium, enables the use of aluminum as the negative electrode current collector. The price of these foils is based on raw materials and manufacturing costs. The foils are 12 microns and 20 microns thick for the copper and aluminum current collectors respectively. The foils used in batteries have additional requirements beyond the cheapest product available. Surface treatments are often necessary to promote adhesion of the electrode to the foil surface. In addition, alloying of the foil may be necessary to achieve the required material properties for long life.

The raw material contributions to the foil price will vary with the volatility of the market price for the metals. Figure 4.1 displays the metal ingot price contribution on a $/m^2 basis. These numbers are based on historical prices for the metals as collected by the USGS.[23]

The values for both aluminum and copper tend to vary significantly over the time period examined. The price for copper is more volatile and always more expensive than aluminum. Analysis of Figure 4.1 reminds the user of the cost model that cost quotes are only valid for a short period. As the market price for raw materials changes, so will the price for the finished product.

Conversations with manufacturers and suppliers lead us to take a price of 3.00 and 0.80 $/m^2 for battery grade copper and aluminum foil respectively. We point out that the current metal ingot price is only a small contribution to the end foil price being about 15 % of the aluminum foil price and 25 % of the copper foil price. Thus, a doubling of the ingot prices would only moderately increase the foil prices. The aluminum foil is produced by rolling of thicker stock foils into thinner and thinner sheets. On the other hand, copper foil is more likely to be produced through an electrodeposition process.

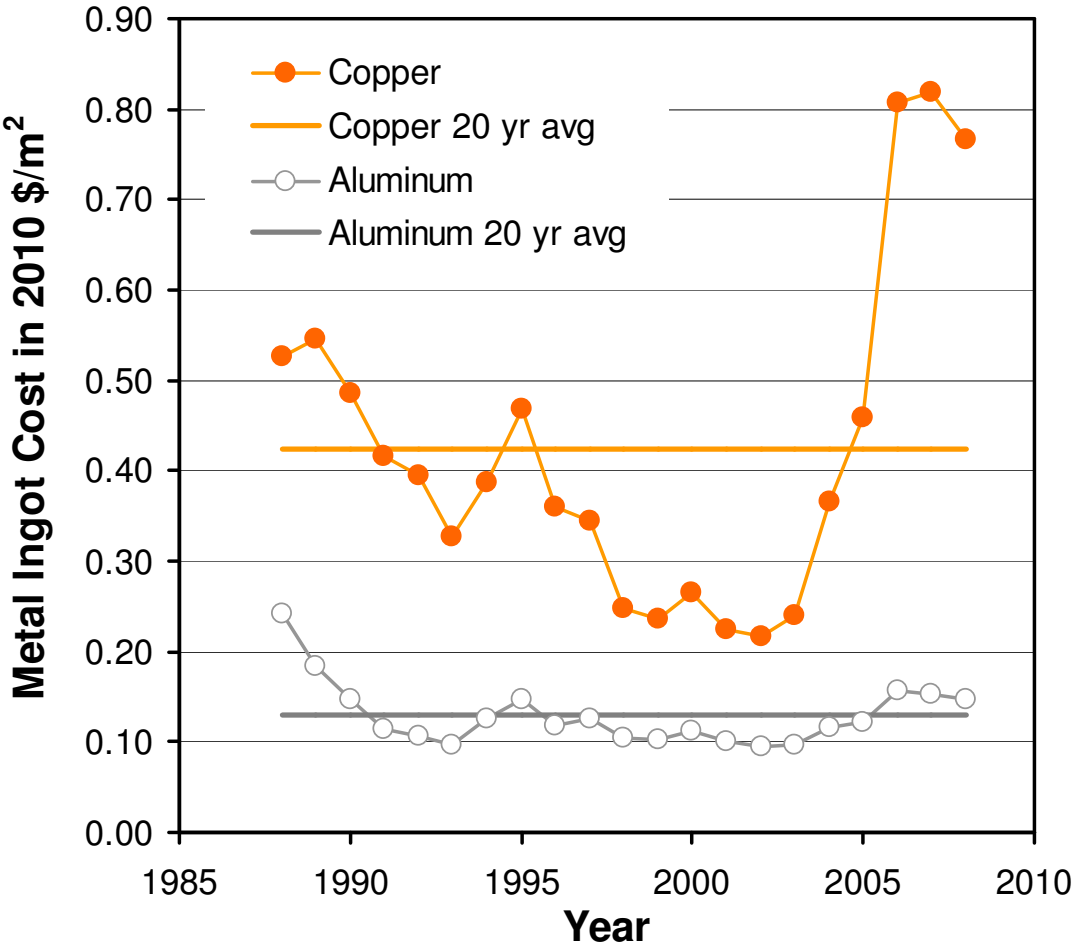

Figure 4.1 Metal ingot cost contribution to the current collector foils over a 20 year period. The average for that period is also shown. All costs are in 2010 US$.

4.2.1.4 Additional Electrode Components

The binder and conductive additive in the positive and negative electrodes add a small but real cost to the battery. The conductive additive, more common for the positive electrode, was priced at 6.80 $/kg for a high purity and moderate surface area carbon black material. The binder, perhaps PVDF or CMC based, is assumed to be 10 $/kg. The *N*-Methyl-2-pyrrolidone (NMP) solvent for the PVDF binder is estimated to be 3.20 $/kg. Most of the NMP is recovered after evaporation and recycled as discussed in section 4.3.3. Only the small amount lost in processing need be replaced. No cost is assumed for water.

4.2.2 Purchased Items Cost

Table 4.2 lists the purchased items for the cell module and battery jacket. The cost of a SOC controller for each cell, or group of parallel cells, is $1.80 plus a small factor for the cell capacity (Ah), which allows for higher cell balancing currents for larger cells. The other components cost

a fixed amount plus an additional factor, which is proportional to their mass, m_i. The cell negative terminal and parallel cell group connection are both made from nickel plated copper sheet and thus have the same cost equation.

Table 4.2 Cost equations for purchased items

Component, *i*	**Cost Equation, $/unit**	**Cost per unit**
SOC controller	$1.80 + 0.005C$	cell or parallel cell group
Cell positive terminal	$0.10 + 4m_i$	cell
Cell negative terminal	$0.10 + 5m_i$	cell
Cell container	$0.10 + 5m_i$	cell
Parallel cell group connection	$0.10 + 5m_i$	parallel cell group
Module terminals	$0.75 + 4m_i$	module
Balance of module (casing)	$1.00 + 3m_i$	module
Battery enclosure & cooling	$50.00 + 7m_i$	battery pack

4.3 Baseline Manufacturing Plant

The baseline plant is designed to produce 100,000 NCA-Gr baseline battery packs per year. The baseline battery pack produced by the plant has sixty, 40-Ah capacity cells, providing a total pack power of 50 kW and total energy of 8.7 kWh. The battery will power 24.4 miles of vehicle travel at 70% of the pack energy and 250 Wh/mile. The schematic diagram of the plant (Fig. 4.2) is designed to illustrate the flow of materials through the plant and the relative floor areas for the processing steps rather than representing a realistic plant layout. The overall manufacturing rate of 100,000 battery packs per year is achieved by operating for three shifts at the equivalent of 300 days per year of fully effective production. There will be more than 300 days of operation, but some days will have less than 100% effectiveness. The exceptions to three-shift operation are the Receiving and Shipping sections, which are active for only two shifts per day. The cost factors for the individual manufacturing steps in the baseline plant are summarized in Table 4.3 and discussed in detail in the sections that follow. Most of the operations are carried out with normal factory atmosphere, but the cell assembly process steps are completed in a dry room atmosphere.

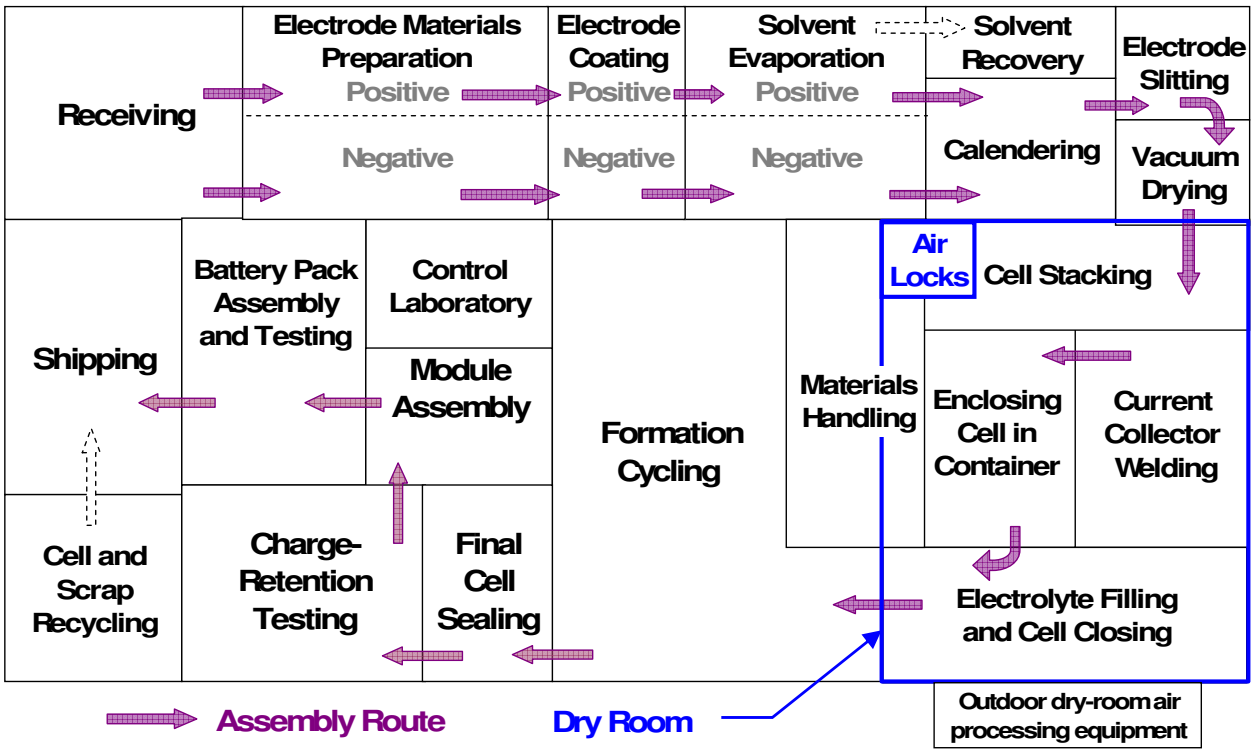

The areas in this diagram for each processing step are approximately proportional to the estimated plant areas in the baseline plant.

Figure 4.2 Baseline lithium-ion battery manufacturing plant schematic diagram. Manufacturing rate: 100,000 NCA-Gr battery packs per year, 50-kW pack power, 40-Ah capacity, 60 cells per battery. Operating year: 300 days with three 8-h shifts (two shifts for receiving and shipping)

4.3.1 Receiving and Shipping

These operations require the moving equipment and storage facilities common to any such factory facilities. The Receiving section handles slightly less than 6,000,000 kg of materials per year and also has facilities to handle and store some of the electrode materials in a dry atmosphere. The Shipping section is required to enclose the battery packs in crates, which requires some automated equipment and more labor than is required for Receiving. Shipping also handles about 400,000 kg of scrap each year, which is broken down and prepared for shipping in the Rejected Cell and Scrap Recycle section. The estimated resources needed for the Receiving and Shipping sections are shown in the table below.

	Rate Factor	Direct Labor	Capital Equip.*	Plant Area, m^2
Receiving	870,000 kWh/y	3 per shift	3.60 mil$ total	600
Off-loading			0.60	
Moving			1.20	
Storage			1.80	
Shipping	870,000 kWh/y	6 per shift	5.0 mil$ total	600

*Total cost including installation

Table 4.3 Summary table of the baseline plant

	Annual Baseline Rate (R_o)		Direct Labor			Cap. Equipment		Plant Area	
			No./shift	Hours/yr	p Factor	$MM	p Factor	m^2	p Factor
Receiving (two-shift operation)	869,420	kWh energy	3	14,400	0.4	3.60	0.6	600	0.5
Materials preparation									
Positive electrode	1,712,524	kg active material	3	21,600	0.5	4.00	0.7	400	0.6
Negative electrode	1,208,957	kg active material	3	21,600	0.5	4.00	0.7	400	0.6
Electrode coating									
Positive electrode	8,169,835	m^2 cell area	4	28,800	0.5	6.00	0.8 (0.2)*	500	0.8
Negative electrode	8,169,835	m^2 cell area	4	28,800	0.5	6.00	0.8 (0.2)*	500	0.8
Solvent recovery	2,309,021	kg NMP	2	14,400	0.4	3.00	0.6	150	0.6
Calendering									
Positive electrode	8,169,835	m^2 cell area	1	7,200	0.5	1.00	0.7	150	0.6
Negative electrode	8,169,835	m^2 cell area	1	7,200	0.5	1.00	0.7	150	0.6
Materials handling[#]	8,169,835	m^2 cell area	4	28,800	0.7	1.50	0.7	600	0.6
Electrode slitting	8,169,835	m^2 cell area	4	28,800	0.5	2.00	0.7	200	0.6
Vacuum drying	8,169,835	m^2 cell area	2	14,400	0.5	1.60	0.7	200	0.6
Control laboratory	869,420	kWh energy	4	28,800	0.5	1.50	0.7	200	0.6
Cell Assembly in Dry Room									
Cell stacking	6,315,789	total cells	6	43,200	0.7	5.00	0.8 (0.3)**	400	0.8
Current collector welding	6,315,789	total cells	6	43,200	0.7	5.00	0.8	400	0.8
Enclosing cell in container	6,315,789	total cells	4	28,800	0.5	3.00	0.7	400	0.6
Electrolyte filling, and cell sealing	6,315,789	total cells	6	43,200	0.5	6.00	0.7	600	0.6
Dry room control and air locks	2,000	m^2 operating area[#]	2	14,400	0.4	20.00	0.6	75	0.4
Formation cycling	6,315,789	total cells	8	57,600	0.7	30.00	0.8 (0.3)**	1,500	0.8
Final cell sealing	6,315,789	total cells	2	14,400	0.5	7.50	0.7	300	0.6
Charge retention testing	6,315,789	total cells	3	21,600	0.4	4.75	0.7	600	0.6
Module assembly	6,000,000	finished cells	6	43,200	0.5	6.00	0.7	400	0.6
Battery pack assembly and testing	100,000	battery packs	6	43,200	0.5	6.00	0.7 (0.3)***	600	0.6
Rejected cell and scrap recycle	6,315,789	total cells	5	36,000	0.7	2.50	0.7	400	0.6
Shipping (two-shift operation)	869,420	kWh energy	6	28,800	0.5	5.00	0.7	600	0.6
Total			95	662,400		135.95		10,325	

[#]One-third of the space for materials handling is within the dry room.

The baseline capital cost electrode coating, C_o, is based on the evaporation of the baseline annual solvent weight (Rs_o). For batteries requiring different solvent evaporation rates Rs, the cost is multiplied by ratio of rates raised to the 0.2 power. Thus, Cost = Co(R/Ro)^0.8*(Rs/Rso)^0.2.

**The baseline costs of the capital equipment for cell stacking and formation cycling is for 40-Ah cells. To correct the baseline cost (C_o) for cells of different capacity, the cost is multiplied by the capacity ratio, (Cap)/ 40 Ah, raised to the 0.3 power. Thus, Cost = C_o*(R/R_o)^0.8*(Cap/40)^0.3.

***The baseline cost of the capital equipment for battery assembly is for a battery with four modules. To correct the baseline cost for a different number of modules (Mod), the cost is multiplied by the ratio of modules, (Mod)/4 raised to the 0.3 power. Cost = C_o*(R/R_o)^0.7*(Mod/4)^0.3.

4.3.2 Electrode Materials Preparation and Delivery to Coating

The electrode materials, which consist of active material, carbon (if necessary), binder and binder solvent, are well mixed in small batches in portable tanks. At the design production rate in the baseline plant, each shift requires three tanks each holding about 1000 liters of positive electrode material mix and three tanks each holding about 900 liters of negative electrode material mix. The section must be capable of exceeding this design rate of production by at least 25% to catch up in case of unscheduled downtime in Materials Preparation or in some of the section immediately following that section. The tanks of prepared materials are moved to the Coating section and pressurized to push the coating paste into the coating mechanism. The estimated resources needed are the following:

Materials Prep.	Rate Factor	Direct Labor	Capital Equip.*	Plant Area, m^2
Positive Materials	1,710,000 kg/y active material	3 per shift	4.0 mil$ total	400
Storage tanks			2.00 mil$	
Mixing tanks			1.00	
Moving equip.			1.00	
Negative Materials	1,210,000 kg/y active material	3 per shift	4.0 mil$ total	400

*Total cost including installation

4.3.3 Electrode Coating on Current-Collector Foil

The positive and negative electrode structures are formed by coating both sides of the current collector foil. In the baseline plant, the coating lines are 1.5 meter wide continuous roll-to-roll coating processes carried out at a line speed of 10 m/min. The first set of coating and drying stations coats one side of the current collector foil, drives off the solvent in a heated oven, and turns the foil over while transferring it to a second set of stations. The second set of coating and drying stations applies and dries the remaining coating before the coated foil is wound into a large roll at the end of the line. The negative and positive coating lines are very similar. However, some of the negative material is coated only on one side to provide the electrodes at the end of the cell stacks. For the baseline plant, a total of 8,170,000 m^2/y of coating (annual cell area) is required for the positive electrode (slightly more for the negative electrode), which allows for the 5% loss of cells expected to fail testing and inspection. A larger area of foil than the coated area must be fed to the coaters to allow for the part of the foil that is not coated so as to provide tabs for welding to the terminals (about 10%) and to allow for trimming losses during electrode slitting (8%). Also, about 30% excess coating capacity must be provided to allow for unscheduled downtime. Only one coating line is needed for each electrode type to meet these needs. If one coating line breaks down, the other coating line may change over temporarily to coat the other electrode material.

The oven sections of the coating line are designed to dry coatings about 100 microns thick at the coating speed of 10 m/min. A thicker coating will require longer ovens at additional capital cost which is provided in the adjustment of costs discussed in section 4.4. For the same annual area throughput, a coating line that coats both sides with a 300-micron coating would cost $7,500,000

rather than the $6,000,000 cost for the 100-micron coater. The binder solvent for the positive electrode in the baseline plant is NMP, which must be recovered by condensation and recycled. About 0.5% of the binder solvent is combusted with a thermal oxidizer and must be replaced. For the negative electrode the binder is water, which need not be recovered. The estimated resources to meet these needs are the following:

Electrode Coating	Rate Factor	Direct Labor	Capital Equip.*	Plant Area, m^2
Positive Electrode	8,170,000 m^2/y cell area	4 per shift	6.0 mil$ total	500
Uncoated area			18%	
Width of coater			1.5 m	
Coating speed			10 m/min	
Number of coaters			One	
Maximum rate			13,000,000 m^2/y	
Excess capacity			30%	
Negative Electrode	8,170,000 m^2/y cell area	4 per shift	6.0 mil$ total	500
Solvent Recovery & Oxidation	1,527,000 kg NMP/y	2 per shift	3.0 mil$ total	150

*Total cost including installation

4.3.4 Calendering

The materials leaving the coating lines may be stored on large rolls (see next section). However, typically the materials leaving the coaters would go directly to the calendering process in which the coatings are compressed by rolling to meet the specified void volume fraction, which will later be filled with electrolyte. The calendering equipment must match the output of the coating equipment producing 8,170,000 m^2/y of cell area with a maximum rate of 13,000,000 m^2 of foil per year to meet contingencies as in coating. The estimated resources to meet these needs are the following:

Calendering	Rate Factor	Direct Labor	Capital Equip.*	Plant Area, m^2
Positive Electrode	8,170,000 m^2/y cell area	1 per shift	1.0 mil$ total	150
Negative Electrode	8,170,000 m^2/y cell area	1 per shift	1.0 mil$ total	150

*Total cost including installation

4.3.5 Inter-Process Materials Handling

For all processes (Fig. 4.2), work in progress must be transported and occasionally stored to permit nearly-continuous operation of the equipment. Storage areas must be provided both inside and outside of the dry room. Raw materials must also be moved to the processing sites, which for those in the dry room means through a separate air lock for materials transfer. One-third of the

total space for Inter-Process Materials Handling is within the dry-room for the baseline plant and also for all other plants. The estimated resources to meet these needs are the following:

Materials Handling	Rate Factor	Direct Labor	Capital Equip.*	Plant Area, m^2
	8,170,000 m^2/y cell area	4 per shift	1.5 mil$ total	600

*Total cost including installation

4.3.6 Electrode Slitting

The coated electrode foils are slit into strips between the coated sections and then into individual electrodes as shown in Fig. 2.2. The estimated scrap loss of foil for this process is about 8%. The estimated resources to meet these needs are the following:

Electrode Slitting	Rate Factor	Direct Labor	Capital Equip.*	Plant Area, m^2
	8,170,000 m^2/y cell area	4 per shift	2.0 mil$ total	200

*Total cost including installation

4.3.7 Final Electrode Drying

In the absence of electrolyte, no harm is done by exposing the electrodes to normal factory air; however, the electrodes must be dried by heating under vacuum prior to cell assembly. Maintaining extremely low moisture conditions during cell assembly is believed to be very important in achieving long battery life. The final drying step coupled with dry room conditions ensures a minimal quantity of moisture will exist in the final product. The pertinent processing rate in determining the resources necessary for drying is the total amount of active materials processed per year (other electrode materials are approximately proportional), which for the baseline plant is 2,950,000 kg/y or 3,275 kg/shift. The individual electrodes exiting from the electrode slitting process are separated into stacks by polarity, loaded into vacuum drying ovens, dried for several hours, and unloaded directly into the dry room. The estimated resources to meet these needs are the following:

Electrode Drying	Rate Factor	Direct Labor	Capital Equip.*	Plant Area, m^2
	2,950,000 kg/y active material	2 per shift	1.6 mil$ total	200
Dryer capacity			600 kg/shift	
Number of dryers			8	
Maximum rate			4,320,000 kg/y	

*Total cost including installation

4.3.8 Control Laboratory

The purpose of the control laboratory is to ensure that the raw materials and the electrodes being fabricated meet specifications. Laboratory personnel collect or supervise collection of samples and carry out analyses. The estimated resources to meet these needs are the following:

	Rate Factor	Direct Labor	Capital Equip.*	Plant Area, m^2
Control Lab	869,000 kWh/y	4 per shift	1.5 mil$ total	200

*Total cost including installation

4.3.9 Cell Stacking

The cells are assembled in four steps, which are carried out in a dry room. The first of these steps is cell stacking. The primary rate factor that determines the cost for all steps in cell assembly is the number of cells assembled per year. For cell stacking an additional cost factor is the capacity of the cells; large cells usually require more electrodes of larger area and thus a more capable, faster cell stacking machine. The method used to determine the extra costs of stacking equipment in detailed in Table 4.3. The capacity of the cells is deemed to have only a minor effect on the other steps in cell assembly and is not taken into account for those steps. The electrodes are inserted in a folded separator sheet, the positive electrodes tabs protrude on one side and the negative electrodes tabs on the other. As in other parts of the plant, excess capacity is provided to allow catching up after unscheduled downtime. The estimated resources to meet these needs for the baseline plant are the following:

Cell Stacking	Rate Factor	Direct Labor	Capital Equip.*	Plant Area, m^2
	6,320,000 cells/y	6 per shift	5.0 mil$ total	400
Stacking rate			4 cells/min	
Number of units			5	
Maximum rate			8,640,000 cells/y	

*Total cost including installation

4.3.10 Current Collector Welding

The current collector tabs for the negative and positive electrodes are welded to their respective terminals by ultrasonic welding. This procedure achieves a connection of near-zero resistance and avoids overheating the electrodes during the welding process. The estimated resources to meet these needs are the following:

Tab Welding	Rate Factor	Direct Labor	Capital Equip.*	Plant Area, m^2
	6,320,000 cells/y	6 per shift	5.0 mil$ total	400
Cell rate			4 cells/min	
Number of units			5	
Maximum rate			8,640,000 cells/y	

*Total cost including installation

4.3.11 Enclosing Cell in Container

The aluminum foil in the pouch container is sufficiently thick (100 microns default thickness) to permit the use of stiff, pre-shaped pouch halves. The pouches are assumed to be purchased as

finished parts. Each cell is enclosed in these containers, which are then partially sealed prior to injecting electrolyte. The estimated resources to meet these needs are the following:

Enclosing cells	Rate Factor	Direct Labor	Capital Equip.*	Plant Area, m^2
	6,320,000 cells/y	4 per shift	3.0 mil$ total	400
Cell rate			4 cells/min	
Number of units			5	
Maximum rate			8,640,000 cells/y	

*Total cost including installation

4.3.12 Electrolyte Filling and Cell Sealing

At this station, the cells are evacuated, filled with electrolyte and temporarily sealed. The estimated resources to meet these needs are the following:

Filling & 1st Seal	Rate Factor	Direct Labor	Capital Equip.*	Plant Area, m^2
	6,320,000 cells/y	6 per shift	6.0 mil$ total	600
Cell rate			4 cells/min	
Number of units			5	
Maximum rate			8,640,000 cells/y	

*Total cost including installation

4.3.13 Dry Room Management

Excellent dry-room atmosphere is required for lithium-ion cell assembly. A maximum dew point temperature of –40 °C is maintained in the room. The load on the dry-room drying apparatus is determined by diffusion of water vapor through the walls, entry of air through the air locks, the number of workers in the room, and the need to admit some fresh air to limit the build up of contaminants such as electrolyte solvent vapor. These load factors are approximately a function of the room area. Because of the importance of the proper functioning of the dry room, two workers are on duty at all times to monitor its performance. The equipment for circulation and purification of the dry air will be located outside of the plant building, adjacent to the dry room. The estimated resources to meet these needs are the following:

	Operating Area	Direct Labor	Capital Equip.*	Air Locks, m^2
Dry Room	2,000 m^2	2 per shift	20.0 mil$ total	75

*Total cost including installation

4.3.14 Formation Cycling, Final Cell Sealing and Charge Retention Testing

Formation cycling is expensive because it takes considerable time and each cell must be monitored separately. For plants to be operated in 2020, we expect some improvements from present day operations because of the urgency to improve and thus save cost. We project that the entire formation cycling and testing can be done in two shifts. These operations consist of

charging the cell, discharging to full depth to measure capacity and impedance, followed by fully recharging the cells. These tests will be carried out in large temperature controlled cycling units that test 500 cells simultaneously, monitor each cell and automatically identify failed cells. The capital cost of the cycling equipment is primarily a function of the annual number of cells to be tested, but to a lesser extent on the capacity of the cells.

The short-term testing described above does not detect cells that have self-discharge rates that are slightly above normal, which could lead to catastrophic failures later. To detect such defects, the cell charge is topped off and the cells are stored for two weeks and then checked for loss of charge. Most of the test period is spent in large racks in compact arrays, without electronic monitoring. Incidentally, the two-week long self-discharge testing requires less floor space than for formation cycling, which lasts only two shifts.

The final cell sealing occurs between the formation cycling and charge-retention storage test. Gas generated during formation cycling may accumulate in the reservoir space that was created during the temporary sealing step. This gas is removed by creating the final seal below the reservoir and trimming off the unwanted portion.

The estimated resources to meet these needs are the following:

	Rate Factor	Direct Labor	Capital Equip.*	Plant Area, m^2
Formation Cycling Cell capacity Number of cyclers Cells per cycler Length of test Testing capacity	6,320,000 cells/y	8 per shift	30.0 mil$ total 40 Ah 35 500 2 shifts 7,875,000 cells/y	1500
Final Cell Sealing	6,320,000 cells/y	2 per shift	2.0 mil$ total	300
Charge Retention Testing rack capacity Racks per stack Number of racks Length of test Testing capacity	6,320,000 cells/y	3 per shift	4.75 mil$ total 500 cells 5 750 14 days 8,040,000	600

*Total cost including installation

4.3.15 Module and Battery Assembly

Approximately 5% of the cells are expected to fail the formation cycling and charge-retention tests and these are sent to the Rejected Cell and Scrap Recycle section. The accepted cells (6,000,000 finished cells per year) are assembled into modules by attaching the terminals through laser welding or mechanical joining with spring loaded devices. Electronic circuit packs are attached that occupy about the same volume as a cell. These operations are carried out at four

automated stations each capable of handling about 280 cells per hour. For the module design being cost estimated in this model, the module is enclosed in an air-tight aluminum container by double seaming. The processing rate that determines the cost of module assembly is the number of finished cells that must be handled per year.

The finished modules are assembled into battery packs with the aid of automated stations. The total cost of these stations is dependant mainly on the number of battery packs to be assembled per year (100,000 for the baseline plant), but to a lesser extent on the number of modules per pack. After assembly, the packs are moved to testing stations where they are discharged as a final check of impedance and to lower the state of charge to a level suitable for shipping. The estimated resources to meet these needs are the following:

	Rate Factor	Direct Labor	Capital Equip.*	Plant Area, m^2
Module Assembly Number of stations Cells/h/station Capacity	6,000,000 cells/y	6 per shift	6.0 mil$ total 4 280 8,060,000 cells/y	400
Battery Pack Assembly Modules/pack Number of stations Packs/h/station Capacity	100,000 packs/y	4 per shift	3.0 mil$ total 4 3 6 130,000 packs	300
Battery Pack Testing	100,000 packs/y	2 per shift	3.0 mil$ total	300

4.3.16 Rejected Cell and Scrap Recycle

Scrap is generated in preparing the electrodes and by the rejection of 5% of the cells that go through formation cycling and charge-retention tests. This scrap is gathered and packaged for shipment for recycling of the materials having value. No credit is taken for the value of the scrap in this model except that the costs of gathering, sorting, packaging and shipping are understated by about that value. The main factor in determining the cost of scrap recycle is the number of cells rejected, which have to be disassembled to recover the scrap, a labor intensive process. The yields of materials in the various processing steps are shown in Table 4.4.

Table 4.4 Materials yields during electrode and cell fabrication

Material	Material Mixing	Coating	Electrode Slitting	Cell Stacking	Electrolyte Filling	Total
Positive Electrode	99	95	99	99		92.2
Negative Electrode	99	95	99	99		92.2
Positive Current Coll.		99	92	99		90.2
Negative Current Coll.		99	92	99		90.2
Separator				98		98.0
Electrolyte					94	94.0

The estimated resources needed for scrap recycle are the following:

	Rate Factor	Direct Labor	Capital Equip.*	Plant Area, m^2
Scrap Recycle Scrap rate	6,320,000 cells/y	5 per shift	2.5 mil$ total 441 kg/shift	400

4.3.17 Baseline Plant Summary

The processing rates and the primary cost factors for the baseline plant are summarized in Table 4.3. The main cost-determining rate of processing for each step is shown in the second column. The requirements for direct labor, capital equipment and plant area, which are shown in detail in the subsections above, are summarized in the table. It is seen that the plant requires a total of 95 workers per shift, $130,450,000 worth of capital equipment, and 10,325 square meters of plant area to manufacture the baseline battery at a rate of 100,000 battery packs per year.

4.4 Adjustment of Costs for Rates Different than those of the Baseline Rates

As noted in Table 4.3, there are many processing rates that must be considered in addition to the overall number of battery packs manufactured per year. Each of these rates affects the costs of one or more steps in the process and may have no effect upon the costs of other steps in the process. For instance, when the user of the model increases the power of the battery packs without increasing the number of cells or their capacity, the model increases the area of the cells and decreases the electrode coatings thicknesses. Such changes would result in an increase in the cost of the coating equipment, the floor area occupied by the equipment, and in the direct labor for that step in the process. It would have no effect on the cost of mixing the materials to be coated because the amounts of these materials per battery back are unchanged under the assumed conditions.

The general approach to cost estimation of multiplying a known cost by the ratio of processing rates raised to a power has also been applied to the capital cost of individual items of equipment.[24]

$$C = C_o(R/R_o)^p \tag{4.1}$$

Here, C_o is the capital cost of an installed equipment item designed for the baseline processing rate, R_o. The power factor, p, relates the capital investment cost and the processing rate for the manufacturing step.

If the value of p were 1.0, it would imply that the cost of the equipment item, or the equipment items if there are several in parallel, would be directly proportional to the processing rate. However, the value of p for the cost of equipment is frequently about 0.6 to 0.7 for many manufacturing process steps because the equipment is larger for the higher processing rates and its cost is less than if it were directly proportional to the processing rate. For process steps

requiring the addition of many identical pieces of equipment for scale up, such as may be true for formation cycling of battery cells, the value of p may be as high as 0.9. The value of p is unlikely to reach 1.0 because the equipment cost includes installation, for which there is some savings even in installing multiple units of the same processing capacity. The relationship between cost and processing rate for two-fold and three-fold rate changes is illustrated in Table 4.5.

Table 4.5 The effect of processing rate (R) on cost for various scale factors

$C/C_o = (R/R_o)^p$		
	Cost Ratio, C/C_o	
Scale Factor, p	$R/R_o = 2$	$R/R_o = 3$
0.25	1.19	1.32
0.3	1.23	1.39
0.4	1.32	1.55
0.5	1.41	1.73
0.6	1.52	1.93
0.7	1.62	2.16
0.8	1.74	2.41
0.95	1.93	2.84
1.0	2.00	3.00

Similar equations have been applied for determining the effect of processing rate on the annual hours of labor and the plant area required for a manufacturing step. In general, the value of p is low for the labor equation, usually only 0.4 to 0.5, because only a relatively small addition to the labor crew permits operation of larger equipment or of operating several more units of the same processing capacity.[24] The value of p for the plant area required for a processing step is slightly less than that for equipment. The floor area required for larger equipment or for more equipment items of the same size is proportionately less than the increase in the processing rate because of the more efficient use of the space occupied by the equipment and the savings in aisle area.

The value of the scale factors (i.e. p factors) for labor, capital equipment, and floor area were estimated for each of the processing steps (Table 4.3). The scale factors selected for the direct labor requirement are usually only 0.4 to 0.5, which indicates considerable unit cost reduction for increasing the plant throughput.

For most processing steps, increasing the processing rate beyond that in the baseline plant would result in a decision to increase automation or use faster equipment to mitigate the costs of higher levels of throughput. Decreasing the processing rate would have the opposite effect. Some steps in the process such as cell stacking, welding of current collectors, and formation cycling do not appear to be easily automated beyond the level intended in the baseline plant and, thus require a higher value for the scale factor of 0.8. This higher scale factor results in achieving fewer reductions in the cost per battery pack with increasing production volume. Additionally, a higher p factor results in a less severe penalty for lower production scale for an individual step in the process.

There are five steps for which the cost of the capital equipment is affected by other factors than the main processing rate for the process step. These are discussed in the footnotes at the bottom of Table 4.3. For these steps, the costs that have been adjusted for the changes in the processing rate from the baseline rate are further adjusted to take into account the other cost factors. The cost of the coating equipment is adjusted for the amount of solvents to be driven off of the positive and negative electrodes; thicker coatings need longer, more expensive ovens to drive off the additional binder solvent or the coater most be operated at lower speeds. The cost of the cell stacking equipment and that of the formation cycling equipment, for which the main cost factor in both cases is the number of cells to be fabricated annually, are also adjusted for the capacity of the cells; larger cells require more expensive equipment. The cost of the capital equipment for battery assembly is primarily a function of the number of cells in the battery, but it is also a function of the number of modules that must be interconnected. This dependence is accounted for in the model with an additional multiplying factor.

A breakdown of the baseline plant capital equipment costs listed in Table 4.3 is illustrated in Fig. 4.3. The largest costs for capital equipment are for formation cycling and testing, cell assembly in the dry room and electrode coating. These capital costs are likely to be dominant in any lithium-ion battery plant in the near future.

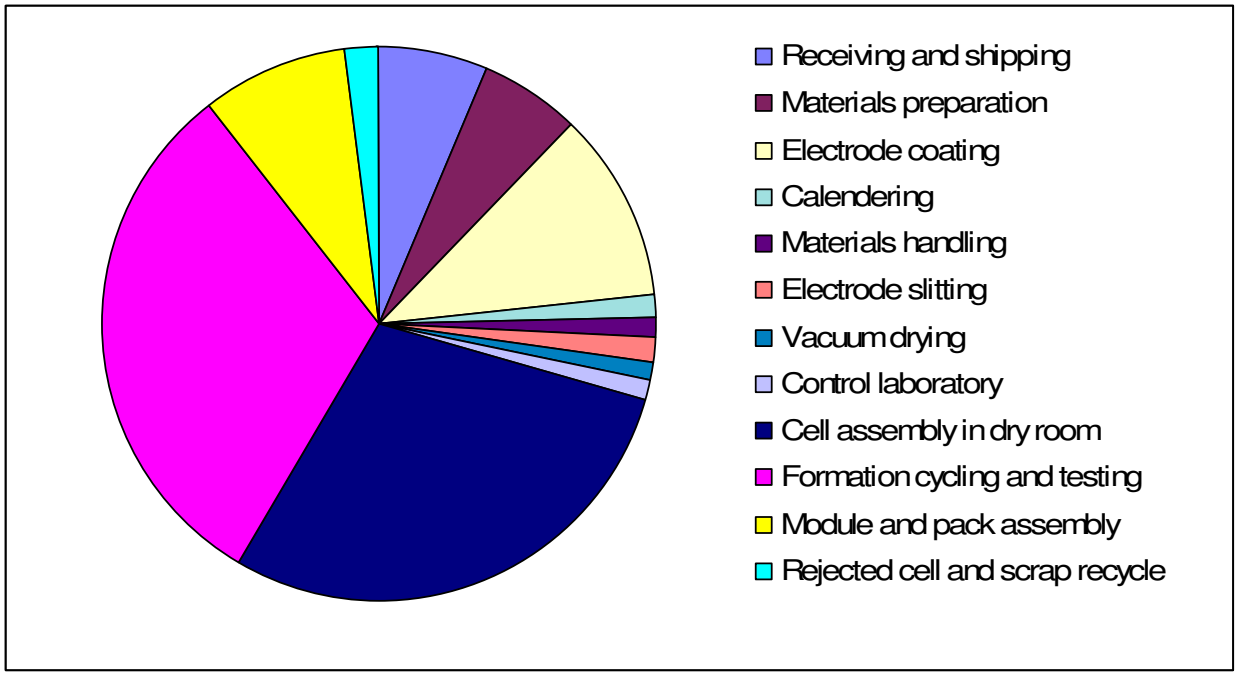

Figure 4.3 Breakdown of installed capital equipment costs for the baseline plant

4.5 Plant Investment Costs

In this model, the calculated investment costs are defined as those directly related with building and operating the plant (Table 4.6). Other costs that may require investment, such as research

and development, are added separately to the unit cost of the battery. The largest investment cost is for the installed capital equipment. Each cost item for the battery under design is adjusted from the estimate of the baseline plant. The plant cost is done in a similar way with a cost of $1,500 per square meter ($140/sq. ft) including land and utilities. Launch costs include plant start-up, employee training and materials that are lost or recycled in early stages of production, beyond the normal amounts. Launch costs are estimated to be 5 % of annual materials costs plus 10 % of annual direct labor and variable overhead (Section 4.6). Working capital is needed to cover the costs of payroll, receivables, and the inventories of raw materials, work in progress and finished product. These working capital costs are partially offset by bills that are payable. We estimate the working capital to be 15 % of the annual variable costs.

Table 4.6 Battery pack manufacturing investment costs

Investment Costs	Description	Method of Calculation
Capital Equipment	Equipment costs including installation	Estimates of costs for each processing step at baseline rates adjusted for actual rates.
Plant Floor Space	Space includes aisles and space for unfinished processing inventory plus land and utility costs.	Estimates of costs for each processing step at baseline rates adjusted for actual rates.
Launch Costs	Plant start-up, training, out-of-spec product.	5% of annual materials cost, 10% of direct labor plus variable overhead.
Working Capital	Cash to meet payroll, receivables, inventories of raw materials and of unfinished and finished product, minus payables.	15% of annual variable costs.

4.6 Unit Costs for Battery Pack

The unit costs of the battery pack are calculated as summarized in Table 4.7.

4.6.1 Variable Costs

The costs of the materials and purchased items are based on the costs discussed in section 4.2, and the annual amounts of materials are adjusted for the yields of materials (section 4.3) and yield of cells. The direct labor is the sum of the labor cost for each step in the process, which are each calculated for the baseline plant and adjusted for the rate associated with the battery under study. Variable overhead is the cost of indirect materials and labor, utilities, and plant maintenance. It is estimated to cost 60 % of direct labor costs.

4.6.2 Fixed Expenses

Fixed expenses include General, Sales, and Administration (GSA), research and development, and depreciation. The cost of GSA includes the plant office, taxes on income and property, cost of sales and insurance. It is estimated by the model as 25 % of direct overhead plus 35 % of depreciation. Research and development (R&D) must be carried out to ensure that the battery packs that are produced in the plant and the means of production continue to be competitive in the world market with respect to performance and price. The greater the investment in the plant and its equipment, the greater is the need to be successful in the R&D effort. Thus, the expenditure has been set at 50 % of the depreciation expense. Depreciation expense provides funding available for future investment in this plant or another venture to replace deteriorating plant and equipment. The equipment and plant are depreciated at straight-line rates for 8-year life (12.5 % per year) and 20-year life (5 % per year).

Table 4.7 Unit cost of battery pack

Variable Costs	Description	Method of Calculation
Materials and Purchased Items	All materials and purchased items in finished product and lost in processing.	Based on prices of materials, cost equations for purchased items and yields.
Direct Labor	Labor costs for operations and immediate supervision.	Estimates of costs for each processing step at baseline rates adjusted for actual rates.
Variable Overhead	Indirect materials, labor, utilities, plant maintenance	60% of direct labor cost.
Fixed Expenses		
General, Sales, and Administration (GSA)	Plant office, taxes on income and property, cost of sales and insurance expenses.	25% of direct labor and variable overhead plus 35% of depreciation.
Research and Development	On-going research needed to upgrade product and maintain competitive position.	50% of depreciation
Depreciation	Provides funds for new investments to replace those in current equipment and plant.	12.5% of capital equipment cost plus 5% of plant floor space cost.
Profit	Return on invested capital after taxes.	5% of total investment costs.
Warranty	Funds set aside for reimbursing customers for battery pack failures.	5.6% added to price based on present worth of projected payments.

4.6.3 Profits

The profit goal for this type of venture varies with the financial structure of the company, especially regarding long-term debt. For the model, the profit is set to provide a 5 % return on the total investment, which is an approximate average for mature manufacturing as vehicle battery production is expected to be in 2020.

4.6.4 Battery Pack Warranty Costs

If a battery module or an entire pack fails, the replacement will cost much more than the original price paid by the OEM. It is important that such events are rare, but provision must be made to reimburse the vehicle owner, especially in the early years of the projected battery life. The extra costs of replacing the battery will result from labor for testing and replacing the battery, inventory costs for stocking replacement batteries, and servicing the battery controller if the new battery is slightly different than the old battery. It is likely that the battery manufacturer will be responsible for the cost of the new battery, which we assume will be equal to the cost of the original battery. The other costs of replacing the battery, to the extent that they are covered by the warranty, are assumed here to be covered by the automobile manufacturer and the dealer. The goal for average battery life is 15 years and a warranted life of 10 years, with full replacement in the first five years and shared cost of replacement for the last five years seems appropriate. The vehicle owner would pay an increasing share of the cost from between 0 % at 5 years to 100 % at 10 or more years. With these assumptions, the cost to the battery manufacturer will be equal to the present worth of the future costs of the new battery or modules as provided in the warranty. The rate of battery failure will vary over the life of the battery with a slightly higher rate early in life, then a low failure rate followed by a gradually increasing failure rate. For purposes of calculation we assume a failure rate of 1.0 % per year throughout the warranty period. With an internal rate of return of 8 % and calculated on a monthly basis, the present value of the future costs would be about 5.6 % of the price of the battery before adding the warranty cost.

4.7 Summary of Baseline Battery Cost

The spreadsheet version of the model, which is discussed in more detail in sections 5 and 6, provides a summary sheet which is illustrated in Table 4.8 for the cost of the baseline battery and that of two others. This breakdown of the battery costs, with a brief summary of the design values, illustrates the effects of the cost factors. The second battery has twice the power of the baseline battery and the third battery has the same power as the baseline battery, but twice the capacity. The number of cells is the same for each battery. The energy storage is slightly higher for the battery with double power because the voltage would be slightly higher during the discharge to determine capacity. The battery with double the capacity has fewer electrodes which are longer and wider, because the cell thickness in maintained, resulting in higher resistance in the current-collector structure. The higher impedance lowers the voltage during the discharge capacity measurements and results in slightly less than twice the energy storage of the baseline battery.

Table 4.8. Summary of results for cost of baseline battery and that of similar batteries with double the power and double the capacity of the baseline battery

	Baseline	Double Power	Double Capacity
Calculated Battery Parameters			
Battery energy storage, kWh	8.7	8.8	17.1
Battery power at 80 % OCV, kW	50.0	100.0	50.0
Required battery power, kW	50.0	100.0	50.0
Capacity, Ah	40	40	80
Number of cells	60	60	60
Battery weight, kg	55.8	69.2	96.9
Battery volume, L	35.9	42.0	58.3
Vehicle electric range, miles	24.3	24.6	47.9
Investment Costs			
Capital equipment cost including installation, mil$	130	149	152
Building, Land and Utilities			
Area, m^2	10,325	12,193	11,744
Cost, $/$m^2$	1,500	1,500	1,500
Building investment, mil$	15	18	18
Launch Costs	10	13	15
Working capital, mil$	28	36	42
Total investment, mil$	184	216	227
Unit Cost of Battery Pack, $			
Variable Cost			
Materials and Purchased Items			
Cell materials	1,350	1,864	2,232
Cell purchased Items	75	75	90
Module and battery	228	234	276
Total	1,652	2,173	2,598
Direct Labor			
Electrode processing	36	52	40
Cell assembly	31	31	31
Formation cycling, testing and sealing	17	17	17
Module and battery assembly	16	16	16
Rejection and recycling	6	6	6
Receiving and shipping	8	8	11
Control laboratory	5	5	7
Total	119	135	128
Variable Overhead	72	81	77
Total Variable Cost	1,843	2,389	2,803
Fixed Expenses			
General, Sales, Administration	107	122	121
Research and Development	85	98	99
Depreciation	171	195	199
Total Fixed Expenses	364	415	419
Profits after taxes	92	108	113
Total unit cost per battery not including warranty, $	2,299	2,912	3,335
Summary of Unit Costs, $			
Materials	1,350	1,864	2,232
Purchased Items	303	309	366
Direct Labor	119	135	128
Variable Overhead	72	81	77
General, Sales, Administration	107	122	121
Research and Development	85	98	99
Depreciation	171	195	199
Profit	92	108	113
Warranty	129	163	187
Price, $	2,428	3,075	3,522

Doubling the power does not add as much cost to the materials and purchased parts as doubling the cell capacity. Most of the labor costs for the three batteries are similar with the major difference being for the labor cost for electrode processing. The double power battery requires greater labor costs principally for coating the larger electrode area. Capital equipment and depreciation costs are higher for both the high power and high capacity battery packs. The increases in capital equipment cost for the high-power battery are for coating, calendering, materials handling and vacuum drying equipment. For the high-capacity battery, the main additional capital equipment costs are for the materials mixing, binder solvent recovery, cell staking and formation cycling steps in the process.

Overall, doubling the power of the battery increases the cost by only 27 %. Doubling the capacity of the cells increases the cost by 45 %, considerably more than for doubling the power. Alternatively, doubling the number of baseline cells and modules within a larger battery jacket (two rows of modules instead of one, twice the voltage, energy, and power) would increase the cost by 83 %.

The summary of unit costs for the baseline battery pack, which is shown at the bottom of Table 4.8, is illustrated in Fig. 4.4. The materials and purchased items are the largest costs for the battery. For larger levels of production, these costs are even more dominant because the scale factors for these items are close to one.

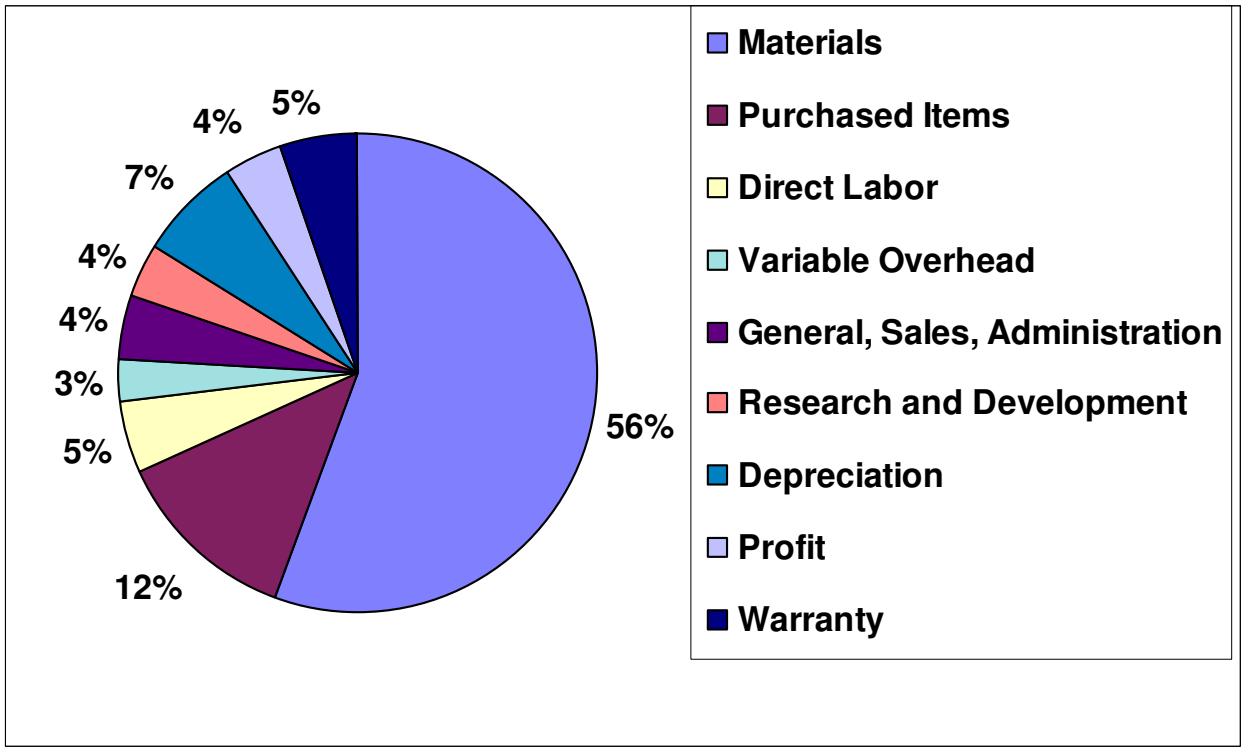

Figure 4.4 Breakdown of unit costs for baseline battery with total price to OEM of $2428.

5 Description of the Spreadsheet Model and Instructions for Use

5.1 Background

Historically, the model has been based on Microsoft® Office Excel spreadsheets. The flexibility afforded by a spreadsheet approach has been extremely useful to the development of the calculations. Until now, the model had been in a constant state of development. Changes to parameters and equations were made rapidly and frequently. The publication of this report represents the first time a version of the model will be "frozen" for open distribution to the public. Advances will continue to be made with the model, such as those discussed in the last section of this report. However, distributions of the revised model will be made in an orderly fashion rather than the continuous improvement approach taken over the last number of years.

5.2 Instructions

The following subsections are a brief explanation of how one may operate the spreadsheet based model. The user is advised to save the original document separately as a back-up copy. Corruption of the calculation is possible and will likely occur during use by someone unfamiliar with the model.

5.2.1 Enabling Calculation

This Microsoft® Office Excel workbook requires the use of iteration. To enable this feature, go to the "Tools" drop-down menu and select "Options." On the calculation tab, check the box next to "Iteration" and change the maximum number of iterations to 1000 (Figure 5.1). Also ensure the calculation is set to automatic and not manual. If the iteration is not turned on, the software will present an error complaining about circular references.

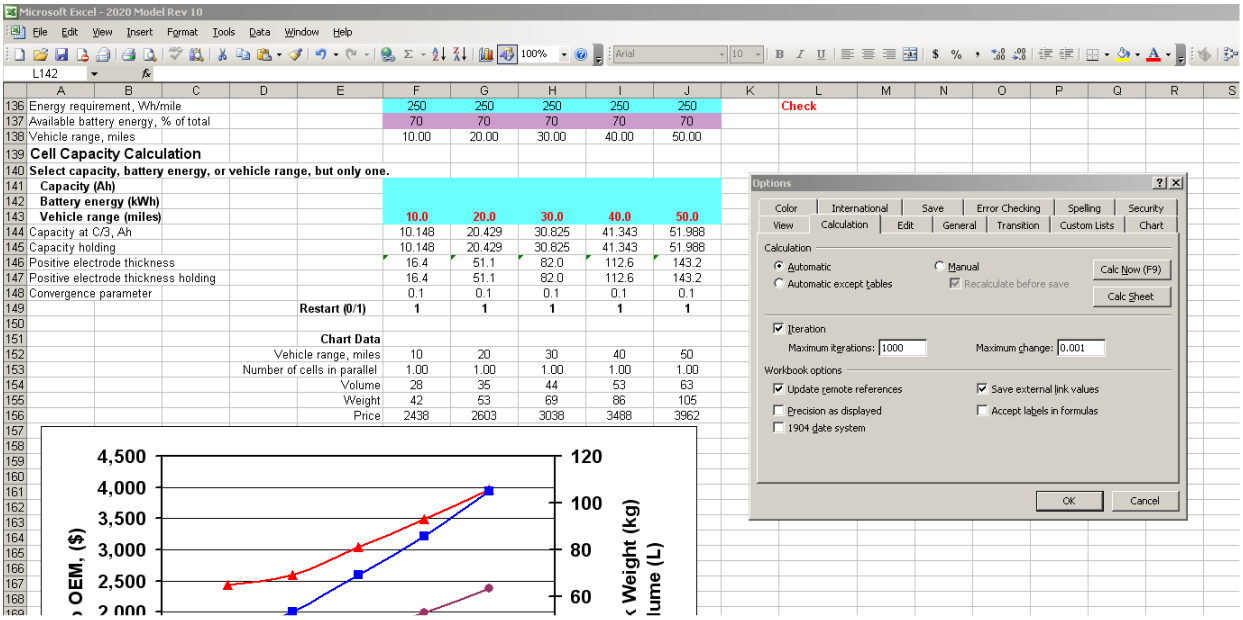

Figure 5.1 Iteration must be enabled for the spreadsheet model to function.

5.2.2 System Selection Worksheet

The cell chemistry is selected by copying the system designated at the top of a column, for instance NCA-G in cell F3, pasting it into cell E3 (Figure 5.2). Any of the values in row E can be overridden by entering the desired value in column L. The selection of the cell chemistry also includes the associated prices at the bottom of the page. These prices can also be overridden by entering the desired values in column L. A full screen shot of the system selection worksheet is in Figure 5.3.

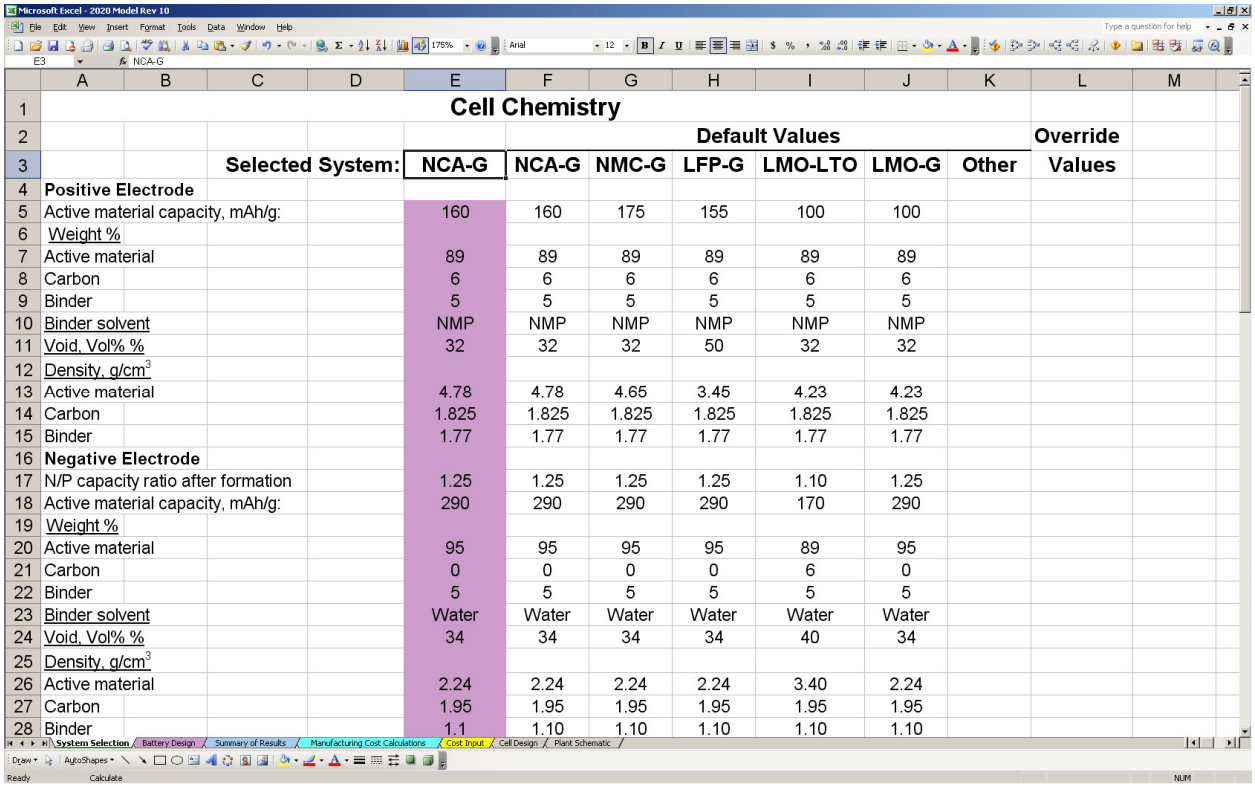

	A	B	C	D	E	F	G	H	I	J	K	L	M
1					Cell Chemistry								
2								Default Values				Override	
3				Selected System:	NCA-G	NCA-G	NMC-G	LFP-G	LMO-LTO	LMO-G	Other	Values	
4	Positive Electrode												
5	Active material capacity, mAh/g:				160	160	175	155	100	100			
6	Weight %												
7	Active material				89	89	89	89	89	89			
8	Carbon				6	6	6	6	6	6			
9	Binder				5	5	5	5	5	5			
10	Binder solvent				NMP	NMP	NMP	NMP	NMP	NMP			
11	Void, Vol% %				32	32	32	50	32	32			
12	Density, g/cm^3												
13	Active material				4.78	4.78	4.65	3.45	4.23	4.23			
14	Carbon				1.825	1.825	1.825	1.825	1.825	1.825			
15	Binder				1.77	1.77	1.77	1.77	1.77	1.77			
16	Negative Electrode												
17	N/P capacity ratio after formation				1.25	1.25	1.25	1.25	1.10	1.25			
18	Active material capacity, mAh/g:				290	290	290	290	170	290			
19	Weight %												
20	Active material				95	95	95	95	89	95			
21	Carbon				0	0	0	0	6	0			
22	Binder				5	5	5	5	5	5			
23	Binder solvent				Water	Water	Water	Water	Water	Water			
24	Void, Vol% %				34	34	34	34	40	34			
25	Density, g/cm^3												
26	Active material				2.24	2.24	2.24	2.24	3.40	2.24			
27	Carbon				1.95	1.95	1.95	1.95	1.95	1.95			
28	Binder				1.1	1.10	1.10	1.10	1.10	1.10			

Figure 5.2 The specific cell chemistry for the battery design is selected on the System Selection worksheet. Any value may be overridden by entering a value in column L.

5.2.3 Battery Design Worksheet

The Battery Design worksheet designs five or more batteries for any type of electric-drive vehicle (Figure 5.4–5.6). The calculated designs are specific for the end batteries requirements specified by the user. From the result, the amounts of materials and the purchased items required for manufacture are easily available to be used in the manufacturing cost calculations found on subsequent worksheets. Although a cell and module format is assumed, the exact format (prismatic, pouch, can, etc) of the battery does not have a dominant effect on the cost for a set cell chemistry system. Our experience teaches us that the amounts of electrode materials and the number, capacity and electrode area of the cells, are the determining cost factors. Nevertheless, a specific design format was selected and is shown on the Cell Design worksheet to provide a basis for calculating the entire cell and battery related costs.

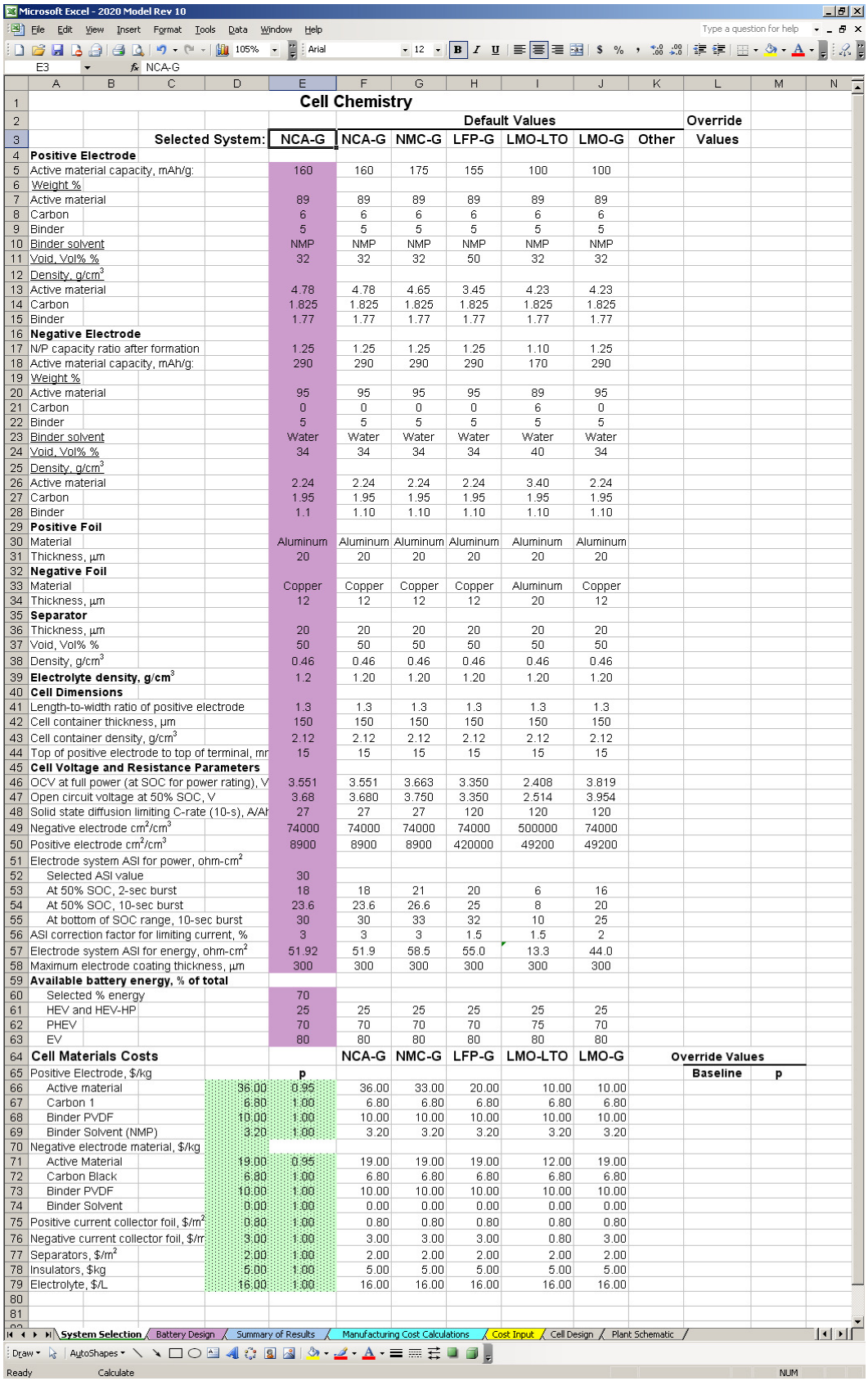

1	**Cell Chemistry**													
2						Default Values							Override	
3				Selected System:	NCA-G	NCA-G	NMC-G	LFP-G	LMO-LTO	LMO-G	Other		Values	
4	**Positive Electrode**													
5	Active material capacity, mAh/g:				160	160	175	155	100	100				
6	Weight %													
7	Active material				89	89	89	89	89	89				
8	Carbon				6	6	6	6	6	6				
9	Binder				5	5	5	5	5	5				
10	Binder solvent				NMP	NMP	NMP	NMP	NMP	NMP				
11	Void, Vol% %				32	32	32	50	32	32				
12	Density, g/cm^3													
13	Active material				4.78	4.78	4.65	3.45	4.23	4.23				
14	Carbon				1.825	1.825	1.825	1.825	1.825	1.825				
15	Binder				1.77	1.77	1.77	1.77	1.77	1.77				
16	**Negative Electrode**													
17	N/P capacity ratio after formation				1.25	1.25	1.25	1.25	1.10	1.25				
18	Active material capacity, mAh/g:				290	290	290	290	170	290				
19	Weight %													
20	Active material				95	95	95	95	89	95				
21	Carbon				0	0	0	0	6	0				
22	Binder				5	5	5	5	5	5				
23	Binder solvent				Water	Water	Water	Water	Water	Water				
24	Void, Vol% %				34	34	34	34	40	34				
25	Density, g/cm^3													
26	Active material				2.24	2.24	2.24	2.24	3.40	2.24				
27	Carbon				1.95	1.95	1.95	1.95	1.95	1.95				
28	Binder				1.1	1.10	1.10	1.10	1.10	1.10				
29	**Positive Foil**													
30	Material				Aluminum	Aluminum	Aluminum	Aluminum	Aluminum	Aluminum				
31	Thickness, µm				20	20	20	20	20	20				
32	**Negative Foil**													
33	Material				Copper	Copper	Copper	Copper	Aluminum	Copper				
34	Thickness, µm				12	12	12	12	20	12				
35	**Separator**													
36	Thickness, µm				20	20	20	20	20	20				
37	Void, Vol% %				50	50	50	50	50	50				
38	Density, g/cm^3				0.46	0.46	0.46	0.46	0.46	0.46				
39	**Electrolyte density, g/cm^3**				1.2	1.20	1.20	1.20	1.20	1.20				
40	**Cell Dimensions**													
41	Length-to-width ratio of positive electrode				1.3	1.3	1.3	1.3	1.3	1.3				
42	Cell container thickness, µm				150	150	150	150	150	150				
43	Cell container density, g/cm^3				2.12	2.12	2.12	2.12	2.12	2.12				
44	Top of positive electrode to top of terminal, mr				15	15	15	15	15	15				
45	**Cell Voltage and Resistance Parameters**													
46	OCV at full power (at SOC for power rating), V				3.551	3.551	3.663	3.350	2.408	3.819				
47	Open circuit voltage at 50% SOC, V				3.68	3.680	3.750	3.350	2.514	3.954				
48	Solid state diffusion limiting C-rate (10-s), A/Ah				27	27	27	120	120	120				
49	Negative electrode cm^2/cm^3				74000	74000	74000	74000	500000	74000				
50	Positive electrode cm^2/cm^3				8900	8900	8900	420000	49200	49200				
51	Electrode system ASI for power, ohm-cm^2													
52	Selected ASI value				30									
53	At 50% SOC, 2-sec burst				18	18	21	20	6	16				
54	At 50% SOC, 10-sec burst				23.6	23.6	26.6	25	8	20				
55	At bottom of SOC range, 10-sec burst				30	30	33	32	10	25				
56	ASI correction factor for limiting current, %				3	3	3	1.5	1.5	2				
57	Electrode system ASI for energy, ohm-cm^2				51.92	51.9	58.5	55.0	13.3	44.0				
58	Maximum electrode coating thickness, µm				300	300	300	300	300	300				
59	**Available battery energy, % of total**													
60	Selected % energy				70									
61	HEV and HEV-HP				25	25	25	25	25	25				
62	PHEV				70	70	70	70	75	70				
63	EV				80	80	80	80	80	80				
64	**Cell Materials Costs**					NCA-G	NCA-G	NMC-G	LFP-G	LMO-LTO	LMO-G		Override Values	
65	Positive Electrode, $/kg				p								Baseline	p
66	Active material			36.00	0.95	36.00	33.00	20.00	10.00	10.00				
67	Carbon 1			6.80	1.00	6.80	6.80	6.80	6.80	6.80				
68	Binder PVDF			10.00	1.00	10.00	10.00	10.00	10.00	10.00				
69	Binder Solvent (NMP)			3.20	1.00	3.20	3.20	3.20	3.20	3.20				
70	Negative electrode material, $/kg													
71	Active Material			19.00	0.95	19.00	19.00	19.00	12.00	19.00				
72	Carbon Black			6.80	1.00	6.80	6.80	6.80	6.80	6.80				
73	Binder PVDF			10.00	1.00	10.00	10.00	10.00	10.00	10.00				
74	Binder Solvent			0.00	1.00	0.00	0.00	0.00	0.00	0.00				
75	Positive current collector foil, $/m^2			0.80	1.00	0.80	0.80	0.80	0.80	0.80				
76	Negative current collector foil, $/m			3.00	1.00	3.00	3.00	3.00	0.80	3.00				
77	Separators, $/m^2			2.00	1.00	2.00	2.00	2.00	2.00	2.00				
78	Insulators, $kg			5.00	1.00	5.00	5.00	5.00	5.00	5.00				
79	Electrolyte, $/L			16.00	1.00	16.00	16.00	16.00	16.00	16.00				
80														
81														

Figure 5.3 System Selection worksheet

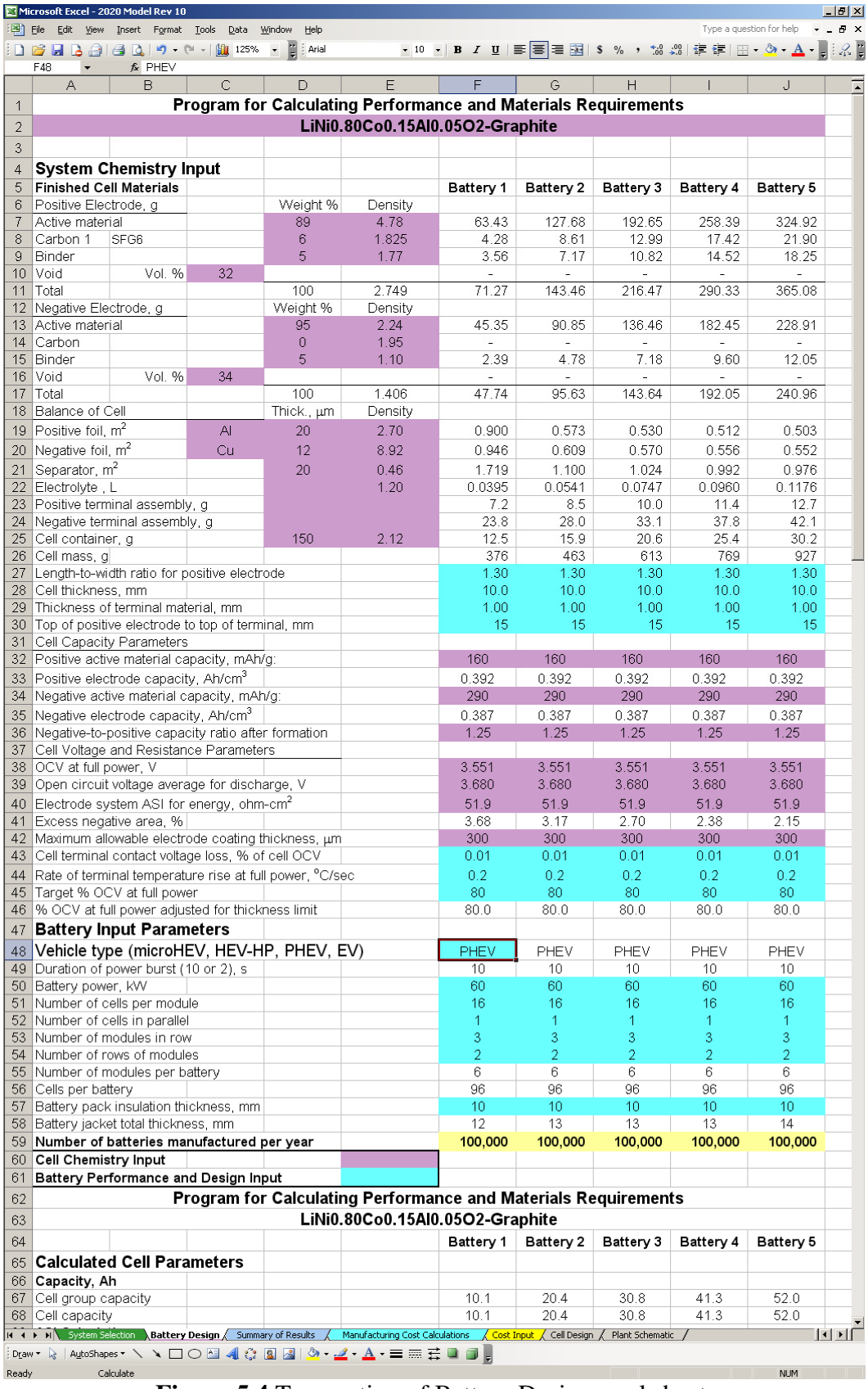

	A	B	C	D	E	F	G	H	I	J
1	**Program for Calculating Performance and Materials Requirements**									
2	**LiNi0.80Co0.15Al0.05O2-Graphite**									
3										
4	**System Chemistry Input**									
5	**Finished Cell Materials**					**Battery 1**	**Battery 2**	**Battery 3**	**Battery 4**	**Battery 5**
6	Positive Electrode, g			Weight %	Density					
7	Active material			89	4.78	63.43	127.68	192.65	258.39	324.92
8	Carbon 1	SFG6		6	1.825	4.28	8.61	12.99	17.42	21.90
9	Binder			5	1.77	3.56	7.17	10.82	14.52	18.25
10	Void	Vol. %	32			-	-	-	-	-
11	Total			100	2.749	71.27	143.46	216.47	290.33	365.08
12	Negative Electrode, g			Weight %	Density					
13	Active material			95	2.24	45.35	90.85	136.46	182.45	228.91
14	Carbon			0	1.95	-	-	-	-	-
15	Binder			5	1.10	2.39	4.78	7.18	9.60	12.05
16	Void	Vol. %	34			-	-	-	-	-
17	Total			100	1.406	47.74	95.63	143.64	192.05	240.96
18	Balance of Cell			Thick., µm	Density					
19	Positive foil, m^2		Al	20	2.70	0.900	0.573	0.530	0.512	0.503
20	Negative foil, m^2		Cu	12	8.92	0.946	0.609	0.570	0.556	0.552
21	Separator, m^2			20	0.46	1.719	1.100	1.024	0.992	0.976
22	Electrolyte , L				1.20	0.0395	0.0541	0.0747	0.0960	0.1176
23	Positive terminal assembly, g					7.2	8.5	10.0	11.4	12.7
24	Negative terminal assembly, g					23.8	28.0	33.1	37.8	42.1
25	Cell container, g			150	2.12	12.5	15.9	20.6	25.4	30.2
26	Cell mass, g					376	463	613	769	927
27	Length-to-width ratio for positive electrode					1.30	1.30	1.30	1.30	1.30
28	Cell thickness, mm					10.0	10.0	10.0	10.0	10.0
29	Thickness of terminal material, mm					1.00	1.00	1.00	1.00	1.00
30	Top of positive electrode to top of terminal, mm					15	15	15	15	15
31	Cell Capacity Parameters									
32	Positive active material capacity, mAh/g:					160	160	160	160	160
33	Positive electrode capacity, Ah/cm^3					0.392	0.392	0.392	0.392	0.392
34	Negative active material capacity, mAh/g:					290	290	290	290	290
35	Negative electrode capacity, Ah/cm^3					0.387	0.387	0.387	0.387	0.387
36	Negative-to-positive capacity ratio after formation					1.25	1.25	1.25	1.25	1.25
37	Cell Voltage and Resistance Parameters									
38	OCV at full power, V					3.551	3.551	3.551	3.551	3.551
39	Open circuit voltage average for discharge, V					3.680	3.680	3.680	3.680	3.680
40	Electrode system ASI for energy, ohm-cm^2					51.9	51.9	51.9	51.9	51.9
41	Excess negative area, %					3.68	3.17	2.70	2.38	2.15
42	Maximum allowable electrode coating thickness, µm					300	300	300	300	300
43	Cell terminal contact voltage loss, % of cell OCV					0.01	0.01	0.01	0.01	0.01
44	Rate of terminal temperature rise at full power, °C/sec					0.2	0.2	0.2	0.2	0.2
45	Target % OCV at full power					80	80	80	80	80
46	% OCV at full power adjusted for thickness limit					80.0	80.0	80.0	80.0	80.0
47	**Battery Input Parameters**									
48	Vehicle type (microHEV, HEV-HP, PHEV, EV)					PHEV	PHEV	PHEV	PHEV	PHEV
49	Duration of power burst (10 or 2), s					10	10	10	10	10
50	Battery power, kW					60	60	60	60	60
51	Number of cells per module					16	16	16	16	16
52	Number of cells in parallel					1	1	1	1	1
53	Number of modules in row					3	3	3	3	3
54	Number of rows of modules					2	2	2	2	2
55	Number of modules per battery					6	6	6	6	6
56	Cells per battery					96	96	96	96	96
57	Battery pack insulation thickness, mm					10	10	10	10	10
58	Battery jacket total thickness, mm					12	13	13	13	14
59	**Number of batteries manufactured per year**					**100,000**	**100,000**	**100,000**	**100,000**	**100,000**
60	**Cell Chemistry Input**									
61	**Battery Performance and Design Input**									
62	**Program for Calculating Performance and Materials Requirements**									
63	**LiNi0.80Co0.15Al0.05O2-Graphite**									
64						**Battery 1**	**Battery 2**	**Battery 3**	**Battery 4**	**Battery 5**
65	**Calculated Cell Parameters**									
66	**Capacity, Ah**									
67	Cell group capacity					10.1	20.4	30.8	41.3	52.0
68	Cell capacity					10.1	20.4	30.8	41.3	52.0

Figure 5.4 Top portion of Battery Design worksheet.

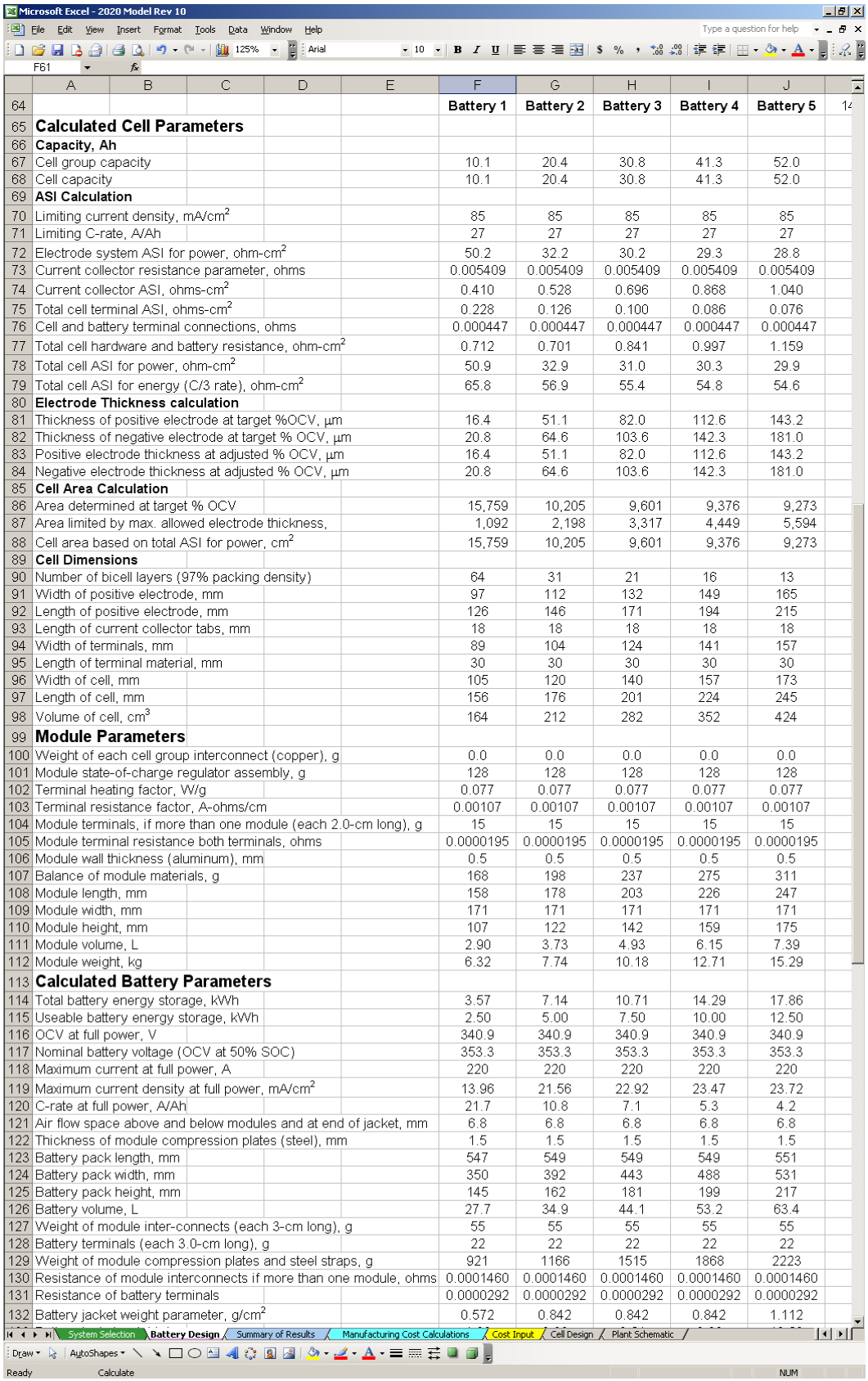

	A	F	G	H	I	J
64		**Battery 1**	**Battery 2**	**Battery 3**	**Battery 4**	**Battery 5**
65	**Calculated Cell Parameters**					
66	**Capacity, Ah**					
67	Cell group capacity	10.1	20.4	30.8	41.3	52.0
68	Cell capacity	10.1	20.4	30.8	41.3	52.0
69	**ASI Calculation**					
70	Limiting current density, mA/cm^2	85	85	85	85	85
71	Limiting C-rate, A/Ah	27	27	27	27	27
72	Electrode system ASI for power, ohm-cm^2	50.2	32.2	30.2	29.3	28.8
73	Current collector resistance parameter, ohms	0.005409	0.005409	0.005409	0.005409	0.005409
74	Current collector ASI, ohms-cm^2	0.410	0.528	0.696	0.868	1.040
75	Total cell terminal ASI, ohms-cm^2	0.228	0.126	0.100	0.086	0.076
76	Cell and battery terminal connections, ohms	0.000447	0.000447	0.000447	0.000447	0.000447
77	Total cell hardware and battery resistance, ohm-cm^2	0.712	0.701	0.841	0.997	1.159
78	Total cell ASI for power, ohm-cm^2	50.9	32.9	31.0	30.3	29.9
79	Total cell ASI for energy (C/3 rate), ohm-cm^2	65.8	56.9	55.4	54.8	54.6
80	**Electrode Thickness calculation**					
81	Thickness of positive electrode at target %OCV, µm	16.4	51.1	82.0	112.6	143.2
82	Thickness of negative electrode at target % OCV, µm	20.8	64.6	103.6	142.3	181.0
83	Positive electrode thickness at adjusted % OCV, µm	16.4	51.1	82.0	112.6	143.2
84	Negative electrode thickness at adjusted % OCV, µm	20.8	64.6	103.6	142.3	181.0
85	**Cell Area Calculation**					
86	Area determined at target % OCV	15,759	10,205	9,601	9,376	9,273
87	Area limited by max. allowed electrode thickness,	1,092	2,198	3,317	4,449	5,594
88	Cell area based on total ASI for power, cm^2	15,759	10,205	9,601	9,376	9,273
89	**Cell Dimensions**					
90	Number of bicell layers (97% packing density)	64	31	21	16	13
91	Width of positive electrode, mm	97	112	132	149	165
92	Length of positive electrode, mm	126	146	171	194	215
93	Length of current collector tabs, mm	18	18	18	18	18
94	Width of terminals, mm	89	104	124	141	157
95	Length of terminal material, mm	30	30	30	30	30
96	Width of cell, mm	105	120	140	157	173
97	Length of cell, mm	156	176	201	224	245
98	Volume of cell, cm^3	164	212	282	352	424
99	**Module Parameters**					
100	Weight of each cell group interconnect (copper), g	0.0	0.0	0.0	0.0	0.0
101	Module state-of-charge regulator assembly, g	128	128	128	128	128
102	Terminal heating factor, W/g	0.077	0.077	0.077	0.077	0.077
103	Terminal resistance factor, A-ohms/cm	0.00107	0.00107	0.00107	0.00107	0.00107
104	Module terminals, if more than one module (each 2.0-cm long), g	15	15	15	15	15
105	Module terminal resistance both terminals, ohms	0.0000195	0.0000195	0.0000195	0.0000195	0.0000195
106	Module wall thickness (aluminum), mm	0.5	0.5	0.5	0.5	0.5
107	Balance of module materials, g	168	198	237	275	311
108	Module length, mm	158	178	203	226	247
109	Module width, mm	171	171	171	171	171
110	Module height, mm	107	122	142	159	175
111	Module volume, L	2.90	3.73	4.93	6.15	7.39
112	Module weight, kg	6.32	7.74	10.18	12.71	15.29
113	**Calculated Battery Parameters**					
114	Total battery energy storage, kWh	3.57	7.14	10.71	14.29	17.86
115	Useable battery energy storage, kWh	2.50	5.00	7.50	10.00	12.50
116	OCV at full power, V	340.9	340.9	340.9	340.9	340.9
117	Nominal battery voltage (OCV at 50% SOC)	353.3	353.3	353.3	353.3	353.3
118	Maximum current at full power, A	220	220	220	220	220
119	Maximum current density at full power, mA/cm^2	13.96	21.56	22.92	23.47	23.72
120	C-rate at full power, A/Ah	21.7	10.8	7.1	5.3	4.2
121	Air flow space above and below modules and at end of jacket, mm	6.8	6.8	6.8	6.8	6.8
122	Thickness of module compression plates (steel), mm	1.5	1.5	1.5	1.5	1.5
123	Battery pack length, mm	547	549	549	549	551
124	Battery pack width, mm	350	392	443	488	531
125	Battery pack height, mm	145	162	181	199	217
126	Battery volume, L	27.7	34.9	44.1	53.2	63.4
127	Weight of module inter-connects (each 3-cm long), g	55	55	55	55	55
128	Battery terminals (each 3.0-cm long), g	22	22	22	22	22
129	Weight of module compression plates and steel straps, g	921	1166	1515	1868	2223
130	Resistance of module interconnects if more than one module, ohms	0.0001460	0.0001460	0.0001460	0.0001460	0.0001460
131	Resistance of battery terminals	0.0000292	0.0000292	0.0000292	0.0000292	0.0000292
132	Battery jacket weight parameter, g/cm^2	0.572	0.842	0.842	0.842	1.112

Figure 5.5 Middle portion of Battery Design worksheet

The Battery Design worksheet automatically receives input from the System Selection worksheet. These values are shown in purple (Figures 5.4 and 5.6) and must not be altered on the Battery Design worksheet. As explained above, cell chemistry values may be adjusted on the System Selection worksheet. The operator provides battery design input in the aqua colored cells (Figures 5.4 and 5.6). It is expected that the default values for the cell design (lines 27 to 30) and the thickness of the battery insulation (line 57) should serve well for most batteries. The battery input parameters on lines 50 to 54 (Figure 5.4) and lines 141 to 143 (Figure 5.6) are the only input values that the operator is required to provide to study a group of batteries. An important variable is the type of vehicle battery, (microHEV, HEV-HP, PHEV, or EV) on line 48 in Figure 5.4. One performs the selection by typing the name of the vehicle battery type in cell F48. While the correct spelling is important, capitalization is not. This selection automatically determines the state of charge at which full power is designated (thus, the open-circuit voltage and ASI for full power) and the length of the power burst (2 seconds for microHEV and 10 seconds for all others).

The cell capacity (lines 141 to 143 in Figure 5.6) can be set in any of three ways: (1) directly specifying the capacity (Ah) on line 141, (2) specifying the total battery energy on line 142 or (3) specifying the electric range of the vehicle (miles). Only one of the three lines should be filled in and the others should be blank. The model will follow the directions of the top-most line with non-zero values.

The number of batteries manufactured per year is selected on line 59 in Figure 5.4. Changing this value from the default value of 100,000, which is the manufacturing rate for the baseline plant, will change the manufacturing cost.

If it is desired to study more than five batteries in the same workbook it is only necessary to add additional columns by copying the battery 5 column to the right as many times as desired. Care should be taken that the appropriate values are maintained when the cells are copied over. The aqua colored cells are typically the source of any problems. The same column additions most also be done for the worksheets on Summary of Results and Manufacturing Cost Calculations.

5.2.4 Remaining Worksheets

The cost calculations are done on the Manufacturing Cost worksheet and the results for the model are shown on the Summary of Results worksheet (Figure 5.7). No parameters need to be entered on these worksheets by the operator; all of the input for these worksheets is from the Battery Design and the Cost Input worksheets. Tables for presentations or for preparing graphs of the data can be assembled at the bottom of either the Battery Design or the Summary of Results worksheet. These tables can be transferred to a blank worksheet for more complex studies. For instance, results for different cell chemistries can be copied and pasted (special paste, values and numbers formats) to a blank worksheet. Preparing a chart has been illustrated in the initial configuration by graphing the data tabulated at the bottom of the Battery Design worksheet. The X-axis description will have to be adjusted if the cell capacity is selected by one of the alternative methods. On the last two worksheets, the cell design and the baseline plant are sketched.

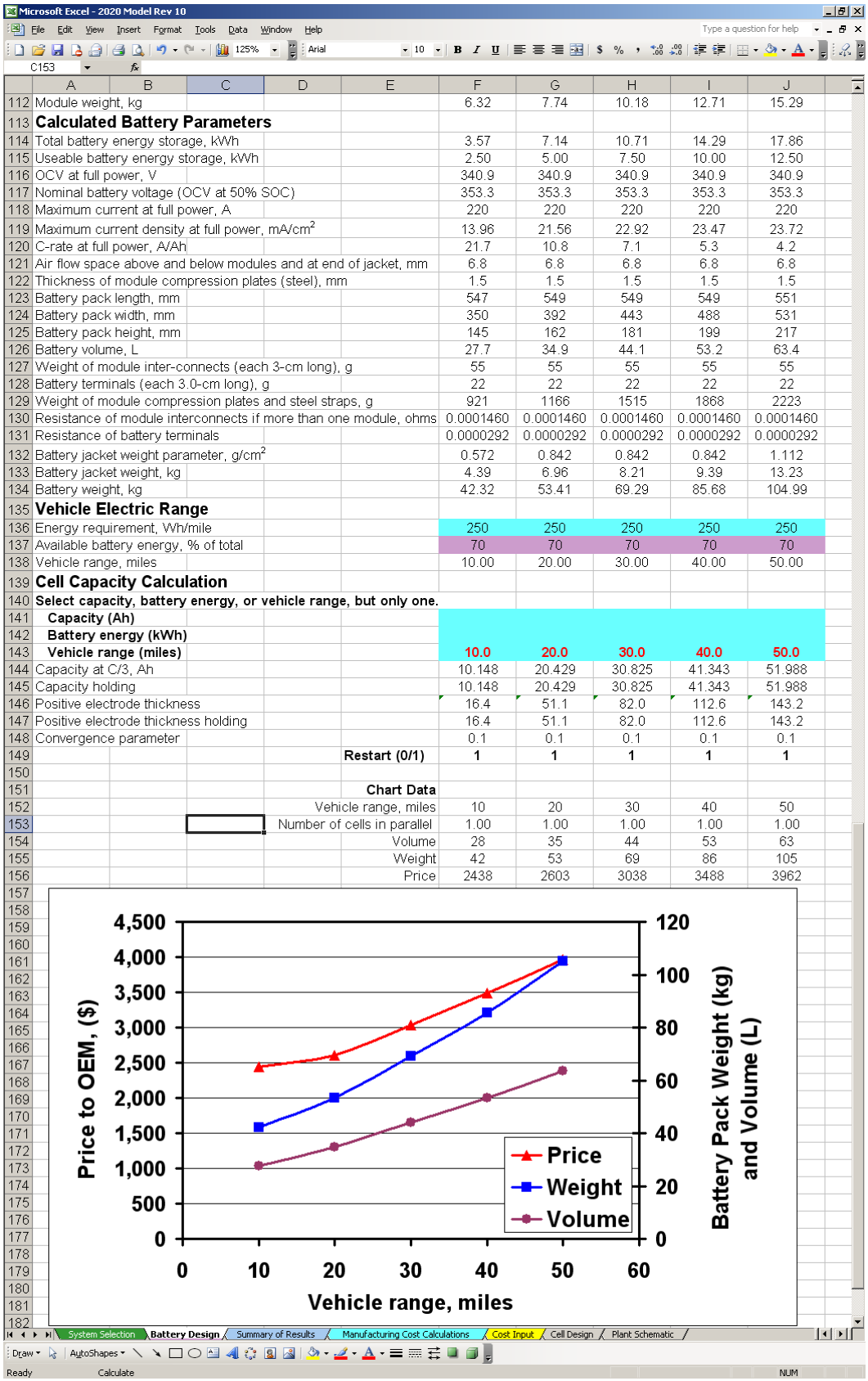

		F	G	H	I	J
112	Module weight, kg	6.32	7.74	10.18	12.71	15.29
113	**Calculated Battery Parameters**					
114	Total battery energy storage, kWh	3.57	7.14	10.71	14.29	17.86
115	Useable battery energy storage, kWh	2.50	5.00	7.50	10.00	12.50
116	OCV at full power, V	340.9	340.9	340.9	340.9	340.9
117	Nominal battery voltage (OCV at 50% SOC)	353.3	353.3	353.3	353.3	353.3
118	Maximum current at full power, A	220	220	220	220	220
119	Maximum current density at full power, mA/cm^2	13.96	21.56	22.92	23.47	23.72
120	C-rate at full power, A/Ah	21.7	10.8	7.1	5.3	4.2
121	Air flow space above and below modules and at end of jacket, mm	6.8	6.8	6.8	6.8	6.8
122	Thickness of module compression plates (steel), mm	1.5	1.5	1.5	1.5	1.5
123	Battery pack length, mm	547	549	549	549	551
124	Battery pack width, mm	350	392	443	488	531
125	Battery pack height, mm	145	162	181	199	217
126	Battery volume, L	27.7	34.9	44.1	53.2	63.4
127	Weight of module inter-connects (each 3-cm long), g	55	55	55	55	55
128	Battery terminals (each 3.0-cm long), g	22	22	22	22	22
129	Weight of module compression plates and steel straps, g	921	1166	1515	1868	2223
130	Resistance of module interconnects if more than one module, ohms	0.0001460	0.0001460	0.0001460	0.0001460	0.0001460
131	Resistance of battery terminals	0.0000292	0.0000292	0.0000292	0.0000292	0.0000292
132	Battery jacket weight parameter, g/cm^2	0.572	0.842	0.842	0.842	1.112
133	Battery jacket weight, kg	4.39	6.96	8.21	9.39	13.23
134	Battery weight, kg	42.32	53.41	69.29	85.68	104.99
135	**Vehicle Electric Range**					
136	Energy requirement, Wh/mile	250	250	250	250	250
137	Available battery energy, % of total	70	70	70	70	70
138	Vehicle range, miles	10.00	20.00	30.00	40.00	50.00
139	**Cell Capacity Calculation**					
140	**Select capacity, battery energy, or vehicle range, but only one.**					
141	**Capacity (Ah)**					
142	**Battery energy (kWh)**					
143	**Vehicle range (miles)**	10.0	20.0	30.0	40.0	50.0
144	Capacity at C/3, Ah	10.148	20.429	30.825	41.343	51.988
145	Capacity holding	10.148	20.429	30.825	41.343	51.988
146	Positive electrode thickness	16.4	51.1	82.0	112.6	143.2
147	Positive electrode thickness holding	16.4	51.1	82.0	112.6	143.2
148	Convergence parameter	0.1	0.1	0.1	0.1	0.1
149	**Restart (0/1)**	**1**	**1**	**1**	**1**	**1**
150						
151	**Chart Data**					
152	Vehicle range, miles	10	20	30	40	50
153	Number of cells in parallel	1.00	1.00	1.00	1.00	1.00
154	Volume	28	35	44	53	63
155	Weight	42	53	69	86	105
156	Price	2438	2603	3038	3488	3962

Figure 5.6 Bottom portion of Battery Design worksheet

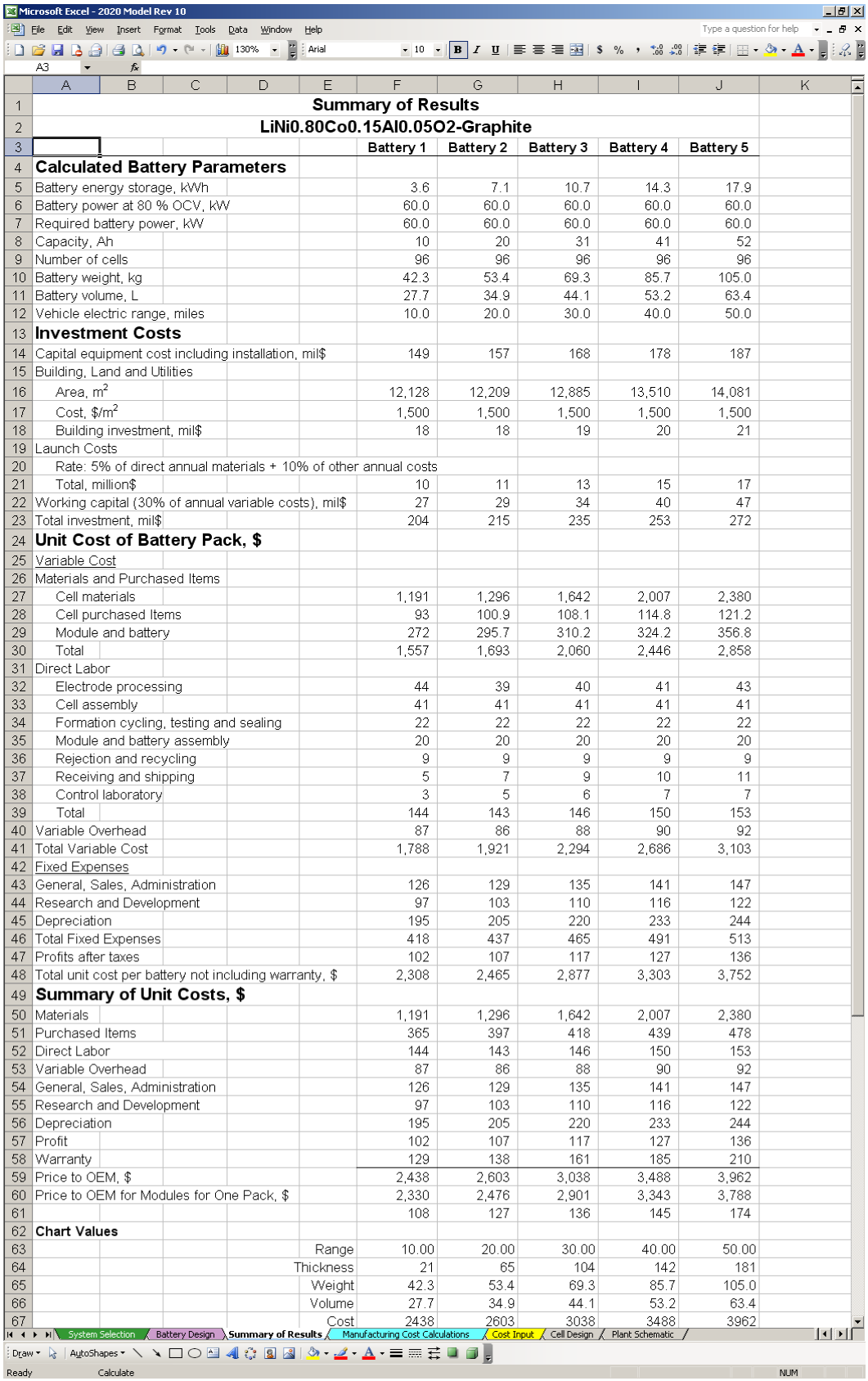

	A	F	G	H	I	J
1	**Summary of Results**					
2	**LiNi0.80Co0.15Al0.05O2-Graphite**					
3		**Battery 1**	**Battery 2**	**Battery 3**	**Battery 4**	**Battery 5**
4	**Calculated Battery Parameters**					
5	Battery energy storage, kWh	3.6	7.1	10.7	14.3	17.9
6	Battery power at 80 % OCV, kW	60.0	60.0	60.0	60.0	60.0
7	Required battery power, kW	60.0	60.0	60.0	60.0	60.0
8	Capacity, Ah	10	20	31	41	52
9	Number of cells	96	96	96	96	96
10	Battery weight, kg	42.3	53.4	69.3	85.7	105.0
11	Battery volume, L	27.7	34.9	44.1	53.2	63.4
12	Vehicle electric range, miles	10.0	20.0	30.0	40.0	50.0
13	**Investment Costs**					
14	Capital equipment cost including installation, mil$	149	157	168	178	187
15	Building, Land and Utilities					
16	Area, m^2	12,128	12,209	12,885	13,510	14,081
17	Cost, $/$m^2$	1,500	1,500	1,500	1,500	1,500
18	Building investment, mil$	18	18	19	20	21
19	Launch Costs					
20	Rate: 5% of direct annual materials + 10% of other annual costs					
21	Total, million$	10	11	13	15	17
22	Working capital (30% of annual variable costs), mil$	27	29	34	40	47
23	Total investment, mil$	204	215	235	253	272
24	**Unit Cost of Battery Pack, $**					
25	Variable Cost					
26	Materials and Purchased Items					
27	Cell materials	1,191	1,296	1,642	2,007	2,380
28	Cell purchased Items	93	100.9	108.1	114.8	121.2
29	Module and battery	272	295.7	310.2	324.2	356.8
30	Total	1,557	1,693	2,060	2,446	2,858
31	Direct Labor					
32	Electrode processing	44	39	40	41	43
33	Cell assembly	41	41	41	41	41
34	Formation cycling, testing and sealing	22	22	22	22	22
35	Module and battery assembly	20	20	20	20	20
36	Rejection and recycling	9	9	9	9	9
37	Receiving and shipping	5	7	9	10	11
38	Control laboratory	3	5	6	7	7
39	Total	144	143	146	150	153
40	Variable Overhead	87	86	88	90	92
41	Total Variable Cost	1,788	1,921	2,294	2,686	3,103
42	Fixed Expenses					
43	General, Sales, Administration	126	129	135	141	147
44	Research and Development	97	103	110	116	122
45	Depreciation	195	205	220	233	244
46	Total Fixed Expenses	418	437	465	491	513
47	Profits after taxes	102	107	117	127	136
48	Total unit cost per battery not including warranty, $	2,308	2,465	2,877	3,303	3,752
49	**Summary of Unit Costs, $**					
50	Materials	1,191	1,296	1,642	2,007	2,380
51	Purchased Items	365	397	418	439	478
52	Direct Labor	144	143	146	150	153
53	Variable Overhead	87	86	88	90	92
54	General, Sales, Administration	126	129	135	141	147
55	Research and Development	97	103	110	116	122
56	Depreciation	195	205	220	233	244
57	Profit	102	107	117	127	136
58	Warranty	129	138	161	185	210
59	Price to OEM, $	2,438	2,603	3,038	3,488	3,962
60	Price to OEM for Modules for One Pack, $	2,330	2,476	2,901	3,343	3,788
61		108	127	136	145	174
62	**Chart Values**					
63	Range	10.00	20.00	30.00	40.00	50.00
64	Thickness	21	65	104	142	181
65	Weight	42.3	53.4	69.3	85.7	105.0
66	Volume	27.7	34.9	44.1	53.2	63.4
67	Cost	2438	2603	3038	3488	3962

Figure 5.7 Summary of Results worksheet

5.3 Battery Design Format Requirements

As the battery design is based off an assumed format (Section 2), certain design requirements are necessary to ensure the modeled battery is physically realistic. For a battery based on a single module, no additional restrictions are required. However, most batteries for transportation applications will use multiple modules. For these applications, the following rules should be followed by the user of the model. An even number of cells should compose each module and an even number of modules should compose each battery pack. These two requirements are to ensure the electrical connections are in the appropriate places in the final battery pack. Finally, the dimensions of the resulting battery pack should be examined. Some final designs may benefit from changing the cell aspect ratio, *H/W*, to fit the end-use application. One example would be, to change the height of the battery pack. Also, for a set number of cells in the pack, changing the number of modules, thus cells per module, allows for adjustment of the pack dimensions.

5.4 Troubleshooting and General Advice

The spreadsheet iterates to find the solution and this sometimes causes error messages to appear after an entry is changed. These errors can usually be removed by first correcting any erroneous entries (non-numeric, two decimal points, etc.). Then the cells may be reset to default values by entering a "0" (i.e. zero) in the restart cell, F149 in Figure 5.6. Finally, entering a "1" in F149 restarts the iteration process leading to a successfully converged answer.

At some point, a user will ask the model to design a battery that is outside the bounds of what is allowable for the selected cell chemistry. The most common error is when too large of a P/E ratio is requested. Two different physical limitations are approached with increasing P/E ratio. First, the electrode thickness is shrinking. At some point, the value will become unrealistic and eventually approach 0 crashing the calculation. At the same time, the C-rate for the active material is approaching the limiting C-rate defined in the Cell Chemistry Worksheet. As this value is approached, the ASI will increase to larger and larger values, which thus demands smaller and smaller electrode thicknesses. Eventually, the calculation will crash.

Common sense approaches to resolve these issues are to use lower designed power or higher designed energy. The C-rate and electrode thickness are easily viewed in the model output. These are found on the Battery Design worksheet in row 120 for the C-rate and rows 81 and 82 for the electrode thickness. Therefore, the user may try designs of increasing P/E ratios and watch to see how the electrode thickness and C-rate is changing. Different cell chemistries will have different sensitivities to the P/E ratio depending on the defined limiting C-rate and calculated ASI for power. What is possible with the LMO-G system will not always be possible with the NCA-G system. P/E ratios that satisfy the expression in Eq. 5.1 generally result in successful battery designs. Higher P/E ratios are allowable in some situations. Note that selecting the microHEV design doubles the allowable C-rate since only two second pulses are used. The limiting C-rate, $r_{C,\lim}$, may be found in cell E48 on the System Selection worksheet and is carried over to row 71 in the Battery Design worksheet.

$$\frac{P}{E} < \frac{r_{C,\lim}}{1.35} \tag{5.1}$$

6. Illustrated Results

The model may be used to study the effects of battery parameters on the performance and the manufactured cost of the designed battery packs. A few examples are given below for the effects of various parameters on battery pack volume, weight and cost.

6.1 Number of Cells in Series

For a set battery pack power, the number of cells in the pack has substantial effects on the price of the pack, the pack voltage and the maximum current. These effects are illustrated (Figure 6.1) for LMO-Gr PHEV20 batteries (providing 20-mile electric range) with 60-kW power. The price of the battery increases by 26% in changing the number of series-connected cells in the pack from 32 to 96. The change in the maximum current would also affect the cost of the motor and the electronic converter and controller, but in the opposite direction. As a result of these offsetting effects on the total cost of the electric drivetrain, a study needs to be done to determine the optimum current at maximum power as a function of the total battery pack power and other parameters (see the Future Work section).

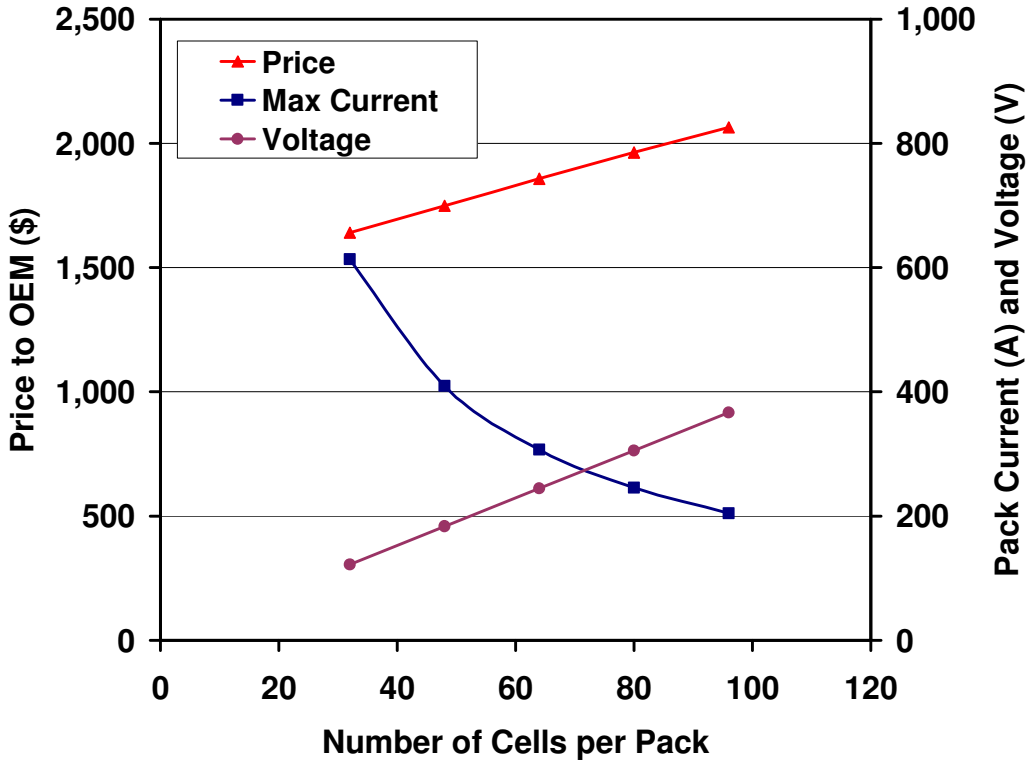

Figure 6.1 The effect of the number of series-connected cells for LMO-Gr, 60-kW, PHEV20 packs with 7.14 kWh total energy (70% useable).

6.2 Battery Packs for HEVs

Lacking a definitive study on the cost of the entire drivetrain to establish the appropriate relationship for battery current, voltage and power, Equation 6.1 is employed in the HEV

examples that follow. Equation 6.1 strikes a balance between very high current and a large number of cells, to aid in selecting the number of cells for a battery of 25 to 150 kW of pack power:

$$\text{Battery Current at full Power (A)} = 1.5 \times \text{Power (kW)} + 200 \qquad (6.1)$$

The number of cells required to match this relationship will differ for each cell chemistry to match the cell open-circuit voltage and impedance of the cell. Also, the selection of the current by this means is only approximate because the voltage is not continuous being defined in terms of a discrete number of cells, which must be an even number for the module design in the model except for single-module battery packs.

Low-powered (25-kW) battery packs for HEVs need to deliver only about 0.15 to 0.25 kWh of energy or a total of about 0.6 to 1.0 kWh. Thus, a cell chemistry that is capable of a high P/E ratio is paramount for these batteries in achieving minimum cost. Some battery chemistries perform much better under these conditions than others as illustrated in Fig. 6.2. The number of cells in these single-module HEV battery packs varies from 33 to 52 to provide a maximum current at full power of 238 ± 2 A, in agreement with Eq. 6.1. It is apparent that the NMC-Gr and NCA-Gr systems studied here are not as well suited to very high P/E requirements as the other systems.

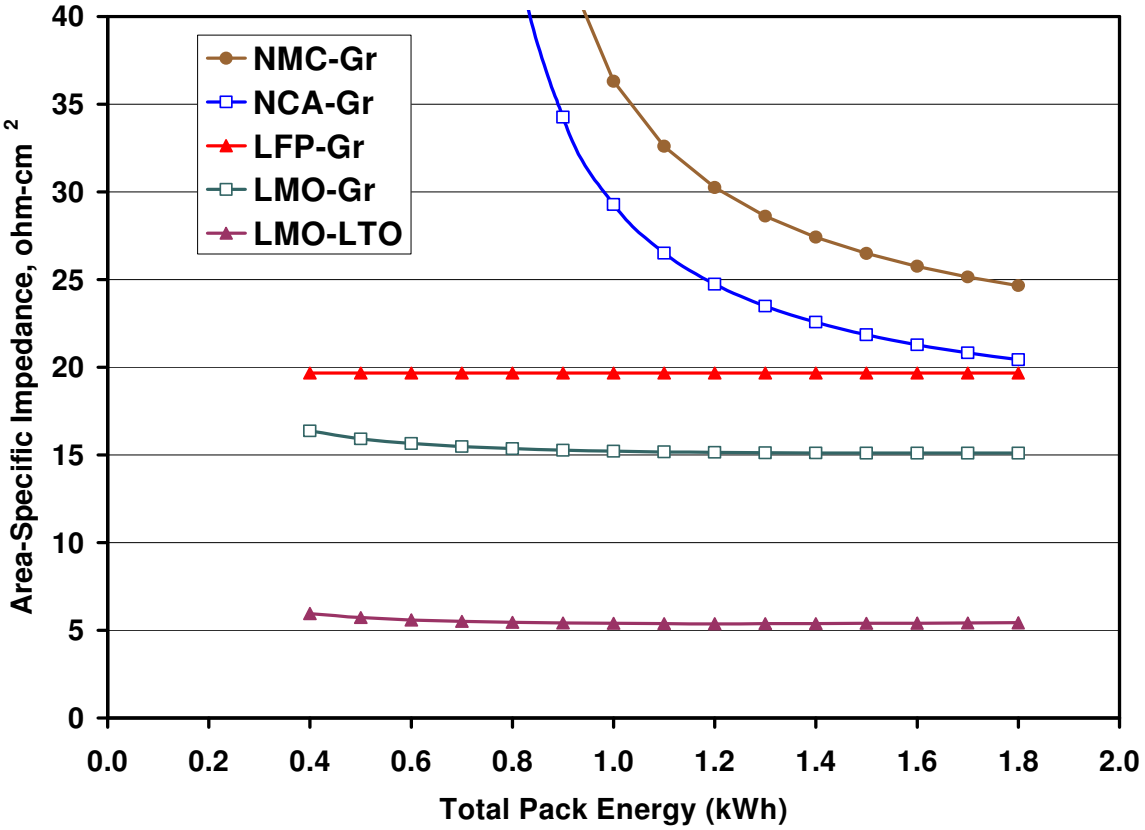

Figure 6.2 Cell area-specific impedance (ASI) for various cell chemistries for 25-kW HEV battery packs delivering full power at about 238 A for 2 sec at 80% OCV

HEV battery packs of about 0.4 kWh of useable energy may be utilized for high power-assist applications. High-powered HEV battery packs of 40 to 100 kW may be required to deliver maximum power for up to 10 seconds. Also, they may be required to deliver moderate power to drive the vehicle electrically at 30 to 50 mph. This latter requirement would also require more useable energy than for the standard HEV battery pack. For this illustration of high-powered HEV battery packs, we have set the energy requirement at 1.6-kWh total energy and 0.4-kWh useable energy. For a moderate-weight sedan with an average energy requirement of 0.25 kWh/mile, the battery pack could power the vehicle for 1.6 miles before being recharged. The battery pack could then be recharged in 1.2 minutes at a rate of 20 kW or at a higher rate if desired.

A comparison of some of the characteristics of LMO-LTO, LFP-Gr, and LMO-Gr battery packs with power capabilities of 25-kW to 100-kW and with 1.6 kWh total energy is shown in Fig. 6.3. As the power of the battery pack is increased, we have increased the number of cells so that both the voltage and the current increase as determined by the relationship of Eq. 6.1. The unevenness in the plotted lines for pack volume results from changes in the number of modules and the dimensions of the packs. The volumes for these high-powered battery packs (Fig. 6.3) as well as their weights (not shown in Fig. 6.3) are all well below the USABC targets for 25-kW battery packs even though most of the battery packs are much more powerful than 25 kW.

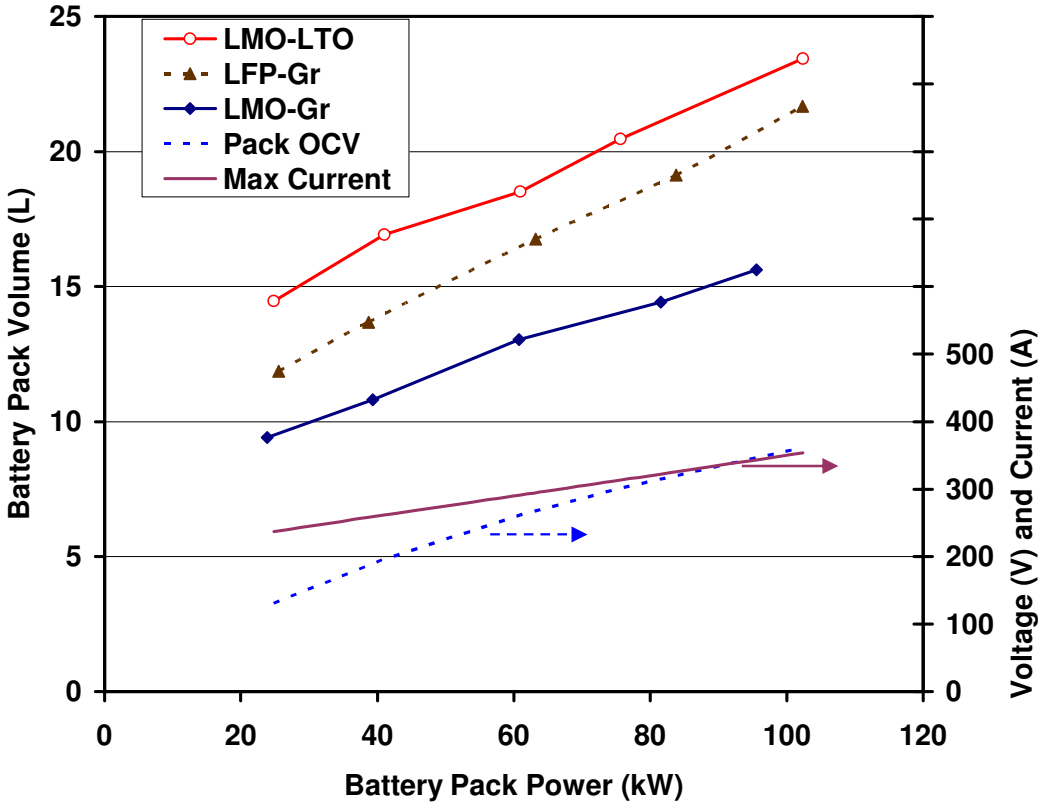

Figure 6.3 Volume, voltage and maximum current for 1.6-kWh lithium-ion battery packs as a function of pack power for packs delivering full power for 10 sec at 80% OCV and 50% SOC. Battery packs have 10-mm insulation thickness.

Many factors affect the costs of manufacturing lithium-ion battery packs. For batteries of high P/E, the chief factors are cell chemistry and pack power as shown in Fig. 6.4, where the prices are plotted for the same batteries as shown in Fig. 6.3, with the addition of the NCA-Gr system. In our attempt to provide high power with a minimum amount of electrode materials with the NCA-Gr system, the area-specific impedance (ASI) became very high as the power was increased resulting in large cell areas and high costs (Fig 6.4). The LMO-Gr system has a significant cost advantage over the other systems in this illustration. These battery chemistries do not have the same probability of meeting the life goal of 15 years, but work is underway throughout the world to meet this need for all of these systems.

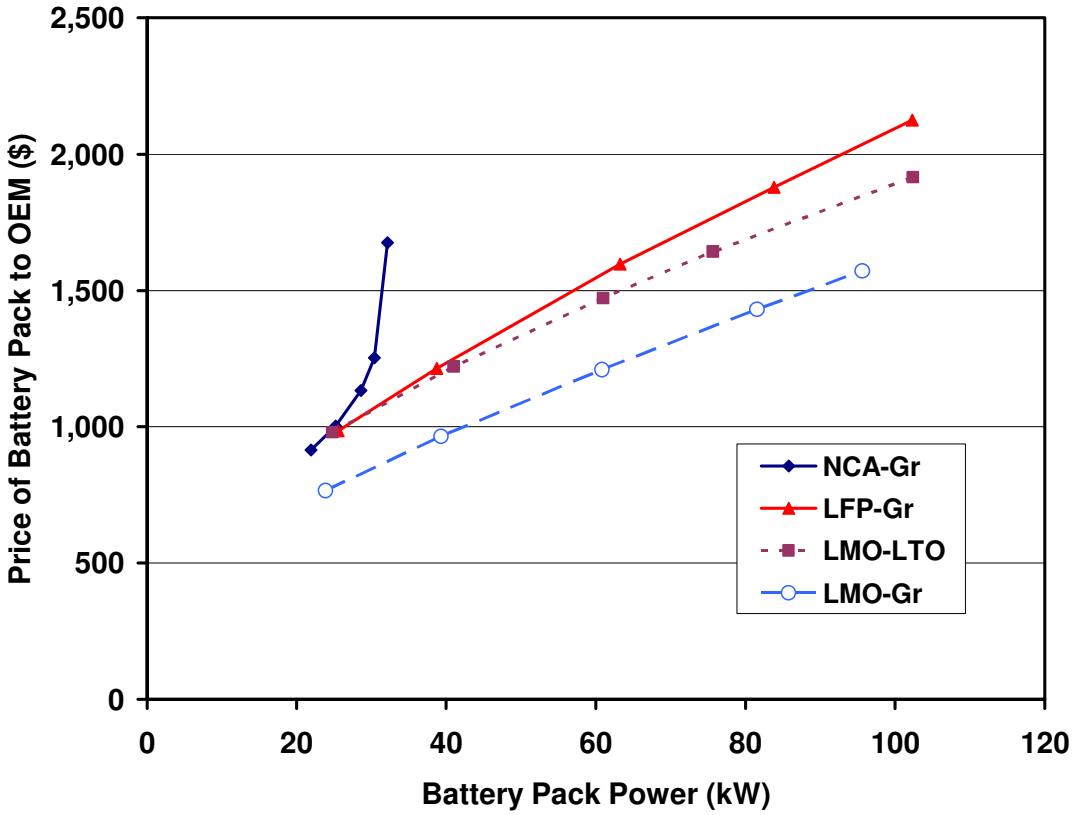

Figure 6.4. Battery pack price to OEMs at 100,000 packs per year manufacturing rate for 1.6-kWh lithium-ion battery packs as a function of pack power for the same battery packs as in Fig. 6.3 with the addition of the NCA-Gr system.

6.3 Battery Packs for EVs

Lithium-ion batteries for PHEVs and EVs do not require a high P/E ratio or low ASI to meet their goals. The most important factors for performance are high specific capacity (mAh/g), high cell voltage, and high electrode density. To compare the performance of EV battery packs made from various Li-ion chemistries, we designed the packs to provide 150 kW of power at 80% OCV at a maximum current of 425 A, which is consistent with Eq. 6.1. Each pack consisted of four modules containing 28, 30, and 32 cells for the cell chemistries LMO-Gr, NMC-Gr, and LFP-Gr, respectively. These selections resulted in nominal (OCV) pack voltages of 429 to 443 V

and within 2 to 13 A of the targeted maximum current of 425 A (Eq. 6.1) for these 150 kW battery packs. On this basis, the NMC-Gr system has excellent power and energy density (Fig. 6.5). The LMO-Gr system does well, despite only moderate specific capacity because of its high voltage. The LFP positive electrode has higher capacity than the LMO chemistry but is hindered by a lower cell voltage and greater electrode porosity resulting from the use of nanostructure particles.

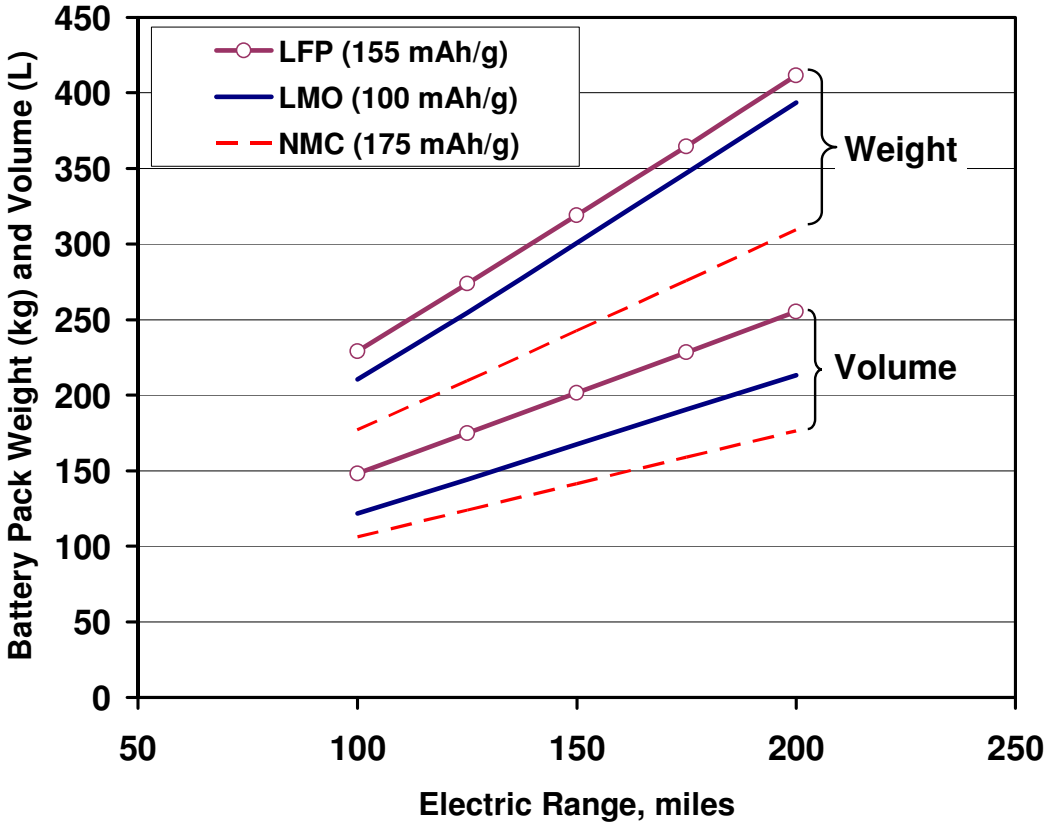

Figure 6.5 Weight and volume of electric vehicle battery packs with lithium iron phosphate (LFP), lithium manganese-spinel (LMO) and lithium nickel-manganese-cobalt (NMC) positive electrodes versus graphite designed to deliver 150 kW of power at about 425 A.

The LMO-Gr system appears to have the lowest price of the three systems in this illustration (Fig. 6.6). By experimenting with the parameter values, it was found that EV battery packs of the NMC-Gr type could match the low price of those in the LMO-Gr system. However, that would require that the specific capacity would be substantially increased and, more importantly, the cost of the NMC would have to be reduced to about $20/kg from $33/kg, perhaps by reducing the cobalt content and increasing the manganese level.

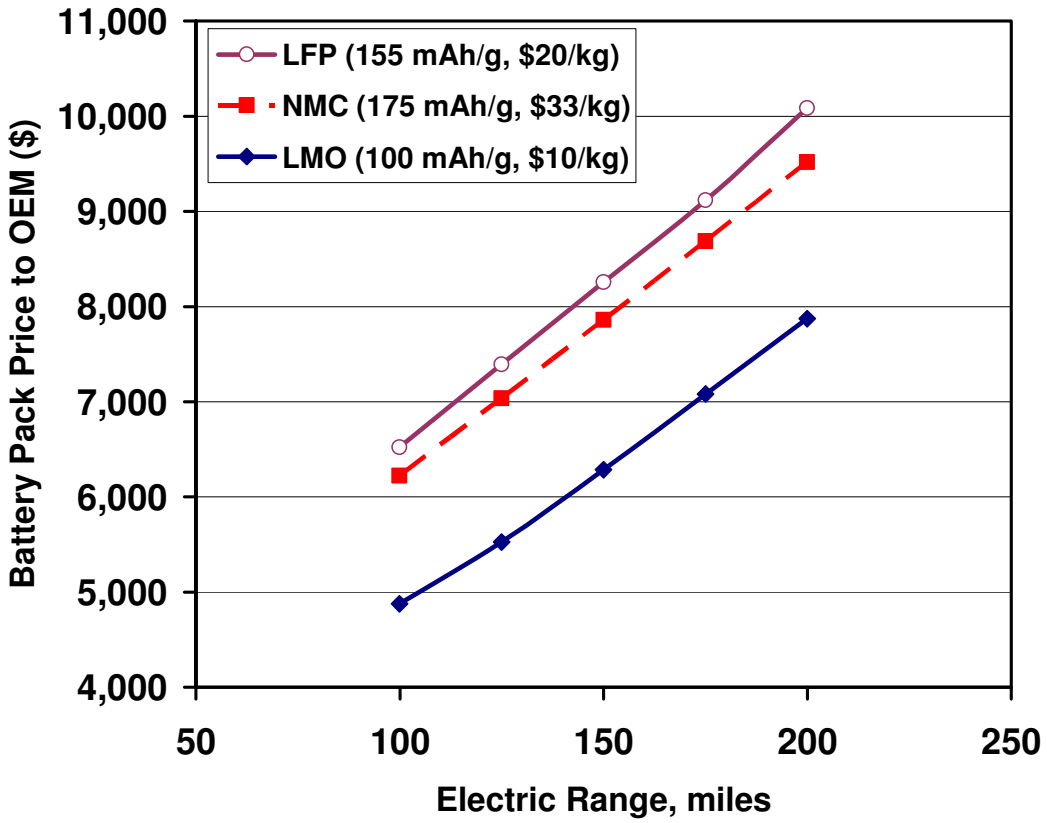

Figure 6.6 Battery pack price to OEM for LFP-G, LMC-G and NMC-G battery packs for same designs as in Fig. 6.5.

6.4 Parallel-Connected Cell Groups and Electrode Thickness Limits

The model also allows the user to create parallel cell groups and to set a maximum electrode thickness. The effect these two unique design factors have on cost are illustrated below in Figure 6.7 for the LMO-Gr and NCA-Gr systems. In this illustration, the EV battery pack design parameters are 100 kW of power, 31 kWh of total energy, and 100 mile range. The nominal battery pack voltage (OCV at 50% SOC) is around 340 V. Two maximum electrode thicknesses of 100 and 200 microns are shown for the two cell chemistries. The thickness of the positive electrode is limiting the LMO-Gr chemistry while the thickness of the negative electrode limits the NCA-Gr chemistry. The LMO-Gr is the least expensive in all cases. However, the difference between the two chemistries lessens with smaller limiting electrode thickness. The costs will become even closer for lower designed P/E ratios. In general, thicker electrodes reduce the cost of the battery pack by lessening the amount of inactive materials used (separator, current collector, etc). Moving to 300 microns allows for greater savings in the LMO-Gr design but not the NCA-Gr design. However, a lower P/E ratio design for NCA-Gr would take advantage of electrode thicknesses greater than 200 microns.

The cell capacity is shown for the NCA-Gr case limited to 100 microns. While the exact values will change with cell chemistry, they will all be similar. The cell capacity is reduced by one half as a single cell is added in parallel. This approach is commonly used by cell manufacturers and

OEMs that cannot reliably produce or successfully operate cells of high capacity for transportation applications (> 60 Ah). However, this approach also increases the price of the battery pack. In this example, the price is increased by ~ $500 when an additional string of cells is incorporated in a parallel arrangement.

The model calculations show that the lowest cost battery pack will utilize thick electrodes and large capacity cells. In current practice, these two approaches have yet to be successfully implemented within the entire community. In the challenge of lowering costs, it is useful to point out the largest gains come from the initial advances (e.g. moving from 100 to 200 micron limit). After that point, the benefits are diminishing.

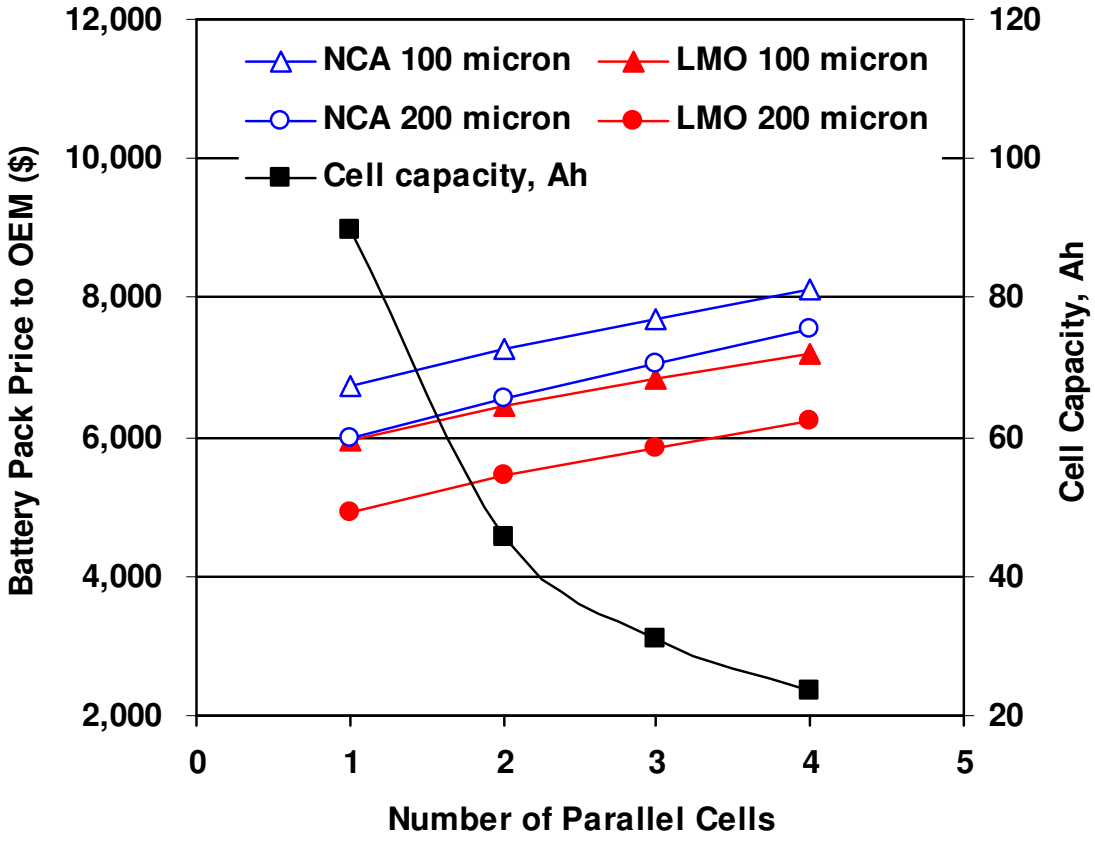

Figure 6.7 Battery pack cost as a function of number of parallel cells and for different maximum electrode thicknesses. The cell capacity is also shown for the NCA-Gr limited to 100 micron electrode thickness.

6.5 Effects of Manufacturing Scale on the Price of the Pack

The effects of manufacturing scale come into the cost calculation even if the annual number of packs produced is unchanged, but the design is altered (e.g. power is increased). For a fixed design, the effect of changing the scale of operations depends on the fraction of the total price that is made up of materials costs. Unit materials costs change little with scale whereas the costs per pack for labor, capital and plant area may decline substantially with increasing production rates, especially at low production rates, Fig. 6.8.

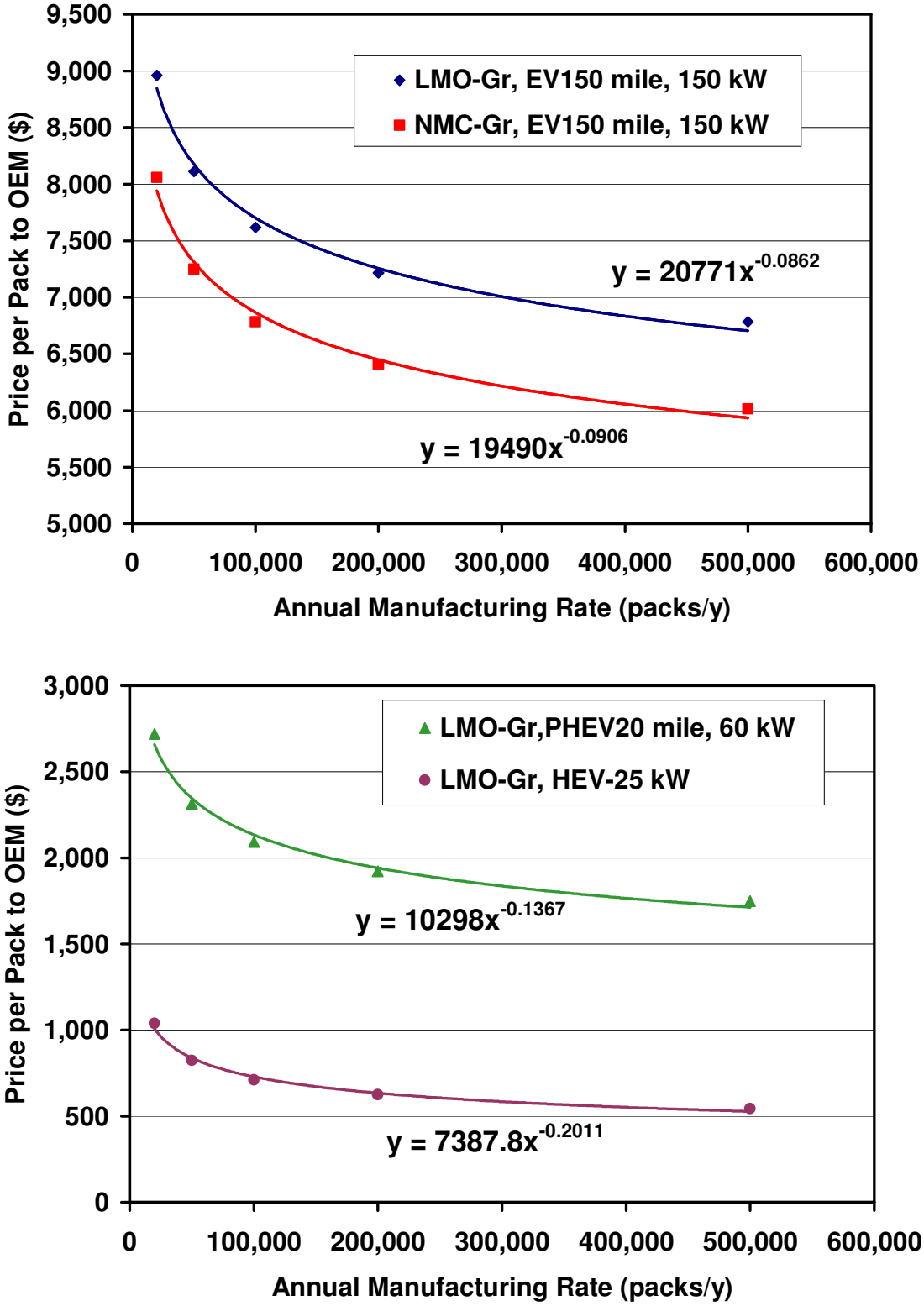

Figure 6.8 The effects of manufacturing rate on the price calculated by the model for battery packs of various cell chemistries, power capabilities and vehicle types

The lines in the graphs are for the best-fit power relationships through the data with power factors of -0.086, -0.091, -0.137, and -0.201 from the top curve to that at the bottom. The least negative power factor is for the battery pack with the highest fraction of materials cost in the total pack cost. The more negative power factors result from a decreasing contribution of materials cost as a fraction of the total pack cost. These power factors for equations of the cost of a single unit can be converted to factors relating the total annual cost of manufacturing similar to Eq. 4.1 by adding 1.0 to each power factor. Thus the factors become 0.914, 0.909, 0.863, and 0.799. These large factors show only a small to moderate effect of scale. When the power curves are compared to the points in each of the graphs of Fig. 6.8, it is apparent that the scale factors approach one as the scale increases. This is because the model assigns a value of 0.95 for the active materials and 1.0 for the balance of the materials. As the production level increases and the materials costs become a larger fraction of the total price of the battery, the scaling power approaches 1.0 and the effect of scale become very small. Likewise, the effect of scale on battery price is much larger for HEV batteries than for EVs because materials costs constitute a smaller portion of the total cost for HEV batteries. Increasing the production rate for HEV batteries will result in a more dramatic reduction in cost than increasing the production rate for EV batteries.

7. Future Work

7.1 Thermal Modeling

The battery design format used in this report provides cooling to the battery pack by blowing air over the top and bottom of the modules. The heat is transferred through the stiff, aluminum pouch material to the module walls. An additional aluminum plate may be placed between cells to enhance heat transfer. This method of cooling will be sufficient for some battery applications, but other applications might require that the battery pack be over-designed to reduce heat generation. Over-design would include providing a battery pack of higher power than called for by the application or providing the power at a very high fraction of the open-circuit voltage (>85%OCV).

We intend to develop an alternative battery design that provides liquid cooling directly to the cells inside the modules. Means of distributing a dielectric coolant to the interior of the modules will be studied. We will carry out thermal modeling studies on the heat generation during vehicle operation on various driving cycles and on the removal of heat from both air-and liquid-cooled battery packs. We intend to investigate the feasibility and cost of these options. The results of these studies will be incorporated into the model in a separate thermal modeling section. This work will be carried out in a cooperative effort with Argonne's Transportation Technology R&D Center, which will perform vehicle simulation tests to determine the rate of heat generation in the battery pack.

7.2 Optimum Battery Voltage for Minimum Drivetrain Cost

For a set cell chemistry and set battery pack power, the cost of the pack increases as the number of cells and the pack voltage are increased (Fig. 6.1). The additional cost results primarily from the cost of additional state-of-charge equalization circuits and the additional number of cells needing formation cycling and testing. The increase in battery pack cost is almost linear with the increase in the number of cells. As the number of cells is decreased, the pack current at maximum power becomes very high and the cost of the balance of the drivetrain increases at an accelerating rate. Thus, there must be a number of cells and an associated pack current at maximum power for which the total cost of the drivetrain is at a minimum. This minimum would be for the current at full power for which the slope of the cost curve for the balance of the drivetrain versus current was equal to the negative of slope of the cost of the pack versus current. This optimum current will increase with the pack power because the slope of the cost-versus-current curve increases with increasing power and, therefore, the optimum current will also increase.

To represent these phenomena in illustrating the model in Section 6, we used an equation (Eq. 6.1) for selecting the current at full power as a function of the battery pack power. This equation is just an estimate and it does not provide for differences in the optimum current that would result from differences in cell chemistries, which are known to affect the battery cost versus power function.

A study is needed to determine the cost of electric motors and the electronic control equipment required for the vehicle and battery pack as a function of power and maximum current capability. Once appropriate cost curves are established, we will determine equations relating the optimum battery current to the desired battery power taking into account the battery chemistry. We intend to do this study with the cooperation of Argonne's Transportation Technology R&D Center.

7.3 Multipurpose Battery Manufacturing Plants

Our cost modeling is based on the concept that a manufacturing plant is constructed to produce a single type of battery pack at a predetermined level of production. In practice, manufacturers will have to produce several types of batteries within the same manufacturing plant and the levels of production may fluctuate. We intend to investigate how this increased flexibility requirement will affect the various manufacturing costs. For example, the cell filling and sealing equipment may be required to handle cells of different dimensions. This would most likely increase the capital cost for this equipment. Alternatively, additional packaging and sealing lines might be needed. We intend to evaluate combinations of vehicle battery packs that are easily integrated into the same plant. The manufacturing cost will most likely increase after these considerations are built into the model.

7.4 Stand-Alone Graphical User Interface for Model

The spreadsheet program described here-in allows versatility in designing the battery and in calculating the costs, but like all complex spreadsheet programs it is not user-friendly to those unfamiliar with the details of calculation. In addition, the model is easily corrupted by a poor choice of input parameters. As a result, the final spreadsheet program will be converted to a stand-alone user-friendly application, primarily with the efforts of Ira Bloom. Visual Basic for Applications will be used to hard code in the model calculations and to also create the graphical interface. The new user interface should allow for a wide distribution of the model while maintaining the ability to change the vast majority of input parameters. The retention of this flexibility should make the model a valuable tool for those interested in batteries regardless of the specific material property or manufacturing cost structure the user seeks to analyze.

REFERENCES

1. M. Anderman, F. Kalhammer, and D. MacArthur. "Advanced Batteries for Electric Vehicles: An Assessment of Performance, Cost, and Availability." California Air Resources Board, June (2000). Available from http://www.arb.ca.gov/msprog/zevprog/2000review/btap report.doc (accessed on December 17, 2010).

2. B. Barnett, D. Ofer, C. McCoy, Y. Yang, T. Rhodes, B. Oh, M. Hastbacka, J. Rempel, and S. Sririramulu "PHEV Battery Cost Assessment," 2009 DOE Merit Review, May (2009). Available from http://www1.eere.energy.gov/vehiclesandfuels/pdfs/merit_review_2009/energy_storage/es_02_barnett.pdf (accessed on December 11, 2010).

3. B. Barnett, J. Rempel, D. Ofer, B. Oh, S. Sriramulu, J. Sinha, M. Hastbacka, and C. McCoy, "PHEV Battery Cost Assessment," 2010 DOE Merit Review, June (2010). Available from http://www1.eere.energy.gov/vehiclesandfuels/pdfs/merit_review_2010/electrochemical_storage/es001_barnett_2010_o.pdf (accessed on December 11, 2010).

4. A. Dinger, R. Martin, X. Mosquet, M. Rabl, D. Rizoulis, M. Russo, and G. Sticher, "Batteries for Electric Vehicles: Challenges, Opportunities, and the Outlook to 2020." The Boston Consulting Group, Available from http://www.bcg.com/documents/file36615.pdf (accessed on December 11, 2010).

5. L. Gaines and R. Cuenca. "Costs of Lithium-Ion Batteries for Vehicles," Center for Transportation Research, Energy Systems Division, Argonne National Laboratory, ANL/ESD-42, Argonne, IL May (2000).

6. F.R. Kalhammer, B.M. Kopf, D.H. Swan, V.P. Roan, M.P. Walsh, "Status and Prospects for Zero Emissions Vehicle Technology: Report of the ARB Independent Expert Panel 2007," California Air Resources Board, April (2007). Available from http://www.arb.ca.gov/msprog/zevprog/zevreview/zev_panel_report.pdf (accessed on December 17, 2010).

7. M. A. Kromer and J. B. Heywood, "Electric Powertrains: Opportunities and Challenges in the U.S. Light-Duty Vehicle Fleet," Sloan Automotive Laboratory, Laboratory for Energy and the Environment, Massachusetts Institute of Technology, LFEE 2007-03 RP, Cambridge, MA (2007).

8. P. Mock, "Assessment of Future Li-Ion Battery Production Costs," presented at *Plug-in 2009*, Long Beach, CA, (2009).

9. National Research Council of the National Academies, "Transitions to Alternative Transportation Technologies – Plug-in Hybrid Electric Vehicles," The National Academies Press, Washington, D.C. (2010). Available from http://www.nap.edu/catalog.php?record_id=12826 (accessed on December 17, 2010).

10. TIAX LLC, "Cost Assessment for Plug-In Hybrid Vehicles (SOW-4656)," Report to US DOE Office of Transportation Technology, October (2007).

11. P.A. Nelson, D.J. Santini, J. Barnes, "Factors Determining the Manufacturing Costs of Lithium-Ion Batteries for PHEVs." *International Electric Vehicles Symposium EVS-24*, Stavanger, Norway, (2009).

12. D.J. Santini, K.G. Gallagher, P.A. Nelson, "Modeling the Manufacturing Costs of Lithium-Ion Batteries for HEVs, PHEVs, and EVs," *International Electric Vehicles Symposium EVS-25*, Shenzhen, China, (2010).

13. P. Nelson, I. Bloom, K. Amine, G. Henriksen, "Design modeling of lithium-ion battery performance," *Journal of Power Sources*, **110**, 437 (2002).

14. P. Nelson, D. Dees, K. Amine, G. Henriksen, "Modeling thermal management of lithium-ion PNGV batteries," *Journal of Power Sources*, **110**, 349 (2002).

15. G.L. Henriksen, K. Amine, J. Liu, and P.A. Nelson, "Materials Cost Evaluation Report for High-Power Li-Ion HEV Batteries," Electrochemical Technology Program, Chemical Technology Division, Argonne National Laboratory, ANL-03/05, Argonne, IL (2002).

16. P. Nelson, K. Amine, A. Rousseau, H. Yomoto, "Advanced Lithium-Ion Batteries for Plug-in Hybrid-Electric Vehicles", *International Electric Vehicles Symposium, EVS-23*, Anaheim, Ca (2007).

17. P. Nelson, "Modeling the Manufacturing Costs of Lithium-Ion Batteries for PHEVs," presented at *Plug-in 2009*, Long Beach, CA, (2009).

18. K.G. Gallagher, P.A. Nelson, and D.W. Dees, "Simplified Calculation of the Area Specific Impedance for Battery Design," *Journal of Power Sources,* **196,** 2289 (2011).

19. A.N. Jansen, K. Amine, and G. L. Henriksen, "Low-Cost Flexible Packaging for High-Power Li-Ion HEV Batteries," Electrochemical Technology Program, Chemical Technology Division, Argonne National Laboratory, ANL-04/09, Argonne, IL (2004).

20. P.A Nelson and A.N. Jansen, "Comparative Costs of Flexible Package Cells and Rigid Cells for Lithium-Ion Hybrid Electric Vehicle Batteries," Electrochemical Technology Program, Chemical Technology Division, Argonne National Laboratory, ANL-06/43, Argonne, IL (2006).

21. J. Euler and W. Nonnenmacher, "Stromverteilun in Porösen Elektroden," *Electrochimica Acta*, **2,** 268 (1960).

22. J.S. Newman and C.W. Tobias, "Theoretical Analysis of Current Distributions in Porous Electrodes," *Journal of the Electrochemical Society*, **109**, 1183 (1962).

23. United States Geological Survery, Commodity Statistics and Information, Available from http://minerals.usgs.gov/minerals/pubs/commodity/ (accessed on December 17, 2010).

24. R.H. Perry, D.W. Green, and J.O. Maloney, *Perry's Chemical Engineers' Handbook,* Sixth Edition, pp: 25-68 (1984).